Guar Gum/Montmorillonite Nanocomposites and Their Potential Application in Drug Delivery

Joanna Dziadkowiec

Thesis submitted to the

Faculty of Graduate and Postdoctoral Studies

in partial fulfillment of the requirements for the

MSc degree in Chemistry

Department of Chemistry

Faculty of Science

University of Ottawa

Acknowledgements

I would like to thank the University of Ottawa members who helped me throughout this project: Rola Mansa, whose precious advice and continual help were truly inspiring and irreplaceable, the members of the Detellier Research Group for their daily laboratory support and insight, and my supervisor, Professor Christian Detellier, who offered his expert guidance and impressive knowledge which strongly motivated and encouraged me during the project.

My acknowledgements go to the University of Aveiro members: dr Ana Quintela and Professor Fernando Rocha who made it possible to work with natural clay samples and introduced valuable geological, engineering and medicinal aspects of clay minerals to me. I would like to thank dr Carla Patinha, Denise Terroso and Maria Cristina Sequeira for their laboratory assistance.

I would like to express my gratitude to the IMACS team for giving me the great opportunity to participate in this excellent Master Program devoted to clay science. I would like to acknowledge Patricia Patrier, Sophie Levesque and Rola Mansa for their constant assistance.

Finally, I would like to thank my parents and Paweł who were always supporting me.

Abstract

Clays are ubiquitous near the Earth's surface. Medicinal properties of these nontoxic minerals have been intuitively recognized since ancient times. Up till now, clays have been used in pharmaceutical formulations as active agents and excipients. Currently, there is an urgent need to seek advanced, functional materials with low environmental impact. Answering to that trend, clay-biopolymer nanocomposites were synthesized in this thesis and applied in a drug delivery system.

In the first part of the thesis, Portuguese clay from a bentonite deposit in Benavila (Portugal) was collected from six sampling sites and characterized. The highest content of clay fraction, approximately 30%, was found in two of the sampling sites. After purification, the smectite-rich samples were analyzed with respect to clay content, mineralogical and chemical composition, physicochemical and mechanical properties. SEM-EDS revealed that the smectite present in the ore is montmorillonite with varying Fe content. This was also indicated by the means of XRD, XRF and FTIR.

The Benavila sample, which was richest in smectite, as well as the sodium Wyoming montmorillonite from the Source Clay Repository (SWy-2) were successfully used to synthesize clay-biopolymer nanocomposites. The chosen biopolymers were the plant-extracted polysaccharides – neutral guar gum and its cationic form. The obtained materials were thoroughly characterized by XRD, TGA and NMR, and the intercalated structure was reported.

The prepared nanocomposites were loaded with an anti-inflammatory drug ibuprofen and tested in an in-vitro release system. The drug-loaded materials were characterized with XRD, TGA and NMR. A membrane diffusion method was chosen as a dissolution testing strategy and the drug was quantified by UV-Vis spectroscopy. The materials exhibited improved properties as a noticeable reduction of release rate was achieved.

.

Table of Contents

List of Tables and Figures

Abbreviations

AAS	Atomic Absorption Spectrometry
BA	Bioaccessibility
BARGE	the Bioaccessibility Research Group of Europe
BSE	Backscattered Electrons
BV	Benavila Sample
CEC	Cation Exchange Capacity
CGG	Cationic Guar Gum
CR	Cumulative Release
DL	Drug Loading
DLE	Drug Loading Efficiency
DTA	Derivative Thermogravimetric Analysis
EDS	Energy Dispersive Spectrometry
FTIR	Fourier Transform Infrared Spectroscopy
IBU	Ibuprofen Sodium Salt
ICP-MS	Inductively Coupled Plasma Mass Spectrometry
IUPAC	International Union of Pure and Applied Chemistry
LDH	Layered Double Hydroxides
LL	Liquid Limit
LOI	Loss on Ignition
MCWO	Molecular Weight Cut-Off
MDDS	Modified Drug Delivery System
NGG	Neutral Guar Gum
NMR	Nuclear Magnetic Resonance

PI	Plasticity Index
PL	Plastic Limit
SE	Secondary Electrons
SEM	Scanning Electron Microscopy
SGF	Simulated Gastric Fluid
SIF	Simulated Intestinal Fluid
SWy-2	Sodium Wyoming Montmorillonite
TEM	Transmission Electron Microscopy
TGA	Thermogravimetric Analysis
UV-Vis	Ultraviolet-Visible Spectroscopy
XRD	X-ray Diffraction
XRF	X-ray Fluorescence Spectroscopy

Part I – Theoretical Introduction

1. Clay Minerals

Clays are ubiquitous near the Earth's surface and have a great potential in material science, which is frequently undervalued. Biopolymers are globally extracted at industrial scale. These two materials have been reported to interact in natural environments (Ueshima & Tazaki, 2001). In this chapter, theoretical aspects of clay minerals, biopolymers, nanocomposites and their application in drug delivery are summarized.

1.1. Terminology

There is no clear, terminological agreement regarding clay and clay minerals. According to the Clay Minerals Society, the term clay is considered as natural, geological material containing clay minerals, other associated minerals and amorphous substances (Guggenheim & Martin, 1995; Moore, 1996). Correspondingly, the term clay minerals refers to natural and synthetic phyllosilicates (Guggenheim & Martin, 1995). Additionally, some non-phyllosilicates, such as layered double hydroxides (LDH) may be also classified as clay minerals (Bergaya & Lagaly, 2013).

1.2. Genesis

The origin of natural clay minerals is very complex and may involve multiple processes. These mainly include: weathering of primary silicates and aluminosilicates as well as other clay minerals, diagenesis and transformation, crystallization from solutions or hydrothermal alterations (Keller, 1970). The formation of clay minerals is often affected by organic matter, microorganisms, and other biological agents (Ueshima & Tazaki, 2001; Velde & Barre, 2010). Additionally, a range of environmental factors such as rock types, fluid chemistry, climate, topography, to name a few, influence the genesis of clay minerals (Meunier, 2005). Synthesis of clay minerals is often troublesome and although, contrary to natural deposits, a pure product can be obtained, clay minerals are not synthesized commercially (except for laponite and LDH) (Jaber *et al*., 2013).

1.3. Structure and Chemistry

Clay minerals are layered phyllosilicates. Layers are major building blocks that comprise of alternate tetrahedral and octahedral sheets. The sheets' framework consists of elementary polyhedra, which are formed by cation-anion bonds.

Generally, Si and Al in 4-fold coordination build the tetrahedral sheets. SiO_4^{4-} and AlO_4^{5-} tetrahedra are bonded together by sharing three oxygen vertices. The fourth oxygen vertex is left free (apical oxygen). In such a two-dimensional lattice, Si^{4+}-Si^{4+} and Si^{4+}-Al^{5+} cation pairs are linked through one O^{2-} anion (Al^{5+}-Al^{5+} pairs are always excluded). The octahedral sheet is formed by cations in 6-fold coordination, where metal cations (such as Al^{3+}, Fe^{3+}, Fe^{2+}, Mg^{2+}) occupy centers of octahedrons. O^{2-} or OH^- anions are present at their vertices. To form a sheet, neighboring octahedrons share six of such vertices. There are two types of octahedral sheets, depending on a cation occupancy. A trioctahedral one is formed when each anion is linked with three cations, whereas, in a dioctahedral sheet, each anion is bonded to two cations, leaving a third site vacant. Tetrahedral and octahedral sheets are linked together through apical oxygen anions of tetrahedra. As such, these oxygen anions simultaneously become vertices of octahedra (Fig. 1) (Meunier, 2005).

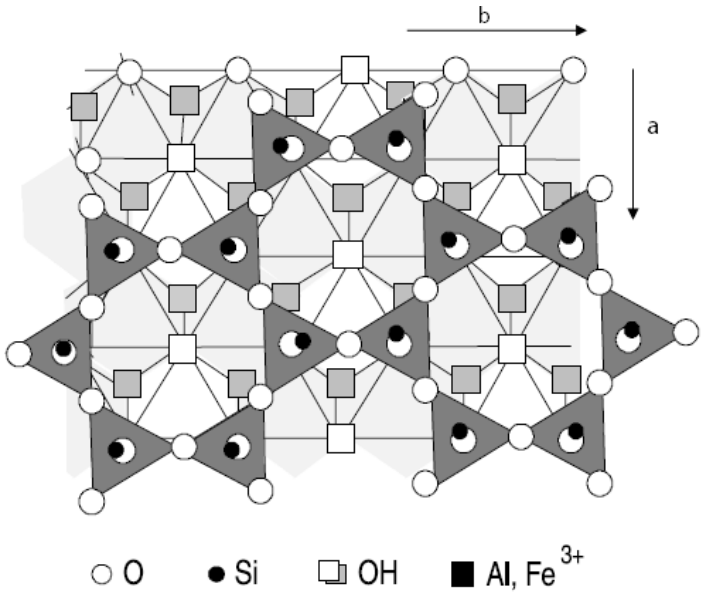

Figure 1. Schematic representation of idealized structures of a tetrahedral sheet, forming hexagonal cavities (dark gray,) and an octahedral sheet (light gray) with vacant sites. In nature, a and b crystallographic dimensions of unit cells of both sheets differ significantly, leading to their distortions of varied degree and a decrease in symmetry (adapted from Meunier, 2005).

There are two basic types of layers that give rise to two different crystal structures of clay minerals – 1:1 layers and 2:1 layers. The 1:1 layers comprise one tetrahedral sheet bonded to one octahedral sheet. Such 1:1 layer units are stacked together in a repeatable manner to form a crystal. The 2:1 layer type consist of one octahedral sheet, sandwiched between two tetrahedral sheets. Similarly, the layers are stacked on each other in the crystallographic direction c (Fig. 2). Crystals of clay

minerals are usually composed of a few layers up to several tens of layers and their dimension is less than 2 μm (Meunier, 2005; Bergaya & Lagaly, 2013).

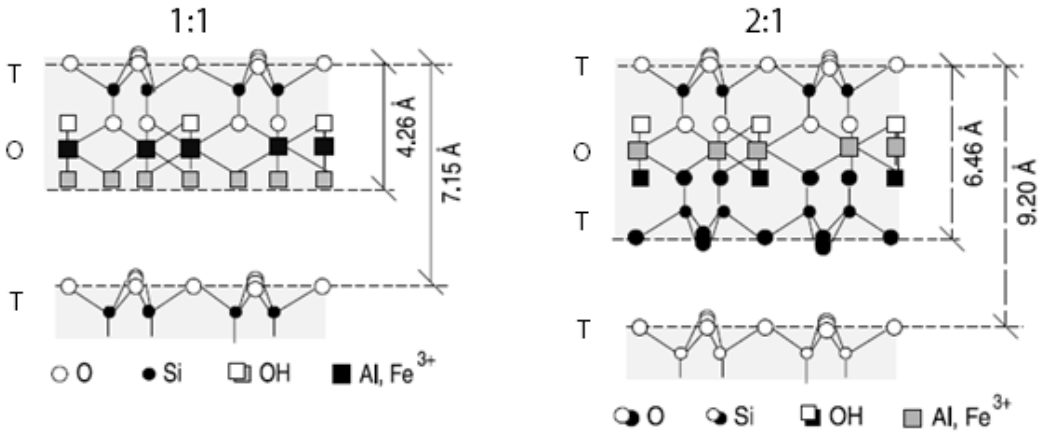

Figure 2. Schematic representation of 1:1 layer and 2:1 layer structures of dioctahedral clay minerals. The typical thickness of layers is indicated. The letters T and O refer to tetrahedral and octahedral sheets, respectively (adapted from Meunier, 2005).

Chemical composition of clay minerals is extremely diversified since they are capable of forming solid solutions with a wide compositional range. Additionally, crystals found in nature are often polyphased – they are comprised of interstratified layers of varied chemistry (Meunier, 2005).

Principal 1:1 phyllosilicates with the simplest chemical formulas are dioctahedral kaolinite ($Si_2O_5Al_2[OH]_4$) and trioctahedral chrysotile ($Si_3O_5Mg_3[OH]_4$). Correspondingly, the 2:1 counterparts are dioctahedral pyrophyllite ($Si_4O_{10}Al_2[OH]_2$) and trioctahedral talc ($Si_4O_{10}Mg_3[OH]_2$) (Velde & Meunier, 2008). Cations present in both tetrahedral and octahedral sheets can be substituted to varied degrees, thus producing solid solutions. There are two main types of cationic substitutions: homovalent (e.g. $Fe^{2+} \rightarrow Mg^{2+}$) and heterovalent (e.g $Al^{3+} \rightarrow Si^{4+}$, $Al^{3+} \rightarrow Mg^{2+}$). The latter induce a deficit of positive charge in the sheets. Generally, this overall negative charge is balanced by the presence of additional sheet of interlayer cations, or by formation of vacancies in certain crystallographic sites. In most cases, 1:1 layer type minerals, do not undergo heterovalent substitutions and the amount of homovalent ones is relatively low. On the contrary, both types of substitutions are frequent for 2:1 layer type phyllosilicates (Meunier, 2005; Velde & Meunier, 2008).

1.4. Smectite Group Clay Minerals

The smectite group comprises 2:1 layer type, swelling clay minerals with relatively low layer charge (0.3 to 0.6 per half unit cell - $O_{10}[OH]_2$) (Velde & Meunier, 2008). This

charge is resultant from cationic substitutions in tetrahedral and/or octahedral sheets. Net electrical neutrality is restored by the presence of interlayer metal cations (such as Ca^{2+}, Na^{+}, Mg^{2+}, K^{+}, etc.) (Fig. 3). One member of smectite group, montmorillonite, is a dioctahedral clay mineral with heterovalent substitutions in octahedral sheets ($Mg^{2+} \rightarrow Al^{3+}$) and the typical chemical formula - $(Na,Ca)_{0.3}(Al,Mg)_2Si_4O_{10}[OH]_2 \bullet n(H_2O)$ (www.webmineral.com). Montmorillonite crystals are flaky, very small (~1 μm) and several nm thick (a few layers) (Velde & Meunier, 2008).

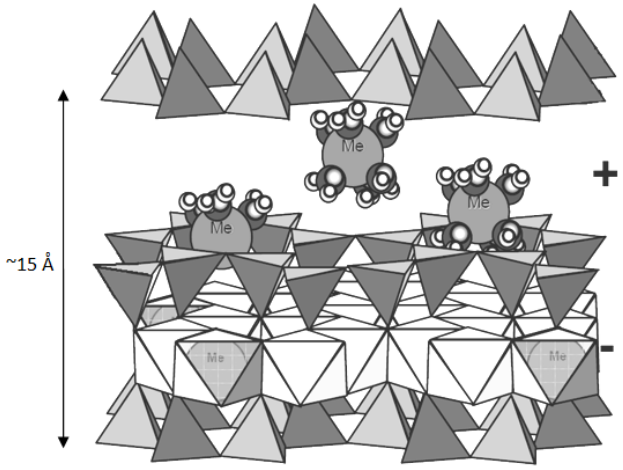

Figure 3. Schematic representation of 2:1 layer type clay mineral – smectite. Negative charge of the layer, due to ionic substitutions in sheets, is balanced out by interlayer cations with associated water molecules. The approximate interlayer spacing for hydrated species with a water bilayer is 15 Å (adapted from Meunier, 2013).

The interlayer cations undergo hydration to a varied extent, depending on their nature and external conditions, what induces a variation of interlayer spacing (d_{001}). Overall, the interlayer thickness results from equilibrium of repulsive forces (negative charge of layers) and attractive forces (electrostatic interaction of cations and layers) (Norrish, 1954). Na^{+}-saturated montmorillonite can undergo infinite swelling upon hydration, leading in a first step to delamination (interaction between layers is conserved) and subsequently, exfoliation of crystallites into single layers (no further interaction) (Meunier, 2005; Bergaya *et al*., 2013).

Most of the interlayer cations are easily exchangeable. This property, along with the presence of active surface adsorption sites, make smectite clay minerals widely useful for adsorption processes and can be quantified by various cation exchange capacity (CEC) assays (Meunier, 2005). Not only inorganic metal cations can be introduced into smectite's interlayer zone. Intercalation of various cationic and neutral, inorganic and organic molecules is commonplace. These include surfactants, oligomer pillars, polymers, biopolymers, drug molecules and many more (Zheng *et al*., 2007; Bergaya & Lagaly, 2011; Mansa & Detellier, 2013; Lambert & Bergaya, 2013). For that

reason, smectite clay minerals are promising materials for advanced applications in many fields.

1.5. Medicinal Use of Clays

Medicinal properties of clays have been intuitively recognized since ancient times. Clays were not only used externally to heal wounds and soothe skin but also consumed. Ingestion of clay or soil (geophagy) was aimed at relieving gastrointestinal ailments and famine, treating mineral nutrient deficiency, and even at curing infectious diseases (Young *et al*., 2011; Carreterro *et al*., 2013). Up till now, natural clays and clay minerals have been used in pharmaceutical formulations as active agents (with therapeutic properties) and excipients (therapeutically inert). However, due to their specific nature, these two functions cannot be separated. Excipients based on clay minerals will exhibit certain therapeutic function, too (Fig. 4). Additionally, their non-toxicity determines feasibility for such purposes.

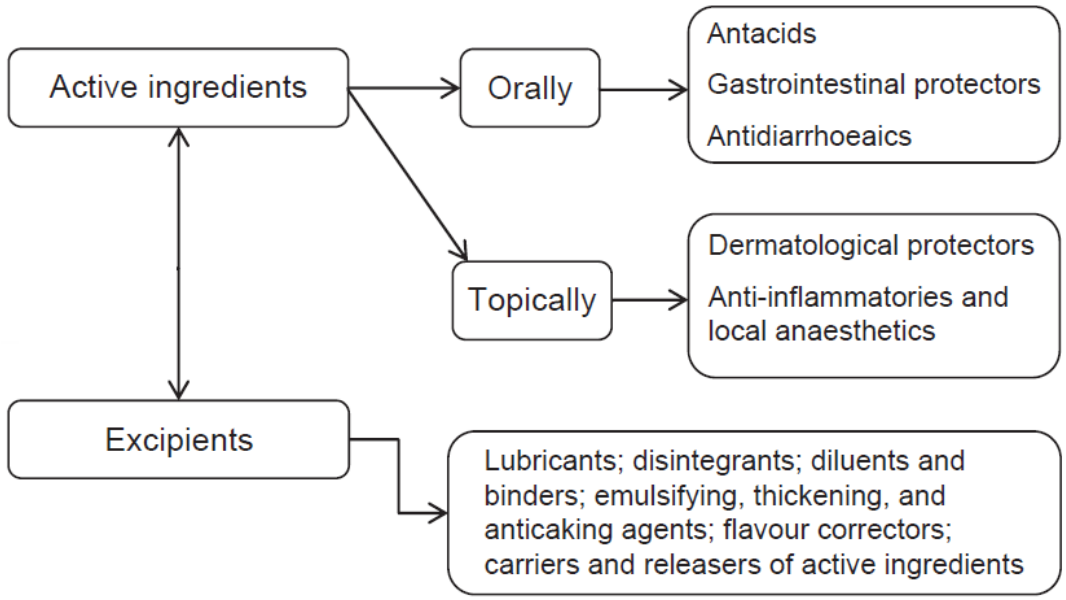

Figure 4. Possible functions of clays and clay minerals as active agents and excipients in drug formulations (adapted from Carreterro et al., 2013).

The basic role of excipients is determination of consistency, form and volume of pharmaceuticals (Carreterro *et al*., 2013). Moreover, clay mineral excipients can improve release characteristics and organoleptic properties of drugs (Kaushik & Dureja, 2014).

The beneficial role of clay minerals results from their physicochemical and physical characteristics. Due to cation exchange capacity and adsorptive potential, they

can interact with drug molecules, facilitating their liberation. Sustained release of drugs, controlled by desorption from clay mineral excipients, was found favorable in case of antibiotics, amphetamines, some anti-inflammatory drugs and others, as well as in intestinal delivery of pharmaceuticals (McGinity & Lach, 1977; Porubcan *et al*., 1978; Zheng *et al*., 2007; Carreterro *et al*., 2013). Clay minerals adsorbing H^+ are capable of reducing gastric acidity (Plantefeve & Rene, 1989). By adsorbing excess water and gases, they have also a prominent anti-diarrheal effect (Dupont & Vernisse, 2009). Smectite can suppress harmful effects caused by microbial toxins, pesticides and bacteria present in the gastrointestinal tract, as indicated by *in vivo* studies (Droy-Lefaix & Tateo, 2006).

Carreterro & Pozo, 2009, describe advantageous rheological, colloidal, thixotropic, mechanical and bioadhesive properties of clay mineral excipients. By making the gastric mucus more viscous and stable, clay minerals can additionally act as gastrointestinal protectors. Since they can adhere to mucous membranes in the gastrointestinal tract, they strengthen mucous gel barrier and inhibit damage that could be induced by aggressive agents, such as pepsin and some anti-inflammatory drugs (More *et al*., 1987, Droy-Lefaix & Tateo, 2006). Non-steroidal anti-inflammatory drugs, for instance aspirin and ibuprofen, are responsible for mucus alteration that may lead to stomach pain, ulceration and other gastropathies (Droy-Lefaix & Tateo, 2006). Peignot *et al*., 1997, demonstrated smectite to be efficient in alleviating ailments caused by ingestion of such drugs.

Importantly, interaction of clay minerals with drug molecules is not always advantageous. Their presence may affect stability and bioavailability of drugs in a negative way. Clay mineral-induced, sustained release may be responsible for lowering blood levels of some drugs below the concentrations necessary for an effective therapeutical action (Carreterro *et al*., 2013). Furthermore, reactive and retentive surfaces of clay minerals may lead to drugs' decomposition upon interaction, leading to a serious health risk. Such phenomenon was reported in the case of digoxin or dexamethasone drugs adsorbed on montmorillonite surface (Porucban *et al*., 1979; Forteza *et al*., 1989). These issues are important in the case of clay mineral excipients and coadministration of drugs and clay minerals.

2. Biopolymers

Biopolymers are natural, non-toxic, polymeric substances, formed by organisms. They are a product of metabolic processes within cells, that include complex, enzyme-

induced polymerization of monomers. According to the IUPAC definition, these macromolecules include proteins, polysaccharides and nucleic acids (IUPAC, 1997). Except for nucleic acids, that convey genetic information, most biopolymers constitute structural or reserve material in cells. Others serve as protective gels, adhesives, etc. or are stress-induced exudates.

Most biopolymeric materials are extracted from plant and animal products. A wide range of biopolymers is also derived from bacterial and fungal exudates (Lenz, 1993). There exist another group of biopolymers that are synthetic and obtained by polymerization of natural substances, for example (poly)lactic acid. Additionally, some authors understand the term biopolymer as a biodegradable polymer, what include certain petroleum-based synthetic polymers (Endres & Siebert-Raths, 2011).

Numerous polysaccharides and proteins are of particular interest for the preparation of materials with a low environmental impact. One important application is the production of bio-based plastics from renewable resources as an alternative to non-degradable, petroleum-based materials. A great deal of research is devoted to medical applications of biopolymers (implants, tissue engineering, drug and gene delivery) (Pilla, 2011; Dutta & Dutta, 2013).

2.1. Polysaccharides

Polysaccharides belong to the most abundant group of natural organic compounds –carbohydrates. They consist of monosaccharide units, which are the simplest carbohydrates. Monosaccharide molecules are polyhydroxy aldehydes (aldoses) or polyhydroxy ketones (ketoses). Predominantly, they exist in cyclic forms, which are built from five-membered furanose or six-membered pyranose ring structures. Sugar molecules in a ring form can adopt α- (axial) or β- (equatorial) orientations at the C-1 atom. The former have glycoside bonds with –OH groups directed down, and the latter directed out from the ring. Aldohexoses (six-carbon aldoses), that are the most abundant in nature, are dextrorotatory (D) D-glucose, D-mannose and D-galactose. Polysaccharides consist of more than ten monosaccharide units that are joined together by oxygen linkages to form a chain. Usually, when monomers are linked axially, polysaccharides can adopt a helical conformation. Those with β-glycoside linkages are generally linear (Petrucci *et al*., 2002; Mathur, 2012). Polysaccharides are synthesized by plants, animals and microorganisms and serve mainly as structural materials (e.g. cellulose, chitin), energy-storage materials (e.g. starch, glycogen) and reserve materials (galactomannans) (Mathur, 2012).

2.2. Guar Gum

Guar gum is a plant-extracted, galactomannan polysaccharide of high molecular weight. Galactomannans are reserve seed sugars of many legume plants. They can be also synthesized by certain microorganisms and bacteria. These branched carbohydrates are copolymers of mannose and galactose. Their main biological function in plants is to supply carbon during germination. Additionally, because of having a high affinity for absorbing water, galactomannans can act as a water reservoir for the plant (Mathur, 2012). The ability of forming paste, colloidal sol or gel, when dispersed in water, is typical for gums (Whistler, 1993). Properties of seed galactomannans depend on molecular weight, mannose to galactose ratio and a mode of galactose branching. Especially, presence of galactose grafts and a placement of hydroxyl groups determines solubility of these gums (Mathur, 2012).

Guar gum is commercially extracted from endosperm of guar plant's seeds. The guar plant *(Cyamopsis tetragonolobus*) is an annual crop cultivated in the Indian Subcontinent (Mathur, 2012). Guar gum molecules comprise of a linear backbone of D-mannopyranose units, linked through β(1→4) glycosidic bonds. D-galactopyranose grafts are side-chained to mannose units at the C-6 position by α(1→6) glycosidic bonds (Fig. 5). The average ratio of mannose to galactose is equal to 1.85:1 (Mathur, 2012).

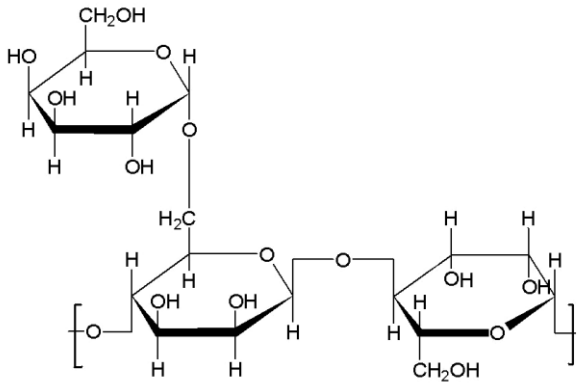

Figure 5. Idealized structure of guar gum. According to the recent studies (Mathur, 2012), galactopyranose grafts have a random distribution.

Guar gum molecules are neutral. Similarly to other biopolymers, they are often chemically modified by simple methods, due to presence of reactive groups in their structure. The functionalized species, with altered properties, may be neutral or charged. One derivative of guar gum is guar 2-hydroxy-3-(trimethylammonio)propyl

ether chloride (cationic guar gum), modified with a quaternary ammonium cation (Fig. 6).

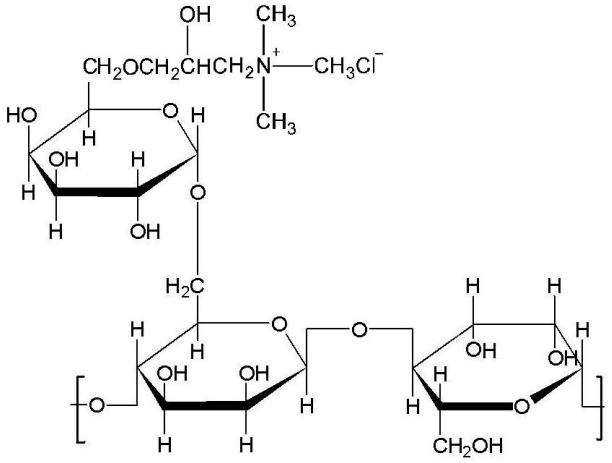

Figure 6. Idealized structure of cationic guar gum, modified with a surfactant, 2-hydroxypropyl-3-N-trimethyl ammonium chloride.

Guar gum and its derivatives are manufactured at industrial scale and have multiple applications in various sectors. Primarily, they are common, highly viscous food hydrocolloids, used as thickeners, binders, stabilizing and emulsifying agents. They are also used as drilling mud ingredients, paper and explosive gel additives, depressants in ore flotation, moisture-retention agents, textile print paste thickeners, etc. Cationic guar has extensive use in cosmetics, where it serves as a viscosity, volume and foam enhancer. Guar gum is used in pharmaceutical formulations and as an excipient with drug release controlling properties (Mathur, 2012).

2.3. Medicinal Use of Guar Gum

Guar gum is a common excipient in pharmaceutical formulations due to its non-toxicity, biodegradability, low cost and useful physicochemical properties. Moreover, it is reported to be therapeutically active (Fig. 7).

As an excipient, guar gum can be applied to control drug release, mainly due to its high viscosity and ability to form gel. To overcome the problem of its swelling, guar gum is usually used in compressed tablets. This dosage form prevents the initial burst release of drugs. Alternatively, various chemical modifications of this biopolymer are introduced (Prabaharan, 2011; Tripathy & Das, 2013). Generally, the aim of controlled release depends strongly on drug characteristics, what brings about multiple strategies of preparing pharmaceutical formulations. The majority of guar gum-based drug formulations is applied in sustained and colon-targeted release systems. As a virtue for the latter, guar gum is prone to enzymatic degradation by microbes in the large

intestine (Prabaharan, 2011). The chemically modified guar gum has been also reported effective in transdermal drug delivery. In such systems, it helps to maintain a constant concentration of a drug being released. (Thakur *et al*., 2009).

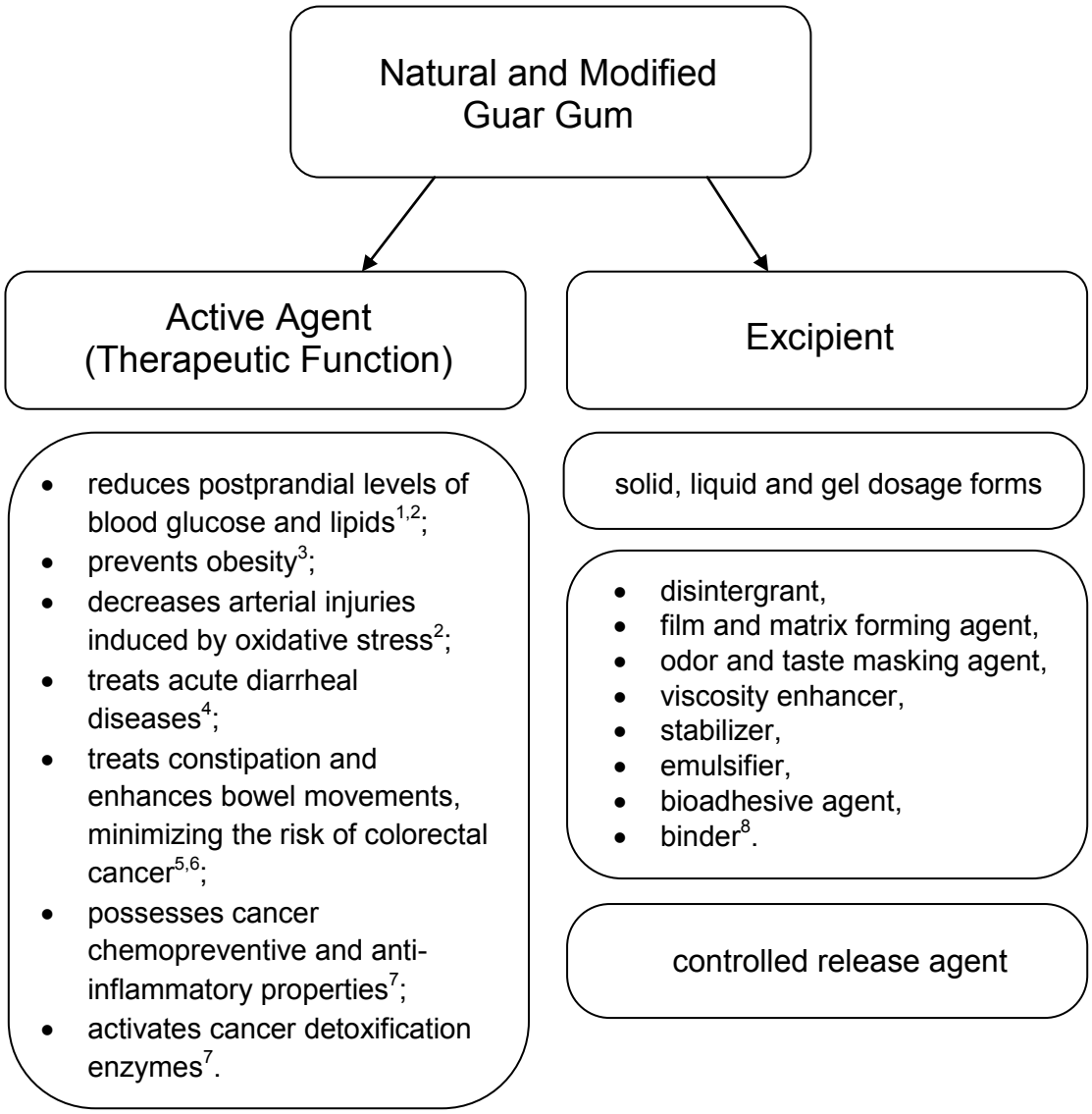

Figure 7. Functions of natural and modified guar gum in pharmaceutical formulations ([1]Takahashi et al., 2009; [2]Kuo et al., 2009; [3]Butt et al., 2007; [4]Alam et al., 2000; [5]Belo et al., 2008; [6]Chaurasia et al., 2006; [7]Gamal-Eldeen et al., 2006; [8]Surendra & Das, 2013).

Native guar gum has been proposed to serve as a cost-effective matrix and a coating in colonic and retarded delivery of various drugs in a pill form, as indicated by numerous *in vitro* and *in vivo* studies (Tripathy & Das, 2013). Basic strategies include layered guar gum compressed matrices (Altaf *et al*., 1998; Krishnaiah *et al*., 2002) and reinforced guar gum tablet coatings (Krishnaiah *et al*., 1998). Some novel strategies

involve preparation of copolymer-matrix tablets, in which guar gum is grafted with various biodegradable polymers. Polyacrylamide-grafted guar gum formulations are suitable for targeted (Sen *et al*., 2010) and sustained drug release (Toti & Aminabhavi, 2003). Recently, systems such as cross-linked microspheres, copolymer microspheres, copolymer micelles, and bigels, based on guar gum are proposed as advanced, colon-targeted (Chourasia & Jain, 2004; Chaurasia *et al*., 2006) and modulative drug releasers (Soppimath *et al*., 2000; Tiwari & Prabaharan, 2012; Singh *et al*., 2014).

3. Nanocomposites

3.1 Composites and Nanocomposites

Composite materials, such as bricks or concrete, have been manufactured since ancient times. Sophisticated composites (e.g. wood, nacre, bones) are broadly found in nature. When constituents with significantly different physical and chemical properties are merged, composite products with new characteristics may be obtained. Nanocomposites are novel, advanced materials that, due to nanometric dimension of one or more components, exhibit superior features to pristine materials or their composites. The uniform definitions of the composite and nanocomposite terms are given by IUPAC (Fig. 8).

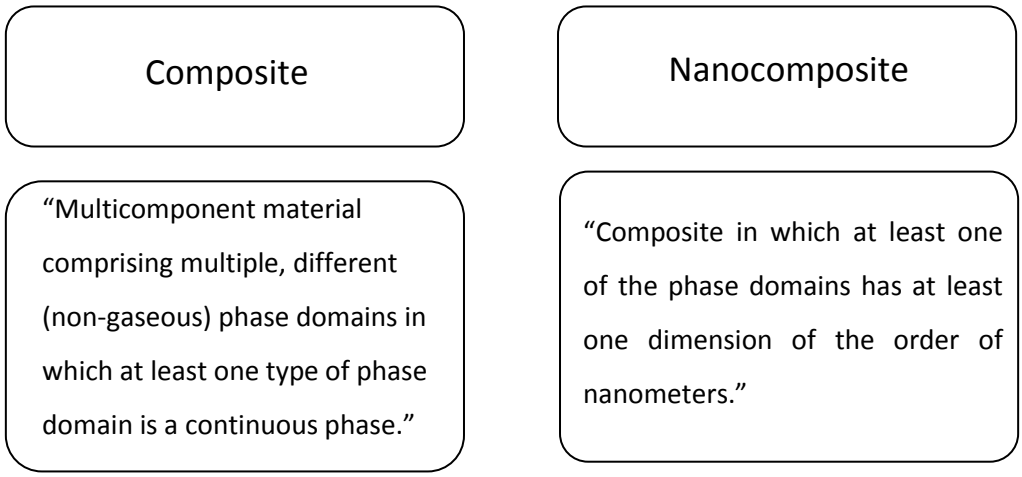

Figure 8. IUPAC definitions of the composite and nanocomposite terms (Alemán et al., 2007).

3.2 Polymer-Clay Nanocomposites - Structure

In polymer-clay nanocomposites, clay layers act a as nanometer-sized phase domain, dispersed in a continuous polymeric matrix. There is no strict regulation regarding the size of a dispersed nanophase, however some authors assume that at

least one dimension should be smaller than 100 nm (Theng, 2012). Polymer is the dominant phase in nanocomposites - the usual content of a clay mineral phase do not exceed several weight percent (Theng, 2012). Such proportion allow a similar processibility as of a pristine polymer, contrary to more ceramic-like materials with higher contents of a clay mineral phase (Okada & Usuki, 2006).

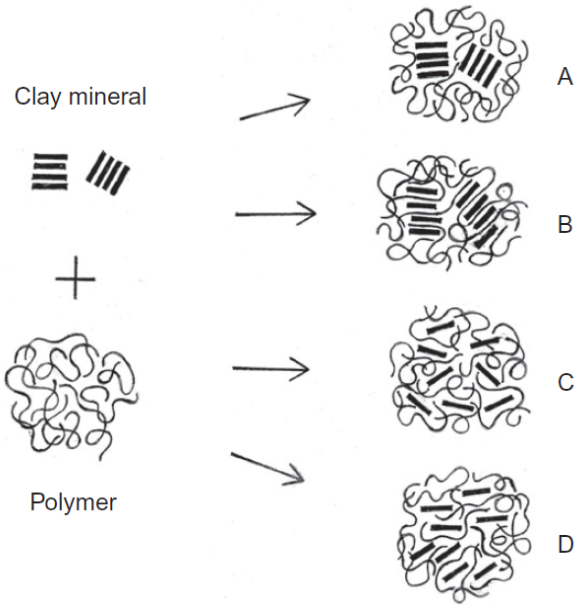

Figure 9. Idealized structures of polymer-clay composites: A – conventional composite with intact clay particles as a filler; B – intercalated nanocomposite; C – exfoliated nanocomposite; D - exfoliated nanocomposite with a long range ordering of clay layers (adapted from Theng, 2012).

When clay mineral particles are simply blended in a polymer matrix, a conventional composite material is obtained, where clay mineral acts as an inorganic filler. Contrary to nanocomposite materials, these microcomposites show little or no improvement of properties and are often prepared to lower the cost of materials (Fig. 9 A) (Okada & Usuki, 2006).

In the case of polymer-clay nanocomposites, two different structures have been identified – intercalated and exfoliated ones. In the first case, polymer chains are present in the interlayer space of a clay mineral, what leads to a noticeable increase of the clay d-spacing. As such, the interaction between individual clay layers is still conserved (Fig. 9B). When single clay layers become more or less homogenously dispersed in the polymeric phase, an exfoliated nanocomposite is obtained

(Fig. 9 C,D). Such nanocomposites are the most desired since the interface between a clay mineral and a polymer is the largest. Due to such enlargement of the reactive surface area of clay mineral, exfoliated nanocomposites generally exhibit superior properties compared to pristine polymers (Theng, 2012; Bergaya *et al*., 2013).

Notably, numerous synthesized nanocomposites exhibit intermediate structures, where intercalated and exfoliated clay mineral morphologies coexist (Theng, 2012; Bergaya *et al*., 2013).

XRD and TEM are two basic tools to determine morphologies of polymer-clay nanocomposites. Intercalated structures can be easily evidenced by an increase in clay mineral interlayer spacing (XRD). Generally, a complete disappearance of (001) basal reflection of a clay mineral is the first indication of exfoliation. However, due to various peak broadening effects (e.g. low clay volume, preferred orientation of clay particles, presence of mixed-layering), the exfoliation phenomenon should be verified by TEM (Theng, 2012).

3.3 Polymer-Clay Nanocomposites - Development

The world's first synthetic plastic, Bakelite, developed more than 100 years ago, was a composite material, as it had to be reinforced with fillers, such as cellulose, due to its brittleness (Baekeland, 1909). Since that time, technologies of reinforcing polymers with inorganic fillers (e.g. talc, $CaCO_3$, carbon black, glass fiber, clay minerals) have been established. Many of such composites, however, exhibit moderate properties in terms of strength, since the interaction between two phases is limited (Okada & Usuki, 2006).

A huge breakthrough came out, when the interface between polymeric matrix and a filler could be strongly enlarged by introducing nanometer-scale, single clay platelets with high surface areas. The first polymer-clay, functional nanocomposite was prepared in 1985 by polymerizing ε-caprolactam in the interlayer space of montmorillonite, yielding a nylon-6-clay nanocomposite (Okada *et al*., 1989). The as-prepared material was introduced in Toyota cars (timing belt covers) in 1989.

This idea originated from previously reported ability of various monomers (e.g. 4-vinyl pyridine, acrylamide, styrene) to be polymerized in smectite's interlayer (Friedlander & Frink, 1964). Such materials were the first examples of intercalated polymer-clay composites (Lambert & Bergaya, 2013). However, only after the invention

of the nylon-6-montmorillonite nanocomposite, with strongly improved mechanical properties, the field of polymer-clay nanocomposites has become intensively researched (Lambert & Bergaya, 2013).

Smectite clay minerals are still the most frequently studied inorganic components of polymer-clay nanocomposites. Nevertheless, a number of kaolinite-polymer and fibrous clay-polymer nanocomposites have been recently developed (Detellier & Letaief, 2013; Ruiz-Hitzky *et al*., 2013).

3.4 Polymer-Clay Nanocomposites – Synthesis

Polymer-clay nanocomposites are diverse materials and their synthesis may involve several processes:

- intercalation from solution,
- intercalation from the melt,
- *in situ* intercalative polymerization,
- *in situ* template synthesis of clay minerals in polymer solutions or gels (Theng, 2012).

Intercalation from solution is often the simplest method of synthesizing polymer-clay nanocomposites. It involves intercalation of polymers soluble in water or, less frequently, in other organic solvents. The preferred clay minerals are the swelling ones, especially Na^+-montmorillonite, however different organoclays may be used to increase compatibility with the polymer. This method is suitable for various non-ionic, cationic and polar polymers. The driving force for their adsorption and intercalation is gain of entropy due to desorption of solvent, which exceeds the loss of the conformational entropy of polymer in the interlayer. In general, intercalated polymers can directly interact with clay siloxane surface by hydrogen bonding, or indirectly, through water molecules that are associated with the interlayer cations (Zeng *et al*., 2005; Theng, 2012).

Intercalation from the melt involves direct blending of organically modified clays (e.g alkylammonium-exchanged smectites) with polymers that are in a molten state. Nanocomposites are processed using twin-screw extruders or twin-roll mills. During the synthesis, a shearing force is applied and organoclay particles break up into stacks and layers leading to exfoliation in a polymer matrix. Intercalation of polymer takes place due to negative enthalpy of mixing and increased entropy, when surfactant molecules are substituted by a polymer (Vaia & Giannelis, 1997; Theng, 2012).

In situ polymerization includes all the methods where various organic monomers are polymerized in the interlayer space of a clay mineral as well as on its external surfaces, yielding a polymer-clay nanocomposite. In some cases, polymerization may occur spontaneously due to interaction of monomers with untreated clay minerals. More often, polymerization is induced by heat treatment, ionizing radiation, chemical initiators, etc. Various modified clay minerals are used in this method – transition metal-exchanged clay minerals and organoclays. *In situ* polymerization is polymer-specific and suitable for poorly soluble polymers (Zeng *et al*., 2005; Theng, 2012).

In situ template synthesis of clay minerals in a polymer matrix is the least common method of polymer-clay nanocomposites preparation. It involves hydrothermal synthesis of a clay mineral (e.g. hectorite) from a gel, where a water-soluble polymer acts as a template (Theng, 2012).

3.5 Polymer-Clay Nanocomposites – Properties and Applications

Generally, polymer-clay nanocomposites exhibit a range of improved properties comparing to conventional composites: mechanical (increased tensile strength and tensile modulus), thermal (increased heat distortion temperatures and flame-retardancy), gas barrier properties, smoothness, paint ability, durability, transparency, and recyclability (Okada & Usuki, 2006; Theng, 2012).

Although polymer-clay nanocomposites have numerous potential applications, few of them have been industrialized and used in commercial products (e.g. nylon-clay, polyolefin-clay or polypropylene-clay nanocomposites in automotive parts, electrical products or food packaging) (Okada & Usuki, 2006). The main, possible applications of polymer-clay nanocomposites include: engineering and structural materials, adhesives, elastomers used for synthetic rubber production, materials with reduced water and gas permeability, packaging materials, optical materials with improved scratch resistance, insulators and conductive materials, fuel cells and many others (Lambert & Bergaya, 2013).

3.6 Biopolymer-Clay Nanocomposites

The first plastic-like materials were manufactured from natural gums, resins, and later from chemically modified natural materials (e.g. natural rubber, nitrocellulose). They were soon replaced with synthetic, petroleum-derived materials. Today, the aspects of biodegradability and sustainable production from renewable resources,

generate again a strong interest in biopolymers. Some of their limitations - improvement of mechanical properties, barrier properties and water sensitivity - seem to be the most challenging issues (Nikolić *et al*., 2012). The broadly researched biopolymer-clay nanocomposites are promising in the field of environmentally friendly plastic materials in various industrial sectors.

Biopolymer-clay nanocomposites are also important for a range of biomedical, pharmaceutical and food industry applications. In these cases, the aspects of biocompatibility, biodegradability in a human body and minimal side effects are the major clinical constraints (Marin *et al*., 2013; Dawson & Oreffo, 2013). In such applications, the design of nanocomposites may differ as: it frequently involves additional components, lower amount of the material is needed or high polymer processibility may be not required.

Multiple biopolymers, mainly polysaccharides and proteins, can react with clay minerals to yield nanocomposites. They are obtained from agro-resources (agro-polymers), extracted from microorganisms and biotechnologically synthesized (biopolyesters) (Averous & Pollet, 2012; Theng, 2012; Lambert & Bergaya, 2013).

Polysaccharides coexist and interact with clay minerals in soil and marine environments (Chenu, 1993; Ueshima & Tazaki, 2001). They become adsorbed and intercalated, driven by electrostatic interactions or a gain in system's entropy (Henao & Mazueau, 2009; Theng, 2012). Most often, polysaccharide-clay nanocomposites are prepared using sugars derived from: plants (e.g. starch, pectin, cellulose, gums), animal products (e.g. chitosan) and microorganisms (e.g. alginate, scleroglucan) (Averous & Pollet, 2012; Lambert & Bergaya, 2013).

Proteins are biopolymer molecules with diverse level of structural complexity. Their structural aspects, shape and pH-dependent charge determine the complex way of interaction with clay minerals. Proteins become adsorbed through entropic (hydrophobic, conformational) and enthalpic (electrostatic, van der Waals) interactions (Theng, 2012). They can be also intercalated in smectite clay minerals (Ensminger & Gieseking, 1941; Talibudeen, 1955; Bae *et al*., 2009). The proteins, most commonly used for preparation of biopolymer-clay nanocomposites are: plant (zein and soy protein, gluten) and animal proteins (casein, whey protein, collagen, gelatin, silk fibroin) (Averous & Pollet, 2012; Lambert & Bergaya, 2013).

Moreover, nanocomposites may be synthesized using biopolymers extracted from microorganisms, such as polyhydroxyalkanoates (produced during bacterial fermentation of sugars and lipids) or synthesized from bio-derived monomers – polylactides, which are both biopolyesters (Averous & Pollet, 2012).

3.7 Medicinal Applications of Biopolymer-Clay Nanocomposites

Biopolymer-clay nanocomposites are a novel class of versatile materials with an expanding range of possible biomedical and pharmaceutical applications. The most intensively researched areas involve drug delivery systems, tissue engineering and regenerative medicine.

Non-toxicity, biocompatibility and biodegradability in human body are the necessary features for such applications. Whereas the term biodegradation is often associated with decomposition initiated and propagated by microorganisms in the environment (Nikolić *et al*., 2012), in a human body it also involves complete elimination of non-toxic degradation products by metabolic processes with limited side effects (Marin *et al*., 2013). Majority of biopolymers are degraded into H_2O and CO_2 in a body by hydrolysis, oxidation and enzymatic reactions and thus are medically suitable (Marin *et al*., 2013). Although clay minerals have been well tested for their non-toxicity in the gastrointestinal tract by multiple bioaccessibility assays (Denys *et al*., 2012), the aspects of biodegradability and cellular response to clay minerals are still in their infancy. However, available studies describe none or minimal loss of cell viability in contact with clay mineral-based materials, at low clay mineral concentration (Gaharwar *et al*., 2010; Dawson & Oreffo, 2013).

Montmorillonite, laponite and sepiolite-based biopolymer nanocomposites are the most frequently researched clay minerals for biomedical applications in the form of dried films and gels, hydrogels, porous scaffolds, and fibrous nanocomposites. Several examples of biodegradable polymers used in these materials include chitin, chitosan, gelatin, cellulose, g-lactic acid, poly(ε-caprolactone, poly(galacturonic acis), various copolymers, etc. (Ruiz-Hitzky *et al*., 2005; Dawson & Oreffo, 2013). Such biopolymer-clay nanocomposites may find numerous potential applications, such as: surgical threads (Zia *et al*., 2011), tissue engineering scaffolds (Depan *et al*., 2009; Ambre *et al*., 2010), wound-dressing (Zheng *et al*., 2002), photodynamic therapy (Perotti *et al*., 2010), etc.

As previously discussed, both clay minerals and biopolymers can act as active agents and excipients in pharmaceutical formulations. Hybrids of these two,

biopolymer-clay nanocomposites may exhibit improved and new properties in modified drug delivery systems (MDDS). By addition of clay minerals, mechanical properties, swelling behavior, a film forming ability, rheological properties, bioadhesion and cellular uptake of biopolymers have been improved. Due to presence of biopolymer, clay mineral dispersions have exhibited increased stability (Viseras *et al*., 2010).

The main functions of MDDS are strongly drug-dependent and involve:

- modulating drug availability (in case of highly soluble drugs),
- improving drug solubility,
- enhancing drug stability in acidic and/or basic media,
- facilitating a controlled rate of drug delivery (i.e. excluding momentary variations in drug concentration),
- facilitating site-specific drug delivery,
- prolonging drug release,
- diminishing gastrointestinal side-effects due to ingestion of some drugs.

Recent examples of the biopolymer-clay nanocomposites were summarized in the table below (Tab. 1). The majority of them are based on natural and organically modified montmorillonite. Additionally, almost all of the systems were designed with the aim of controlled, targeted and prolonged drug release, as indicated by *in vitro* studies. To the best of my knowledge, whereas there are several modified drug delivery systems based on guar gum (e.g. Toti & Aminabhavi, 2003), there is a very limited number of studies concerning guar gum-clay nanocomposites for such applications (e.g. Yang *et al*., 2013).

Authors	Biopolymer	Clay Mineral	Drug	Dosage Form	Properties (*In Vitro* Testing)
Si-Shen *et al*., 2009	poly(lactide)-vitamin E derivative	Na^+-Mtm	anticancer - Docetaxel	nanoparticles	prolonged delivery, enhanced oral bioavailability, possible reduction of side effects
Pongjanyakul & Suksri, 2009	sodium alginate	Mtm/Saponite	Nicotine	films	prolonged buccal delivery
Depan *et al*., 2009	chitosan-g-lactic acid	Na^+-Mtm	Ibuprofen	films, porous scaffolds	very slow release of drug
Cojocariu *et al*., 2012	chitosan crosslinked with glutaraldehyde	Organo-Mtm	Paracetamol, Theophylline	hydrogel beads	controllable release by increasing amount of clay, burst release slightly improved
Wang *et al*., 2009	chitosan-g-poly(acrylic acid), alginate	Palygorskite	Diclofenac Sodium	hydrogel beads	pH-sensitive and controlled release
Abdeen *et al*., 2013	triphenyl-chloro acetylated chitosan phoshonium salt	Na^+-Mtm	Ibuprofen	-	sustained-release carrier, pH-sensitive
Yang *et al*., 2013	guar gum-g-poly(acrylic acid), alginate	Palygorskite	Diclofenac Sodium	hydrogel beads	eliminated burst release effect, decrease of cumulative drug release with increasing palygorskite content
Liu *et al*., 2013	quaternized carboxymethyl chitosan, alginate	Organo-Mtm	Bovine Serum Albumin	hydrogel beads (microspheres)	increased encapsulation efficiency due to clay, controlled release
Campbell *et al*., 2010	poly-ε-caprolactone	Organo-Mtm, Organofluoromica	Ibuprofen	compressed discs	adjustable mechanical properties, retarded release
Jain & Datta, 2014	poly(lactic-co-glycolic acid)	Mtm	antidepressant Venlafaxine	-	controlled release (minimizing drug administration frequency and side effects)
Mahdavinia *et al*., 2015	hydroxypropyl methylcellulose-g-poly(acrylamide)	Laponite, magnetic particles	Diclofenac Sodium	hydrogel	pH-responsive and magnetic-field controlled release
Wang *et al*., 2014	2-hydroxypropyltrimethyl ammonium chloride chitosan	Halloysite, magnetic particles	antibacterial drug Ofloxacin -	microspheres	promising systems for magnetically driven targeted delivery
Namazi & Belali, 2015	starch-g-lactic acid	Mtm	antidepressant - Fluoxetine	films	sustained release at pH 10 due to clay mineral incorporation
Rao *et al*., 2014	sodium hyaluronate/poly(hydroxyethyl methacrylate)	Halloysite	anticancer drug - 5-Fluoroacil	hydrogel films	pH-sensitive and controlled release, potential system for colonic delivery
Lal & Datta, 2015	poly(lactic-co-glycolic acid)	Mtm	hypertensive drug - Atenolol	-	prolonged gastric residence for poorly available drug, possible reduction of side effect due to lower doses

Table 1. Examples of recent biopolymer-clay nanocomposite systems with a potential application in drug delivery (mtm- montmorillonite).

4. Principal Techniques of Characterization

4.1. X-ray diffraction

X-ray diffraction is a principal technique in identification and characterization of clay minerals, due to their characteristic interlayer spacing values. XRD diffractograms may provide information on structure, hydration state, polytypes, stacking faults, presence of mixed-layer clays or clay crystallinity. A great deal of research is given to quantitative XRD analyses (Moore & Reynolds, 1997; Środoń, 2013). Undoubtedly, X-ray diffraction is an irreplaceable tool to study clay intercalation processes and novel materials such as clay nanocomposites.

X-rays are electromagnetic waves with lengths between 10 – 10^{-3} nm and energies of 100 eV to 10 MeV. A continuous beam of X-rays is produced upon application of high voltage between two electrodes. The electrons released from a cathode lose their energy when colliding with an anode target, and X-rays of different wavelengths are generated. Some of these electrons are able to excite atoms in the anode material, and upon their relaxation, characteristic X-rays are emitted. These characteristic X-rays have a discrete energy values related to the anode metal and a shell from which the electrons were ejected (Waseda *et al*., 2011).

When an incident X-ray beam enters a crystalline material with a periodic arrangement of atoms, it becomes diffracted. There is a certain condition for diffraction to occur, which is described by Bragg law:

$$2d \sin \theta = n \lambda,$$

where d corresponds to an interplanar spacing between adjacent atomic planes (d-spacing), θ is an X-ray incidence angle with respect to a normal plane, λ is X-ray wavelength and n is reflection's order, which corresponds to a difference in a number of wavelengths between neighboring crystal planes (Fig. 10). (Pansu & Gautheyrou, 2006; Waseda *et al*., 2011).

A typical XRD diffractometer is an instrument that consists of an X-ray source, a sample holder and an X-ray detector. Usually, X-rays are generated in an X-ray tube and they pass through a monochromator to filter the chosen, characteristic wavelength. The filtered beam enters the sample, which is scanned with the beam at a varied 2θ angle of incidence, which typically ranges from 2 to 90°. After interacting with the sample, a set of scattered beams is detected and recorded as a function of diffraction

2θ angles and corresponding intensities. Usually, such a set is unique for each crystalline substance and enables their identification (He, 2009; Waseda *et al*., 2011).

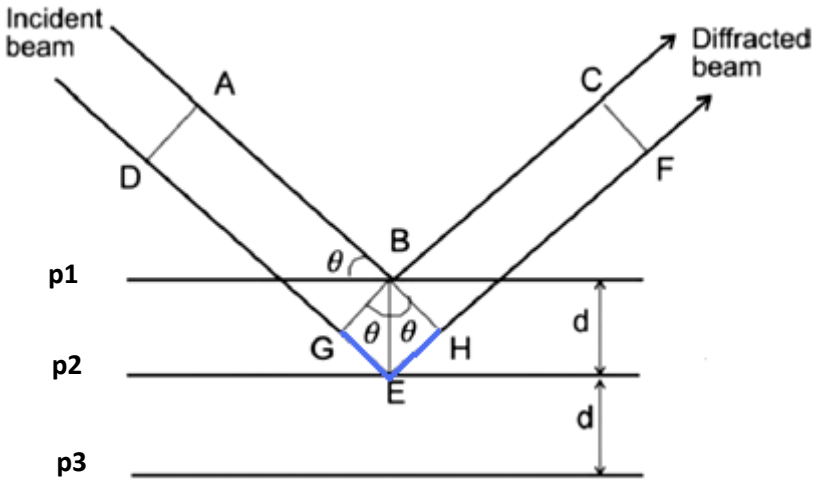

Figure 10. Schematic representation of a diffraction phenomenon by a crystalline substance. The incident beam of X-rays strikes the parallel and reticular crystal planes p that are separated by a constant distance d. The X-ray beam is reflected in the incidental angle θ. The beam will be diffracted if all the rays reflected by the planes p1, p2, p3 are in phase. According to Bragg Law, this only takes place if the path difference (blue line) between radiations ABC and DEF is equal to a whole number of wavelengths (adapted from Pansu & Gautheyrou, 2006).

There are two major techniques used in preparation of clay samples – random powders and oriented aggregates. The first one produces an hkl series of reflections, as randomly oriented crystals in powder represent all possible orientations of crystal planes. In this manner, a complete diffractogram is obtained upon scanning a sample as there are always some crystals in position to diffract an X-ray beam. The second technique involves sedimentation of clay suspension onto a glass slide. As such, clay layers are aligned parallel to the diffractometer plane and a set of intensified 00l reflections can be obtained. The resultant diffractograms are free of other hk reflections and allow a more precise determination of a clay interlayer spacing (Moore & Reynolds, 1997; Środoń, 2013). This is especially vital in a study of clay intercalation complexes, where increase of a basal spacing is monitored by changes in the 001 plane reflection's position or its total disappearance (exfoliation). In a complete approach, oriented preparations are analyzed in four states: air-dried, ethylene glycol-saturated and heated to 300°C and 550°C, what assures proper identification of clays (Środoń, 2013).

4.2. X-ray Fluorescence Spectrometry

X-ray Fluorescence Spectrometry (XRF) is a common, established technique for the chemical analysis of geological samples. Although it has less accuracy than Inductively Coupled Plasma Mass Spectrometry (ICP-MS), it can be applied in quantification of major, minor and even trace elements with a satisfactory accuracy (Anzelmo & Lindsay, 1987).

X-rays are produced upon irradiating atoms with high energy sources. If the energy is high enough, an inner shell electron can be ejected, leaving an atom in an unstable, ionized state. This resultant excess energy can be dissipated in several ways. One possibility is emission of a characteristic X-ray photon, when an electron from a higher shell fills the vacancy created by the ejected photon (fluorescence) (Fig. 11). Only certain transitions from outer shells are allowed. The term characteristic denotes that as-produced photons have fixed energy values specific for particular transitions and elements. By determining energies of these X-ray photons, elements constituting the sample can be identified. This process is principal for XRF. Additionally, Auger electrons can be emitted from the sample, leading to production of UV and visible light emissions. Energy is also dissipated in the form of heat. Additionally, the X-rays, that were used to irradiate the sample, lose their energy when upon striking the sample. As a result a continuous X-ray spectrum is produced (Anzelmo & Lindsay, 1987; Jenkins, 1999).

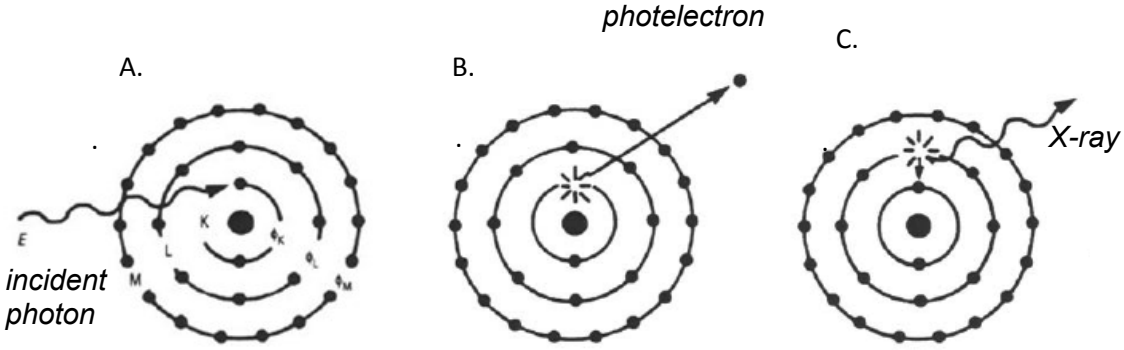

Figure 11. Schematic representation of X-ray fluorescence phenomenon: A – photo-electric ionization, B – emission of photoelectron, C – relaxation by emission of characteristic, fluorescent X-ray (adapted from Jenkins, 1999).

The goal of the XRF experiment is to measure energy and intensity of the emitted, characteristic X-rays. The resultant spectrum contains sets of characteristic lines from all detectable elements, which are superimposed above the background induced by other processes.

A typical XRF spectrometer consists of three main components: a source of X-rays, a dispersion system that separates the X-rays produced by the sample, a detector and an intensity measuring system. There are two main types of XRF spectrometers that differ in construction of dispersion systems: energy-dispersive spectrometers (EDXRF) and wavelength-dispersive spectrometers (WDXRF). The first are equipped with solid-state detectors that measure all excited lines simultaneously and the results are stored in multichannel memory. The latter produces spectra of wavelengths versus intensity. Wavelengths are spatially dispersed by a Bragg diffraction crystal and, at the same time, photons are counted by an appropriate counter for intensity data (Anzelmo & Lindsay, 1987; Jenkins, 1999).

The accuracy of the method depends mostly on the particular instrument design. There is a wide range of XRF instruments, including portable ones. The main advantages of XRF are: fast and simultaneous multielemental analysis, ability to analyze almost all the elements qualitatively and quantitatively, and non-destructivity, in most cases (Jenkins, 1999).

4.3. Nuclear Magnetic Resonance Spectroscopy

Nuclear Magnetic Resonance (NMR) Spectroscopy is a unique tool in investigation of local environments of atoms in molecules and crystals. Depending on a physical state of samples, liquid- and solid-state NMR can be distinguished.

Solid state NMR provides detailed information on atomic structures of solids. Furthermore, it is able to monitor some dynamical processes occurring in these materials, such as phase transitions. Contrary to X-ray diffraction, NMR handles even the most disordered samples (MacKenzie & Smith, 2002). This technique is commonly applied to clay minerals in order to study their structure and to monitor different processes of clay modification, including syntheses of hybrid organoclay materials.

Usually, most nuclei have even mass number and even charge and because of that they have zero spin. For the others, a non-zero spin is due to physical spinning of a nucleus. These ones are useful for an NMR experiment. Upon placing such a nucleus in a strong magnetic field, splitting of energy levels between different spin states occurs. As a result of these energy transitions, absorption or emission of a photon in radiofrequency takes place. Nuclei with different structural environments will absorb photons at slightly different frequencies, what enables identification of varied local atomic structures (MacKenzie & Smith, 2002). The measured resonance frequencies are usually reported with respect to standard compounds as chemical shifts [ppm].

A typical NMR experiment involves three stages (Fig. 12). In the first step, a nuclear spin system is placed in an external magnetic field. Subsequently, a pulse of radiofrequency is applied upon the system, causing its perturbation and splitting of energy levels between different spin states. In the last stage, when the system returns to its initial state, a signal which contains frequency information is detected. This signal, induced by transverse magnetization, is expressed as a function of time (free induction decay FID) and frequency information is extracted from it mathematically by Fourier Transformation (MacKenzie & Smith, 2002).

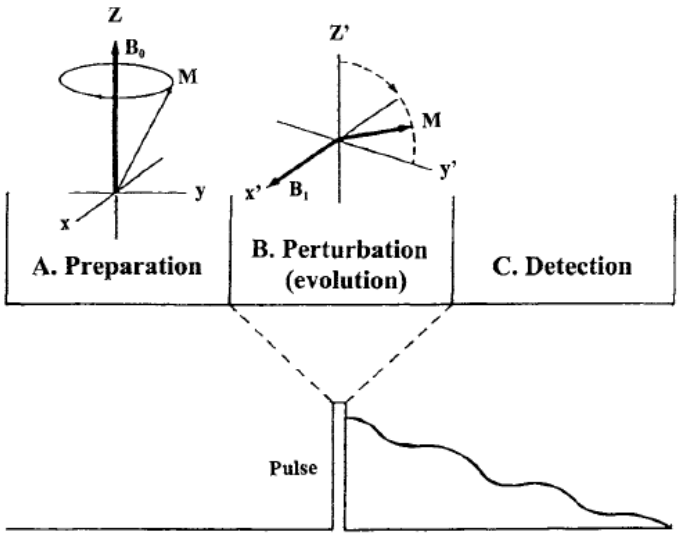

Figure 12. NMR experimental stages. In the preparation stage, external magnetic field B_0 is applied. In the perturbation stage, net magnetization of a sample becomes oriented perpendicularly to B_0.. Subsequently, the precessing spin system induces voltage in the coil which is detected as a signal (adapted from MacKenzie & Smith, 2002).

Unlike liquid-state NMR, a solid state experiment produces less resolved spectra. There are a number of interactions involving nuclei that cause spectra to broaden. They are connected with the chemical shift anisotropy caused by crystal orientation in the external magnetic field, dipolar interactions between magnetic moments of neighboring nuclei, J-coupling between bonded spins, paramagnetic interactions, quadrupolar interactions and structural anisotropies of electronic shielding. To overcome these effects, some special NMR techniques were developed. Most of the interactions can be significantly reduced by spinning a sample around an axis inclined at 54,44° with respect to the external magnetic field (magic angle spinning – MAS). The MAS technique helps to cancel out the anisotropy of first-order interactions (chemical shift anisotropy, spin dipolar interactions, J-coupling, first-order quadrupolar interactions) (MacKenzie & Smith, 2002; Sanz & Massiot, 2013).

To further remove interactions between dipole moments of two different nuclei, decoupling techniques can be applied. Most often, heteronuclear broadening due to ^{1}H is cancelled out by decoupling. In case of less abundant nuclei, such as ^{13}C, it is common to use a cross-polarization technique (CP). In this experiment, magnetization is transferred from a more abundant nucleus, typically ^{1}H, to the scarcer one. Magnetization level is then determined by protons and signal to noise ratio can be improved by collecting more scans per specific time. In the case of second-order quadrupolar interactions, higher external magnetic fields are required to minimize them. Another solution to this problem can be two-dimensional NMR that allows separation of second-order quadrupolar interactions (MacKenzie & Smith, 2002; Sanz & Massiot, 2013).

In clay science, NMR can provide data about a local atomic structure such as structural networks, crystallographic sites, structural distortions and distribution of cations (Sanz & Massiot, 2013). NMR helps to study the structural effects of thermal and chemical modification of clays. Moreover, it plays an important role in the study of clay interaction with organic molecules. They include clay-organic interactions in soils, clay intercalation complexes, including grafting and pillaring processes and clay-polymer nanocomposites (Baldock *et al*., 1992; Aznar & Ruiz-Hitzky, 1988; Fafard & Detellier, 2015). ^{13}C and ^{29}Si are the most frequently used nuclei in such studies.

4.4. Thermogravimetric Analysis

Thermal analysis include all the methods in which specific properties of samples are studied as a function of temperature (Fig. 13). One of them, Thermogravimetic Analysis (TGA) is a technique that measures a change of sample's mass on controlled heating (Heal, 2002). TGA is a very useful technique in clay mineral studies. Most of the materials, including clays, display unique behavior when exposed to heat. This allows not only their identification but also a detailed characterization of transformations induced on heating (Haines, 2002). As such, TGA complements identification and characterization of clays, including hybrid clay materials.

In a TGA experiment, the studied property is sample's mass. The goal of the experiment is to determine any steps of weight loss and corresponding temperatures. Typically, mass change is followed when the sample is heated from room temperature to 1000 °C. The heating rate is usually kept constant during the experiment. The sample is kept in a furnace. Both furnace's and sample's temperatures are precisely monitored. Simultaneously, mass of the sample is being continuously determined by

a balance. As a result, mass or mass percent as a function of temperature is plotted (Heal, 2002; Wunderlich, 2005).

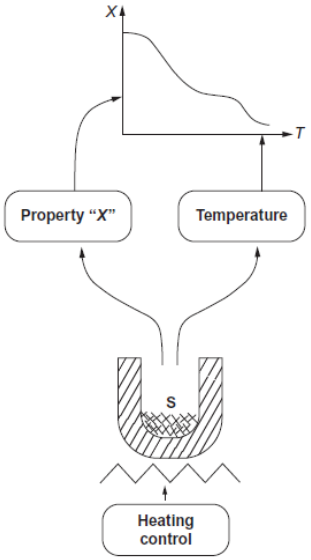

Figure 13. General principle of thermal analyses (adapted from Rouquerol et al., 2013).

Derivative Thermogravimetric Analysis (DTG) is an alternative way of presenting TGA results. A TGA experimental curve is mathematically transformed into its derivative with respect to time. As a result, instead of mass percent, the rate of mass change is plotted as a function of temperature. In this way, the points of inflection in the TGA curve become more pronounced as maxima in DTG curve, what allows more detailed description of occurring thermal events and improves resolution. Additionally, positions of DTG peaks can help to determine temperatures at which reactions are the fastest. Thus, they can serve as characteristic features in identification of substances (Brown, 1998; Heal, 2002).

In a typical TGA apparatus, a sample is placed in a small, inert crucible, attached to a microbalance. Modern equipment requires a sample of 1 to 100 mg depending on the design. The crucible is placed inside a furnace. The furnace construction should allow heat exchange with the sample with a minimum thermal lag. The sample is usually pyrolised in inert gas such as nitrogen. Another type of experiment involves air or oxygen. In this case, sample may be oxidized or burned, depending on how it reacts with oxygen (Brown, 1998; Heal, 2002).

In TGA, it is highly important is to control the temperature of system. Most often, it is controlled by thermocouples. A thermocouple is made of two metals fused into a junction. Across it, there is a standard electromotive force, which is constant at given

temperature. There are two such thermocouples, where one is held at constant reference temperature controlled electronically. The other one measures the changing temperature of the sample. A second, separate thermocouple system controls the temperature of the furnace. Control unit produces output data expressed in μV, which is processed digitally to temperature values (Heal, 2002).

TGA is insensitive to processes that take place without a mass change (Rouquerol *et al*., 2013). This is why it is common to use multiple techniques of thermal analyses simultaneously, which aids more complete characterization of studied materials. Other very frequently used conventional techniques (temperature-controlled) are Differential Thermal Analysis (DTA) and Differential Scanning Calorimetry (DSC). In these techniques, samples are heated or cooled alongside the inert reference (Laye, 2002). It is also possible to study composition of gases evolved during a TGA experiment when a thermobalance is coupled to a mass spectrometer (Wunderlich, 2005). Recent advancements give raise to techniques in which heating or cooling rates depend on sample behavior – sample controlled thermal analysis (SCTA). In general, these techniques can improve resolution of overlapping processes and provide better data for kinetic studies (Wunderlich, 2005; Rouquerol *et al*., 2013).

Conventional thermal analysis is frequently applied in clay science. Most importantly, DTA and TGA experiments can be used to identify certain clays since the experimental curves are usually characteristic for each groups of minerals. TGA enables quantitative analysis of dehydroxylation steps of clay minerals. DTA provides information about desorption of surface water, dehydroxylation of clays, phase transformations, crystallization of new phases and reveals endothermic or exothermic nature of processes (Rouquerol *et al*., 2013). Thermal analysis is vital for characterization of various modified clays and hybrid clay-organic materials. It has been successfully applied to study catalytic properties of clays, pillaring processes of clays, thermal stability of clay-polymer nanocomposites, clay suitability for ceramic industry, organic matter content in clayey soils and many more (Leszczynska *et al*., 2007; Plante *et al*., 2009; Gil *et al*., 2011; Letaief & Detellier, 2011).

4.5. Scanning Electron Microscopy

Scanning electron microscopy (SEM) is a unique tool to observe sample topography and compositional differences, developed back in the 1950s. Nowadays, due to many technological improvements, it allows to observe nanometric objects, such as clays, with a 2 nm resolution (Reimer, 1998). In comparison, traditional optical microscopy fails to resolve objects smaller than 0,2 μm, which is restricted by a visible

light wavelength and observation of individual clay crystals is impossible. Although Transmission Electron Microscopy (TEM) allows to obtain even better resolution, SEM is irreplaceable to observe three-dimension-like images of clays (Kogure, 2013). Scanning electron microscopes are usually equipped with X-ray spectrometers to perform chemical microanalyses.

In principal, a magnified image of a sample is formed when sample's surface is scanned with a convergent electron beam. The sample is bombarded with electrons having energy of 5-30 keV. Primary electrons of normal incidence interact with the sample, which emits several types of signals: secondary electrons (SE), backscattered electrons (BSE), characteristic and continuous X-rays, Auger electrons and cathodoluminescence, which can be recognized and counted by appropriate detectors (Fig. 14). Most of the energy of primary electrons is, however, dissipated in the form of heat. The first two are the key emissions in the image formation. Characteristic X-rays are used for qualitative and quantitative elemental analyses (Reimer, 1998; Reed, 2005).

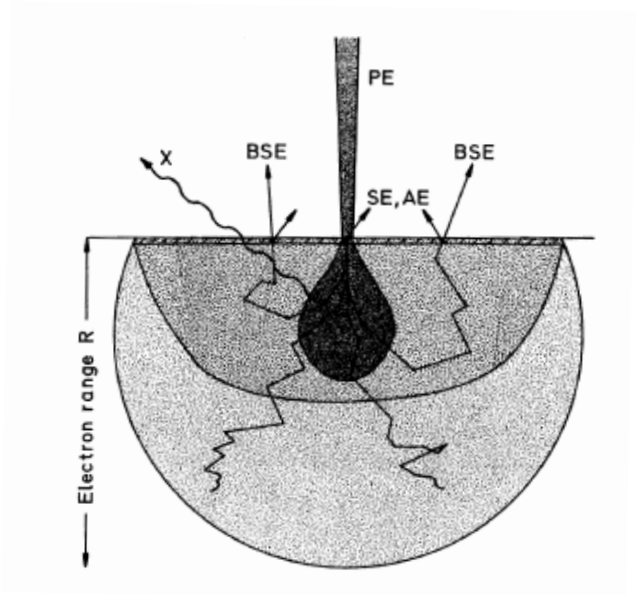

Figure 14. Schematic representation of electron-specimen interactions containing origin and information depth of different phenomena: PE – incident, primary electrons; SE – secondary electrons; BSE – backscattered electrons; AE – Auger electrons; X- X-rays (adapted from Reimer, 1998).

SE allow to obtain high-quality images of surface morphology. They may be produced both by incident electrons when they enter a sample or by BSE when they emerge. SE ejected from the sample possess relatively low energy (a few eV). As such, only the ones produced near the surface (up to several nm deep) are able to escape the sample. The SE yield is proportional to the angle between a specimen's

surface and an electron probe. Typically, the more declined the surface, the brighter it appears in the image, since the electron signal is enhanced at the edges. This phenomenon highlights edges, steps and other discontinuous geometries. SE signal is only slightly composition-dependent (Reed, 2005; Kogure, 2013).

BSE are the primary beam electrons that were scattered inelastically or elastically by the atoms from the sample's surface. They reveal compositional variations of a sample as the fraction of BSE is strongly dependent on atomic number of elements. As such, brightness of BSE images is a function of the average atomic number of the surface's pixel scanned at time. To eliminate topographic effect, the samples should be polished. Because BSE travel longer distances in the sample before emerging, the spatial resolution is worse than for SE (Reed, 2005; Kogure 2013).

A typical scanning electron microscope consists of a source of electrons, a set of electron lenses that focus the beam on the sample, beam-deflection coils, suitable electron detectors and an image-display system. It has a vacuum system and a specimen stage (Reed, 2005). Different parameters govern the quality and resolution of SEM images. The latter is closely related to the probe size (electron beam diameter). The smaller probe size diameter, the better. Recently, the introduction of field emission electron guns, has led to a significant improvement of images resolution (high-resolution SEM imaging). Additionally, corrections of spherical and chromatic aberrations of an objective lens in the microscope upgrade the images (Kogure, 2013).

SEM microscopes can be equipped with X-ray spectrometers to perform chemical analysis in micro-regions. Most commonly these are energy-dispersive spectrometers (EDS) that record emitted X-rays of all energies at the same time. Characteristic X-rays provide compositional information as their energy varies with element's atomic number. In a detector's output, X-ray photon energy is plotted as a function of intensity (Reed, 2005; Kogure 2013). Quantitative chemical micro-analysis can reach relative precision of about 2%. The EDS detection limit for an element is about 0,1 % and the minimum area that can be analyzed is around 2 μm in diameter (Friel, 2003).

4.6. UV-Vis Spectroscopy

Spectroscopy in the ultraviolet (190 – 400 nm) and visible (400 – 780 nm) regions of the light spectrum (UV-Vis spectroscopy) is a technique that enables observation of electrons in excited states. Compared with other spectroscopic techniques, UV-Vis spectroscopy is more precise and reproducible in quantitative analysis. However, it is less efficient in molecular structure elucidations and identification of substances.

As such, it is a powerful tool to determine concentrations of various solutes. Very often, UV-Vis spectroscopy is applied to quantification of pharmaceuticals. Recently, it was used to study metal complexes, semiconductors and metal nanoparticles (Gauglitz, 2001; Sablinskas *et al*., 2014).

UV-Vis spectrophotometry is a more specific term that denotes measurement of transmitted or reflected light's beam intensity as a function of its wavelength (Raty *et al*., 2004).

Electrons become excited when they interact with electromagnetic radiation of a frequency that matches the difference between two electronic states. This energy difference depends both on the molecule's electronic structure and its environment. The electronic transition takes place from the highest occupied molecular orbital to the lowest unoccupied molecular orbital. This phenomenon is called absorption (Gauglitz, 2001). When radiation enters the medium, it may be partially reflected, scattered and absorbed. The remaining part of the light is transmitted (Fig. 15) (Steiner, 2014).

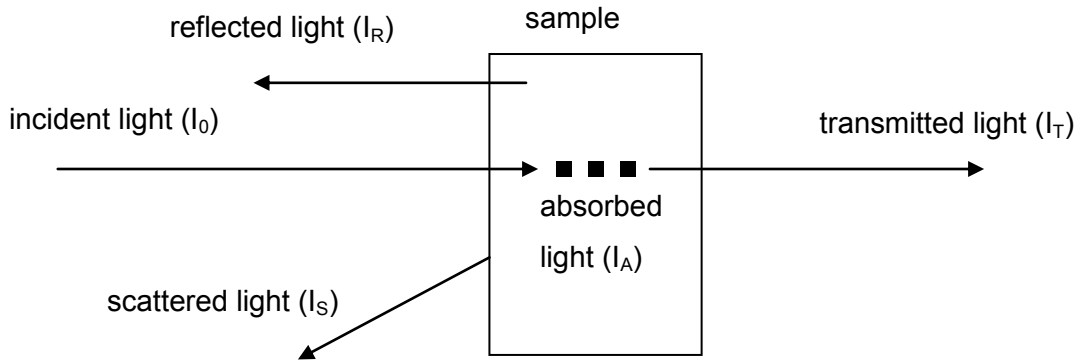

Figure 15. Interaction of incident light with a sample (adapted from Steiner, 2014).

There is a relationship between absorption and scattering and amount of particles that absorb this radiation. It is expressed by the Beer-Lambert Law:

$$I = I_0 e^{-\alpha(\lambda)d}$$

where I_0 is the intensity of the incident beam, α is the absorption coefficient, λ is the radiation wavelength of the light and d is the thickness of a liquid sample (Raty *et al*., 2004). The assumption is made that the radiation is monochromatic and perpendicular to the sample. Additionally, there should be no chemical change of the molecule during the measurement or it should not interact with the solvent. Usually, Beer-Lambert Law

is expressed as a proportional relationship between absorbance and molar concentration of solutions:

$$A = \varepsilon(\lambda) \cdot c \cdot d$$

where A is internal absorbance [-], ε(λ) is the molar absorption coefficient [$L/mol^{-1} \cdot cm^{-1}$], c is concentration [mol/L] and d is sample thickness [cm] (Gauglitz, 2001). Absorbance represents logarithmic attenuation of light in a sample and can be expressed as transmittance T, according to the relationship:

$$A = \log_{10}(1/T)$$

(Raty *et al*., 2004).

Spectrometers that measure transmission of light through absorbing media are based on Beer-Lambert Law. Transmission is the most common mode of spectroscopic measurements. The simplest UV-Vis spectrometers are single-beam instruments that consist of a polychromatic light source, a monochromator, a sample chamber and a detector. In these devices, spectra of background and sample are measured subsequently. The spectra can be also obtained using more sophisticated dual beam dispersive scanning devices or dispersive multichannel instruments. In a typical optical layout of the former, there is a light source, a monochromator, a chopper, sample and reference compartments and a detector (Fig. 16). The chopper is a rotating mirror that generates sample and reference beams and recombines them. The multichannel instruments have a different layout and another optical elements. Additionally, there are double-beam spectrometers that allow a synchronous measurement of a sample and a reference (Steiner, 2014).

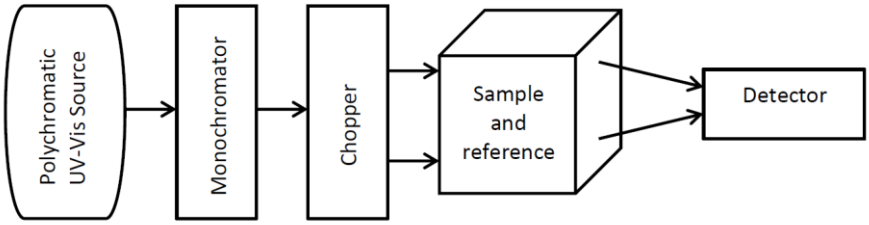

Figure 16. Block diagram of UV-Vis scanning spectrometer (adapted from Steiner, 2014).

Usually, the used light sources are separate for the UV and the visible region. These can be deuterium lamps (180 – 350 nm), tungsten filament and halogen lamps (330 – 900 nm). There are also various solutions for monochromators, among which filter ones are the cheapest. These optical elements have a prism or a diffraction

grating that turns, allowing the measurement of complete spectra. Along with the slit, dispersion of the monochromator determines beam resolution. Typically used detectors are silicon diodes or photomultipliers (Steiner, 2014; Gauglitz, 2001)

Part II: Characterization of Portuguese Clay – Benavila Bentonite

1. Aims

The main goal of this part of the thesis was to characterize Benavila bentonite ore and choose the sample that would be most suitable for a nanocomposite's synthesis.

The well-established utility of clay minerals to interact with various polymers and biopolymers is often limited to commercial clay products and clay minerals supplied from the Source Clay Repository. As mineral resources are highly diverse, exploring less recognized clay minerals is a substantial insight into clay mineral-polymer interactions.

2. Materials and Methods

2.1 Geography and Sampling Sites

Six bentonite samples were collected in the central-east part of Portugal, close to Benavila town, which belongs to Portalegre district and Avis municipality (Fig. 17). Typically, approximately 5 kg of each sample was placed in a plastic bag and stored for a further treatment. Due to low accessibility of the land (fenced private properties), all the sampling was done along the public roads. The first three sampling sites (BV1E, BV1W and BV2) are not well recognized, whereas the other three (BV3, BV4, BV5) are more frequently sampled, especially BV3 and BV5, that usually exhibit the highest clay mineral content.

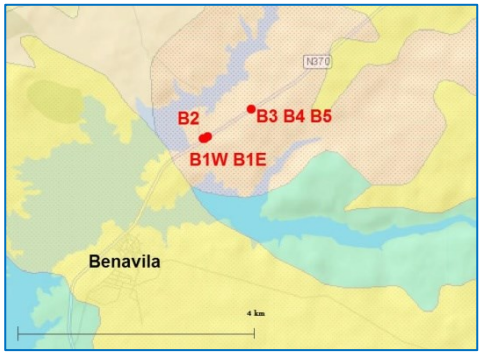

Figure 18. Benavila sampling sites (LNEG portal, 2014).

Figure 17. General view on the Benavila bentonite sampling site (source: Google Maps, retrieved in 2014).

sample symbol	coordinates		altitude [m a.s.l.]
BV1E	-7.8596 W	39.1240 N	150
BV1W	- 7.8594 W	39.1240 N	150
BV2	-7.8589 W	39.1243 N	156
BV3	-7.8522 W	39.1275 N	158
BV4	-7.8522 W	39.1275 N	158
BV5	-7.8522 W	39.1275 N	158

coordinate system WGS84

Table 2. Geographical coordinates of the sampling sites for the six Benavila bentonite samples.

Figure 19. Detailed view on the Benavila sampling sites – BV5, BV4 and BV3 sampling sites significantly differ in color (BV3,BV5 – greenish; BV4 – grayish). The discontinuity in color correlates with a presence of a fault zone - photos by C. Costa, University of Aveiro, 2014.

2.2 Geology

Benavila bentonite, sampled in the Hercynian Massif, is a residual rock that originated from the weathering of Benavila granodiorites (Fig. 20). This alteration product can be dated as a paleogenic deposit (Rebelo et. al, 2010).

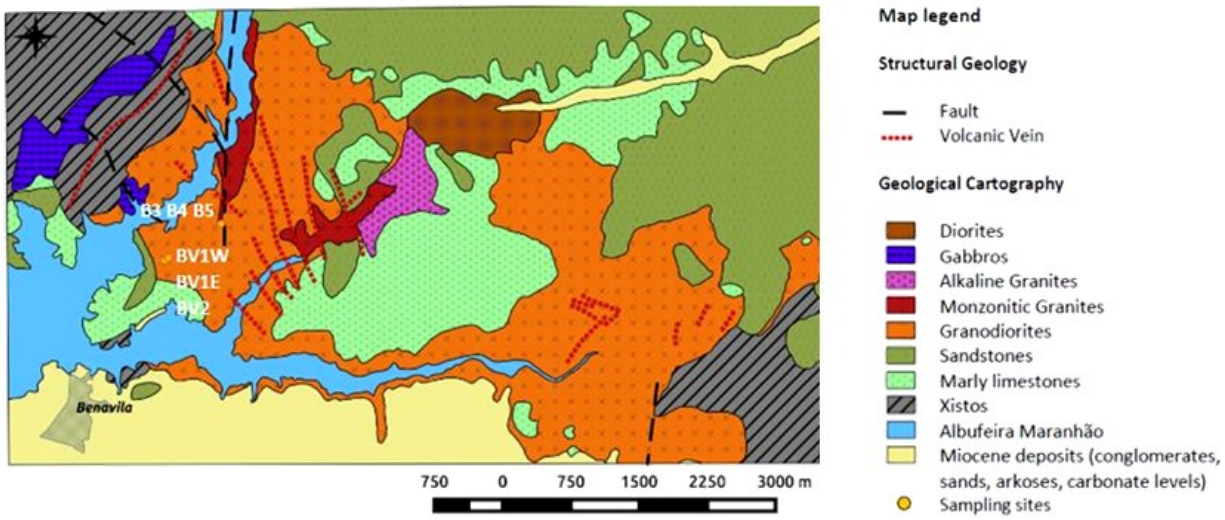

Figure 20. Geological map of the Benavila region with a marked location of Benavila bentonite sampling sites - by João Ribeiro, UA, adapted from Peinador Fernandes, 1964.

Granodiorites are usually intermediate to acid igneous rocks that are rich in quartz (> 20%), plagioclases, and have a minor content of alkali feldspars and mafic minerals, such as biotite and hornblende. They are most often associated with orogenic or island arc magmatism. As an alteration process depends not only on chemistry and mineralogy of the weathered rock, but also on the interacting fluid composition, topography, climate, biological activity, etc., the resulting products of this process vary significantly. In the case of Benavila granodiorites, the altered products consist mainly of Fe-rich smectite and different amounts of typical associated minerals (Dias *et al*., 2004). Because of the respectively high content of smectite, Benavila bentonite is considered as one of the most important clay deposits in Portugal (Dias *et al*., 2004).

2.3 Clay purification

Bentonite samples were purified in order to separate fractions < 63 μm (silt-clay fraction) and < 2 μm (clay fraction).

In the first step, a wet sieving procedure was performed in order to separate the silt-clay fraction (<63 μm) from the bulk bentonite samples. This fraction contains clay minerals and associated minerals. Typically, about 1 kg of each sample was disaggregated in distilled water using a mechanical stirrer. The further separation was

done manually, using a sieve with a mesh size 63 μm and distilled water. The sieving was continued until the screened suspension was clear. The material over 63 μm (sand - gravel fraction) was dried at 50°C and weighted to estimate distribution of fractions in the bulk samples. The fraction <63 μm was dried at 50°C, ground with an agate mortar and stored for further analyses.

Subsequently, sedimentation according to Stokes Law was performed in order to separate the fraction under 2 μm (clay fraction). Stokes Law allows to determine the particles' settling velocity as a function of their size. The time of settling for particles > 2 μm was calculated according to the equation below:

$$t = \frac{18\,\eta h}{g d^2 (\rho_p - \rho_w)}$$

where:

t- settling time [s]; h- height of water column [m] (0.1 or 0.2 m); η – water dynamic viscosity (close to 1 in 20 °C); g- gravitational acceleration (9.81 m/s^2); d – the equivalent spherical diameter ($2*10^{-6}$ m); ρ_p – particle density (for all the particles the assumed density was that of quartz – 2650 kg/m^3); p_w – water density in 20 °C

The calculated settling time for h = 0.2 m and d = $2*10^{-6}$ m was equal to about 14 hours and 50 minutes. Portions of 10 g of ground clay (<63 μm) were suspended in 1L of distilled water. Four drops of antiflocculating agent (1% sodium hexametaphosphate) were added to prevent flocculation. The suspension was sonicated for 1 min and transferred into plastic cylinders. After the proper time, necessary for the particles to settle, the 20 cm of supernatant was collected and dried at 50 °C. The material was ground with an agate mortar and stored for further analyses. A little amount of suspensions of the fraction <2 μm, was used to prepare oriented aggregates for XRD analysis.

2.4 Grain Size Distribution

The grain size distribution of Benavila bentonite samples was estimated on the basis of the wet sieving procedure, which allowed to determine approximate amounts of sand-gravel fraction (>63 μm) and silt-clay fraction (<63 μm), dried at 50 °C. The amount of clay fraction (<2 μm) was determined by an X-ray beam particle size analyzer (Micromeritics® Sedigraph 5100), for the samples BV5, BV4 and BV3 (single measurements).

2.5 X-ray Diffraction

The mineralogical composition of the Benavila bentonite samples (fraction <63 μm) was determined using a Philips/Panalytical X'pert-Pro MPD, with Cu Kα radiation (λ = 1,5405 Å), and a step size of 0,02° 2θ s^{-1}, in the 2θ angle range 4-65°. The randomly oriented powder mounts were prepared by a back-loading method.

The identification of clay minerals was carried out using oriented aggregates. Suspensions of clay fraction <2 μm, were deposited on thin glass slides and air dried. Diffraction patterns were measured with a step size 0,02° in the 2θ angle range 4-20°. Afterwards, diffractograms of the slides, saturated with ethylene glycol (24 h), and heated to 500°C, were recorded in order to differentiate between particular clay minerals.

The mineral phases were identified according to: www.webmineral.com; Brindley & Brown, 1980; Meunier, 2005 and Crystallography Open Database (www.crystallography.net). Semi-quantification of mineralogical composition was performed by a method adapted from Martins *et al*., 2007, and verified using the results of XRF chemical analysis. In this very simple method, estimated quantification is performed on the basis of certain, diagnostic peak areas for each identified mineral which are subsequently divided by corresponding empirical factors (Table 3). The peak areas were calculated using Macdiff and OriginLab 8 Pro software.

	Peak [Å]	Empirical factor
Chosen minerals (random preparations)		
Quartz	3.34	2
Phyllosilicates	4.45	0.1/0.2*
K-feldspars	3.21	1
Plagioclases	3.18	1
Calcite	3.03	1
Anatase	3.52	1
Anhydrite	3.49	1.5
Dolomite	2.88	1
Hematite	2.68	1.3
Pyrite	2,71	1
Siderite	2.79	1
Clays (oriented preparations)		
Illite	10.0 (natural specimen)	0.5
Kaolinite	7.0 (natural specimen)	1
Chlorite	7.0 (specimen heated to 500°C)	1.25
Smectite	17.0 (glycolated specimen)	4

Table 3. Diagnostic peaks and data used in XRD semi-quantification, adapted from Martins et al., 2007 (depending on clay crystallinity).*

2.6. X-ray Fluorescence

The chemical composition was determined by X-ray fluorescence spectroscopy (XRF) using a Philips Panalytical PW1404 X-ray fluorescence wavelength dispersive spectrometer for major, minor and trace elements. Typically, for the analysis, a pressed powder pellet was made out of about 12 g of the sample. The uncertainty of the analysis is not given due to single measurements.

2.7. Bioaccessibility

Bioaccessibility (BA) refers to the maximum amount of certain element available for absorption in the animal or human gastrointestinal tract (Van de Wiele *et al*., 2007). There are many possible methodologies used in determining BA that differ in gastrointestinal fluids composition, digestion conditions and time. In-vitro bioaccessibility was assessed according to the unified BARGE method (BARGE, Unified BARGE Method, 2010) for the two samples BV3 < 2µm and BV5 < 2µm, only in gastric solutions.

Typically, 0,6 g of each dried and ground samples were placed in a plastic tube. The samples were subjected to synthetic gastric fluid prepared according to the unified compositions (BARGE - UBM Procedure, 2010). Such acidic fluid (pH 1.1 +/- 0.1) simulates the stomach conditions and it is composed of: inorganic salts (KCl, NaH_2PO_4, NaCl, $CaCl_2$, NH_4Cl), hydrochloric acid (37%), enzymes (mucine, pepsin, bovine serum albumin), urea, glucose, glucuronic acid and glucosamine hydrochloride. In an experiment, 13.5 mL of the synthetic gastric fluid was added to each sample, pH was adjusted to 1.2 and the tubes were shaken for 10 s by hand. After that, pH was measured and adjusted to 1.2 again, if necessary. The tubes were placed in the end-over-end rotator and then heated to 37°C for 1 hour, to simulate human body temperature. After 1 h, pH was measured again and if it was >1,5 the procedure was repeated. If the pH was <1,5 the tubes were centrifuged for 15 min at 4500*g, the supernatant was collected, acidified with 500 µl of concentrated HNO_3 and the element concentration in these gastric samples was measured by ICP-MS. The same measurements were performed for a blank sample and repeated for one of the samples (BV3 < 2µm).

The bioaccessible fraction (relative bioaccessibility) is expressed as a percentage of the bioaccessible concentration (%BA) of certain element, calculated using the following equation:

$$\%\ BA = \frac{concentration\ of\ the\ bioaccesible\ element\ (ppm)}{total\ concentration\ of\ the\ element\ (ppm)} * 100\%$$

The total concentration of the elements for the BV3 <2μm and BV5 <2μm was measured by XRF. Because of different accuracy of ICP-MS and XRF methods and the fact that uncertainty of the chemical analysis results is not given (due to single measurements), the bioacessibile fraction values should be considered as estimated.

2.8. Effective Cation Exchange Capacity and Exchangeable Cations

Cation exchange capacity (CEC) was determined by an adapted ammonium acetate method (Gomes, 1988 and Meunier, 2005).

Typically, about 5.0 g of a clay sample, dried at 50°C was suspended in a 1M ammonium acetate solution for 24 hours and, thus, saturated with NH_4^+ cations. Measured pH at this point was slightly above 7 for all clay suspensions. Afterwards, the clay sample was separated by filtration using a glass fiber filter paper (Macherey-Nagel MN640d). At this point, 100 mL of the filtrate was collected and analyzed by Atomic Adsorption Spectrometry (University of Aveiro) for quantitative determination of exchangeable cations, using the multi-element GBC 906 Spectrometer or by Inductively Coupled Plasma Mass Spectrometry, using Agilent 7700 X Spectrometer (University of Ottawa). Afterwards, the sample was washed with ethanol (96%) until the excess ammonia was not detected anymore by the Nessler reagent. NH_4^+ exchangeable cations were then quantified by a Kjeldahl-type distillation. Following the procedure, the dry filter residue was placed in a Florence flask with the addition of 2.0 g of MgO and 200 mL of distilled water. Ammonium was collected into an Erlenmayer flask with 50 mL of 4% boric acid and 6 drops of indicator (0,1% bromocresol green) until the total volume of solution reached 150 mL. The amount of ammonia was determined by acid titration (0,1 M HCl) until the solution's color turned from blue to light green/yellow. Effective cation exchange capacity was calculated according to the formula below:

$$\mathbf{CEC\ (meq/100g) = V_{HCl} * 0,1 * 100/m}$$

where m- sample mass [g]; V_{HCl} – volume of 0,1 M HCl [mL].

2.9 Scanning Electron Microscopy

Scanning electron microscopy was performed for three samples: BV5, BV4 and BV3 (fraction <2μm) using a Hitachi SEM S-4100 scanning electron microscope equipped with Bruker Quantax 400 Energy Dispersive Spectrometer (EDS) for point chemical

analyses. The SEM images were acquired with a tungsten filament working at 20 kV and the EDS was performed at 15 kV. The main goal of the analysis was a determination of the smectite types in the samples and a calculation of the smectite average chemical formulas.

2.10. Fourier Transform Infrared Spectroscopy

FTIR transmission spectra were recorded for the fraction <2 μm of the three samples: BV3 BV4, and BV5 using a Bruker Tensor 27 spectrometer, in the 4000 cm^{-1} to 400 cm^{-1} frequency region, with 128 scans and a resolution of 4cm^{-1}. KBr pellets were prepared using 1,5 to 2,0 g of sample and 200 g of KBr. The main objectives of the FTIR measurements were to aid XRD and SEM-EDX techniques in identifying the clay type, to verify octahedral composition, and to reveal any impurities that cannot be evidenced by the means of XRD, e.g. organic matter.

2.11. Mechanical Properties – Plasticity

Plasticity was expressed using the plasticity index. Plasticity index (PI) was determined using the standardized methods based on Attenberg limits - liquid and plastic limit.

Liquid limit (LL) corresponds to the state in which the clay becomes wet and can no longer maintain a given shape (Andrade *et al*., 2010). It was determined by a fall-cone test, according to the standard ISO/TS 17892-6/12 using a 80 g/30° cone. Plastic limit (PL) corresponds to the amount of water which is necessary to make clay plastic (it is possible to form 3 mm-diameter clay rods between the palms of the hands). It was determined according to the Attenberg limits for soils (ISO/TS 17892-12-2004). Both LL and PL are expressed as the water content in clay in weight %. Plasticity index (PI %) was calculated as a difference between LL (%) and PL (%).

3. Results and Discussion

3.1 Grain Size Distribution

Figure 21 presents the estimated grain size distribution of Benavila bentonite bulk samples. The sand-gravel fraction (>63 μm), composed of associated minerals, is dominant in all the samples. Its amount ranges from ~78 % in BV1W to ~37 % in BV3 sample. The amount of silt-clay fraction (>63 μm) was found between ~22 % and ~63 %, respectively. The clay fraction (<2 μm), which mainly contains clay minerals, constitutes several percent (BV2, BV1E and BV1W – the exact amount was not

determined by sedigraph analysis) up to ~31 % (BV3). Thus, it can be concluded that the most suitable samples for synthesis of the nanocomposite are the BV3 and BV5, as they are richest in clay fraction (~31 and ~29 %, respectively). For the remaining samples, separation of the clay fraction would be cumbersome and not economical. In spite of this, the BV3 and BV5 samples were subjected to a more thorough characterization.

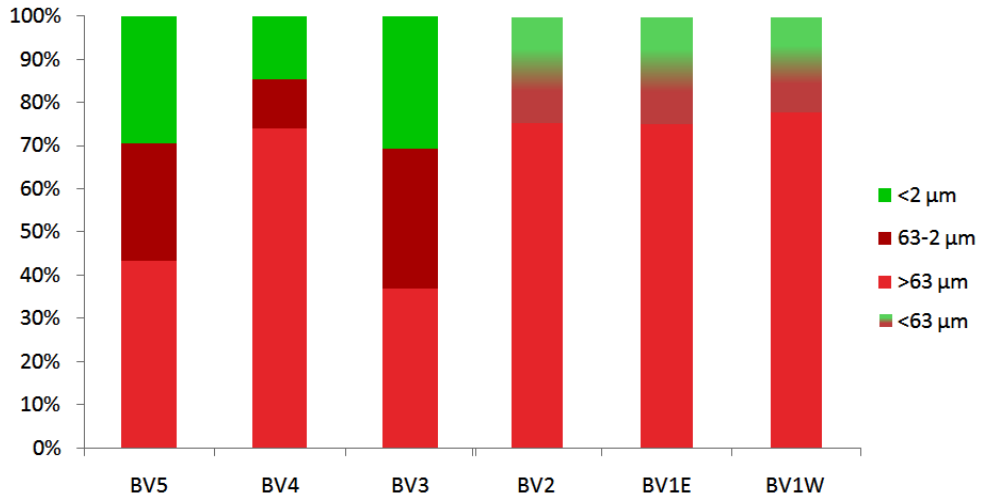

Figure 21. Estimated grain size distribution based on the wet sieving separation procedure and the sedigraph analysis.

When sampling a geological deposit one should take into consideration its homogeneity. Mineral deposits form over long periods of time and are exposed to changing environmental conditions, which makes them inherently heterogeneous. When dealing with deposits, the life cycle of which only begins, it is especially challenging to assess its true geologic properties (Camus, 2002). The Benavila bentonite deposit is industrially unexploited and information about its characteristics is limited to research literature, which is based on rather sparse sample data (e.g. Dias et al., 2004; Santos et al., 2006; Rebelo et. al, 2010). Desirably, the biggest possible amount of material should be sampled, both vertically through the deposit and horizontally along it. The choice of sampling sites, number of samples taken, and the mass of the sample are generally the main factors that determine the accuracy of sampling. In this project, the amount of each sample was limited to ~ 5 kg and the rock was sampled from the exposed, accessible outcrop. Such method of sampling should be efficient to decide about the general character and quality of the deposit, and to observe some major variations within certain parts of the deposit. The homogeneity

within each sample was assured by performing wet sieving, during which substantial amounts of sample (~ 1 to 3 kg) are used.

3.2 Mineralogical Characterization and Semi-Quantification

The mineralogical composition of the six Benavila bentonite samples (silt-clay fraction < 63 µm), along with the estimated quantitative data, are presented in Table 4. XRD analysis revealed that the samples are composed of different amounts of clay minerals and associated minerals. In all the cases, the dominant clay mineral is smectite. The most abundant associated minerals are calcite and primary silicates.

	Mineral (%) (fraction <63 µm)	BV5	BV4	BV3	BV2	BV1E	BV1W
Clay minerals	Total Phyllosilicates	68	69	76	61	72	48
	Smectite	64	66	74	60	71	48
	Chlorite	4	-	3	-	1	<1
	Illite-mica	-	1	-	-	<1	<1
	Kaolinite	-	2	-	1	-	-
	I/S	-	<1	-	<1	<1	<1
Associated minerals	Calcite	**18**	2	**21**	4	9	4
	Dolomite	3	1	<1	1	0	0
	Quartz	1	7	<1	6	4	**10**
	Cristobalite/Opal	4	2	-	-	5	-
	K-feldspars	2	3	1	2	2	7
	Plagioclases	1	**12**	<1	**21**	3	**17**
	Hornblende	1	-	<1	3	2	9
	Muscovite	-	4	-	-	-	-
	Anatase	1	<1	1	1	<1	1
	Fe-ox/hydroxides	<1	1	<1	1	2	3
	Anhydrite	-	<1	-	<1	<1	<1
	Apatite	-	-	-	<1	<1	1

Table 4. Mineralogical composition of the Benavila bentonite samples (fraction <63 µm) and semi-quantification data corrected with respect to their chemical composition (determined by XRF).

The calculated, total amount of phyllosilicates varies from ~48% (BV2) to ~76% (BV3). Apart from smectite, other clay minerals are present in trace amounts: chlorite, illite, kaolinite, and mixed layer illite/smectite.

The carbonate content (calcite and dolomite) is especially high in BV5, BV3 and BV1E samples. The samples that are not rich in carbonates, have a high content of plagioclases and K-feldspars. Plagioclases are especially abundant in the BV4, BV2

and BV1W samples. Quartz content is rather small for all the samples, except for the BV1W (~10%). The other identified minerals, present in smaller amounts, are aluminosilicates: hornblende and muscovite (only in BV4 sample), titanium oxides – anatase, iron oxides/hydroxides and traces of Ca-apatites and anhydrite.

The mineralogical composition of the Benavila samples reflects their geological origin. Granodiorite's weathering products usually contain quartz, plagioclases, clay minerals and other minor phases. As for quartz, the prevalent part of it has been removed with a sand-gravel fraction (> 63 μm).

The samples most abundant in clay minerals were purified. XRD diffractograms of the BV3 and BV5 samples (Fig. 22) present the mineral composition of the samples before and after the extraction of the clay fraction (<2 μm).

It can be clearly seen that the purification procedure was efficient and the purified clay samples contain almost no accessory minerals apart from calcite, which was quite abundant in the silt fraction. BV5 <2 μm may contain traces of anatase. According to semi-quantification results, clay minerals were enriched (>90%) in both samples.

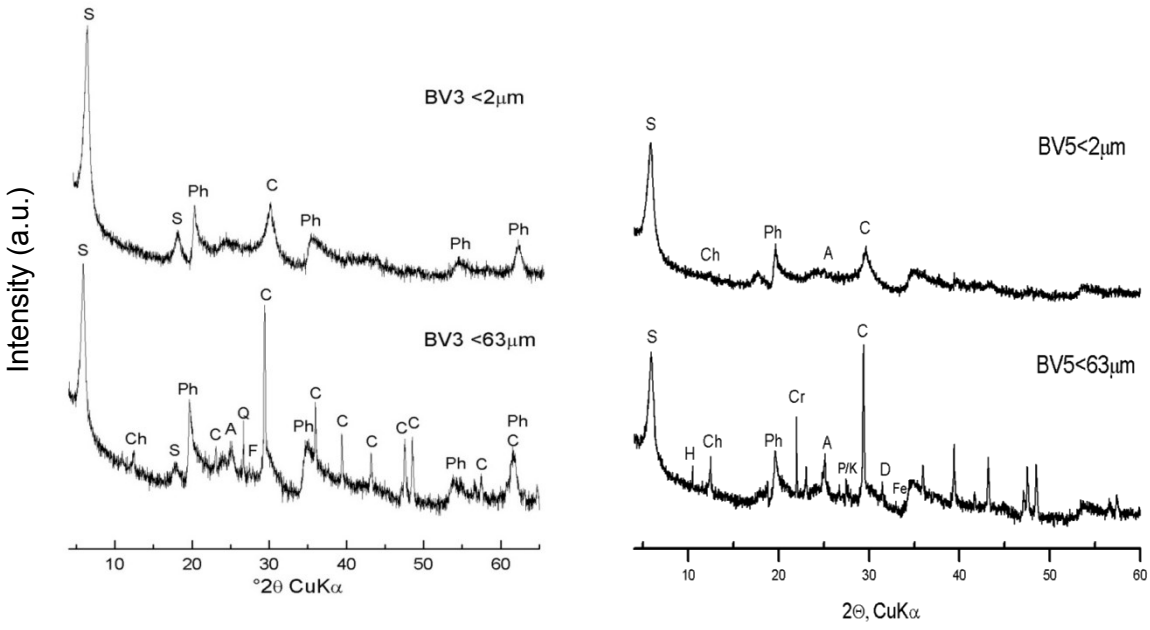

Figure 22. XRD diffractograms of BV3 and BV5 clay samples before and after separation of clay fraction. The symbols correspond to the main identified mineral phases: S – smectite, Ch – chlorite, Ph – phyllosilicates, C – calcite, A – anatase, F – feldspars, Q – quartz, H – hornblende, Cr- cristobalite, P/K – plagioclases and K-feldspars, D- dolomite, Fe- iron (hydro)xides.

3.3 Chemical Composition

Chemical composition of the silt-clay fraction (<63 μm) and clay fraction (<2 μm) was determined by X-ray fluorescence spectroscopy (XRF) (Fig. 23; Fig. 24).

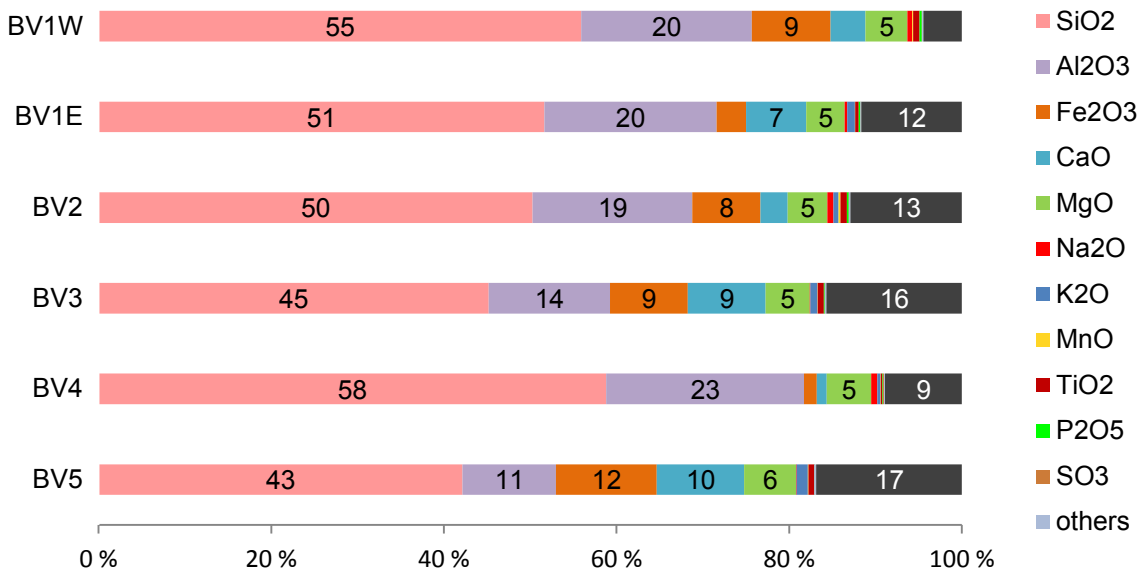

Figure 23. Chemical composition of Benavila bentonite samples (<63 μm) determined by XRF for major elements (LOI – loss on ignition; single measurements).

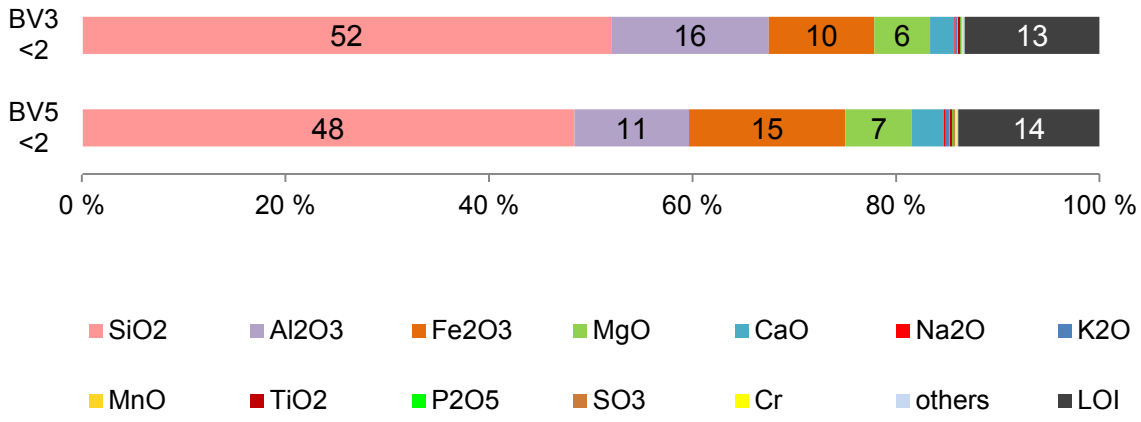

Figure 24. Chemical composition of Benavila bentonite samples (<2 μm) determined by XRF for major elements (LOI – loss on ignition; single measurements).

The chemical composition of the samples, regarding the major elements, is in a good agreement with their mineral composition (Table 4). The most abundant element is silicon (SiO_2 represents ~50% of the bulk compositions). The main mineral phases in the samples are Si-rich phyllosilicates and primary silicates such as quartz, plagioclases, feldspars, amphiboles and muscovite. Their presence also contributes

to high amount of Al as most of them are alumino-silicates. The sample that is the most abundant in these two elements is BV4 with a higher content of plagioclases and quartz.

Another abundant element in the samples is iron. Some part of Fe may be attributed to iron minerals – Fe oxides and hydroxides, and smectite. However, a major amount of Fe, indicated by XRF, cannot be associated with any of the present minerals (Tab. 4). Possibly, Fe-rich phases are present in the sample, that are difficult to identify by XRD. This is due to a peak superimposition (magnetite-maghemite group minerals) or very low crystallinity of iron minerals (such as ferrihydrite). The latter can be supported by the fact that the clay fraction (<2 μm) is slightly enriched in iron with respect to the silt-clay fraction (<63 μm).

The dominant source of calcium is calcite. It is also present in plagioclases, smectite, dolomite and apatite. The samples richest in Ca (BV3 and BV5 <63 μm), contain also the highest amount of calcite. This is also well reflected by the biggest loss on ignition (LOI) for these two samples, since LOI corresponds mainly to water loss and carbonate decomposition.

After separation of the clay fraction (<2 μm), BV5 and BV3 samples were slightly enriched in Si, Al, Fe and Mg and depleted in Ca. This suggests that the main impurity, calcite, was partially removed (Fig. 24).

Like all natural Earth materials, the Benavila bentonite samples have varied elemental composition, as evidenced by XRF analysis (Table 5). The concentrations of minor and trace elements were compared with a typical distribution of elements in major geological units. The concentrations of elements in Table 5, highlighted in light blue, are only slightly above the typical values reported by Turekian *et al.* (1961). The table's fields highlighted in red signify the biggest element concentration among the bulk Benavila samples <63 μm. In conclusion, the BV5 and BV2 samples are richest in most analyzed minor elements, including heavy elements. Among all the minor elements, the content of chromium is relatively high. Cr abundance is linked with the sample origin (alteration of magmatic rocks – granodiorites, containing Cr-bearing minerals) (Oze *et al*., 2006).

The content of minor elements in the clay fractions (BV3 and BV5 <2 μm) is comparable with their concentration in bulk samples. Only Ni and Rb exhibit significantly higher abundances. Cr content is not reduced, which suggests that Cr may be associated with clay minerals and iron minerals (Oze *et al*., 2006).

(ppm)	BV5	BV4	BV3	BV2	BV1E	BV1W	BV5 <2µm	BV3 <2µm
As	35	19	29	43	28	41	31	27
Bi	13	7	12	12	9	11	11	10
Br	12	17	12	33	16	20	ND	37
Cd	ND	ND	ND	5	ND	ND	4	ND
Ce	15	49	21	144	49	116	19	ND
Co	22	ND	9	16	7	14	16	5
Cr	1330	10	480	180	38	170	1520	460
Cs	7	6	6	7	5	9	6	ND
Cu	41	8	25	30	19	30	32	17
Ga	13	21	16	22	19	20	14	17
La	ND	26	ND	74	26	62	ND	ND
Mo	2	ND	1	2	1	2	2	1
Nb	5	7	6	17	11	16	3	2
Nd	ND	16	12	61	26	52	ND	ND
Ni	112	11	24	43	13	24	69	23
Pb	9	25	8	18	13	15	9	8
Rb	3	55	15		28		13	8
Sc	47	3	33	32	19	39	38	33
Se	6	3	5	5	4	5	6	5
Sm	ND	ND	ND	13	ND	11	ND	ND
Sn	7	3	4	8	5	9	9	ND
Sr	84	112	93	114	79	97	99	84
Ta	11	6	8	9	6	7	7	8
Th	ND	17	ND	10	4	18	ND	ND
Tl	14	8	12	12	11	12	13	11
U	3	3	2	5	3	4	2	2
V	133	31	129	103	35	124	80	102
W	8	ND	ND	ND	ND	ND	ND	ND
Y	11	13	16	65	21	48	1	1
Zn	66	29	52	56	25	56	55	54

Table 5. Chemical composition of Benavila bentonite samples (<63 µm and <2 µm) determined by XRF for minor elements (ND – not detected). Error not provided (single measurements).

3.4. Bioaccessibility

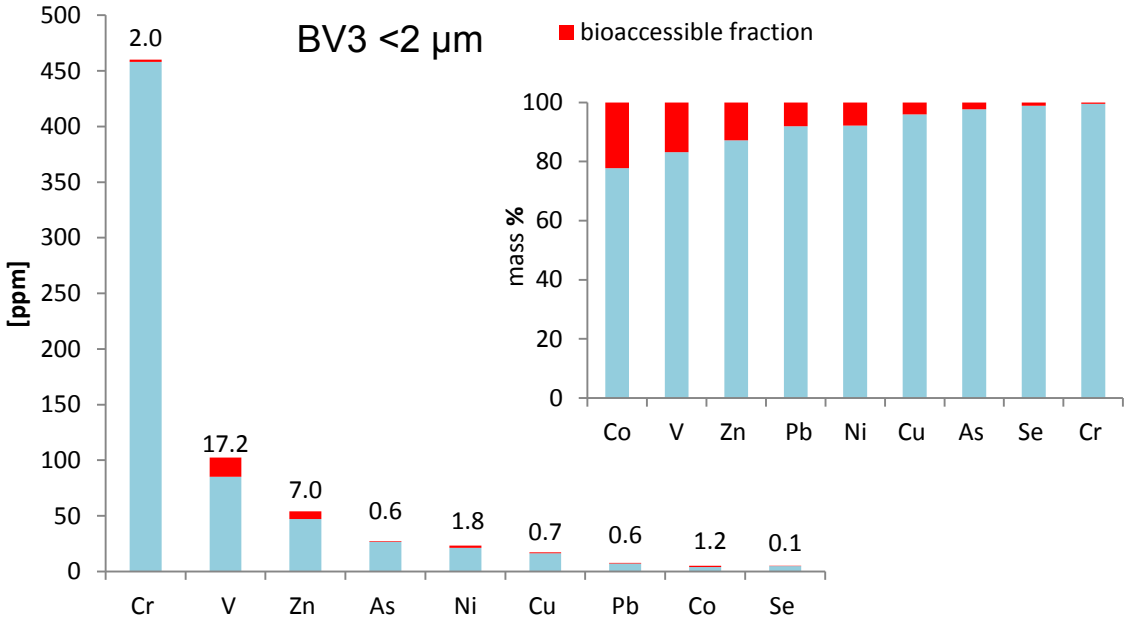

Figure 25. Estimated bioaccessible fraction (BA) determined in gastric solutions (left: ppm and right: %) with respect to total concentration of chosen, potentially harmful elements for the BV3 <2 µm sample. The amount of bioaccessible fraction in ppm is indicated above the columns for each element. Error not provided (single measurements).

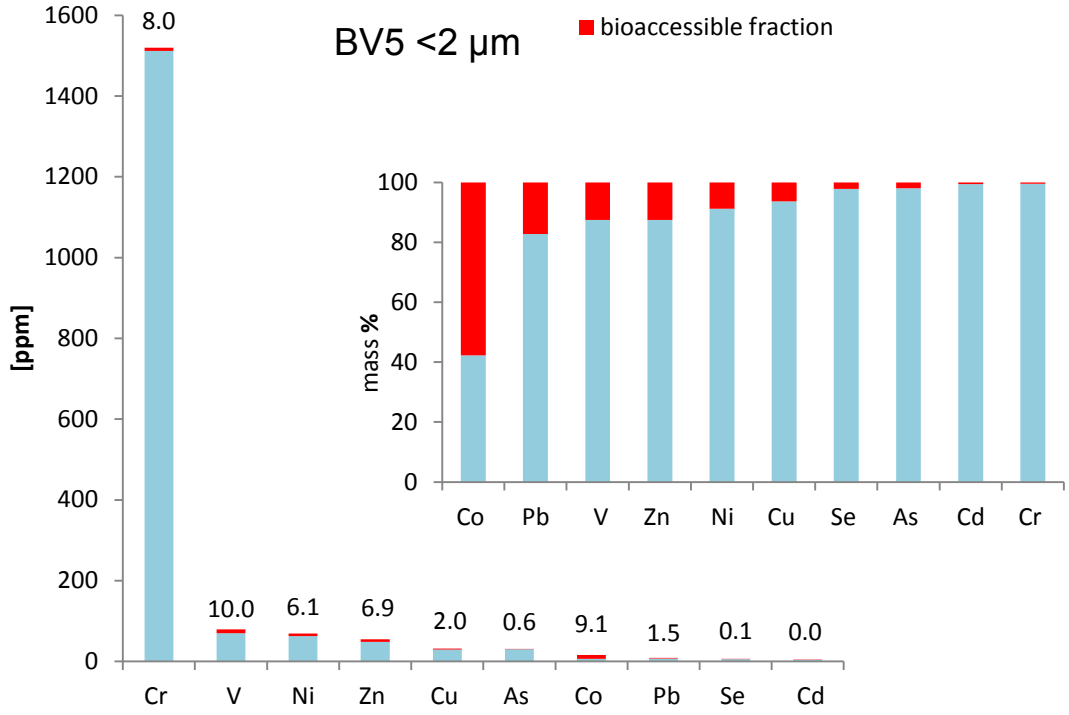

Figure 26. Estimated bioaccessible fraction (BA) determined in gastric solutions (left: ppm and right: %) with respect to total concentration of chosen, potentially harmful elements for the BV5 <2 µm sample. The amount of bioaccessible fraction in ppm is indicated above the columns for each element. Error not provided (single measurements).

Generally, clay minerals are non-toxic, even when they are ingested. However, since the Benavila smectites might be a potential ingredients of pharmaceutical formulations and they contain several potentially harmful elements, it is important to determine their accessibility in human gastrointestinal tract. Especially, Cr concentration is elevated in the chosen samples (BV3 <2 μm and BV5 <2 μm).

Regulations concerning the maximum concentration of certain elements in pharmaceutical formulations are not uniform throughout the world, however, they are quite strict and in many cases daily allowed concentrations are below several ppm (Health Canada, 2009; EMEA, 2008). According to U.S Pharmacopeial Convention (2012), the most toxic elements for human health are As, Cd, Hg and Pb and their permissible daily oral dose in an inorganic form is 1.5, 25, 15 and 5 μg, respectively. The same source states that Cr is not considered dangerous in pharmaceutical formulations.

The important parameter in assessing health risk connected with ingestion of heavy metals is their bioavailability. It refers to the fraction of these elements that reaches the human or animal systemic circulation (Van de Wiele *et al*., 2007). As it is only possible to assess it in *in vivo* test, it is a strongly problematic issue for ethical reasons. One solution is to estimate bioavailability of toxic elements by determining their bioaccessible fraction. Bioaccessibility refers to the maximum amount of certain element that is available for absorption in the animal or human gastrointestinal tract (Van de Wiele *et al*., 2007).

Fig. 25 and Fig. 26 present bioaccessible fraction (BA%) of several, potentially harmful heavy metals in two Benavila samples subjected to gastric solutions. When assessing bioaccessibility, two parameters are of great significance: BA% of elements and their total concentrations in the sample. Because of that, the bioaccessible fraction is also presented with respect to total amounts of elements (in ppm). Co is the most bioaccessible element in both samples (58 % - BV5 and 22% - BV3). However, with respect to total amount of Co, bioaccessible amount reaches several ppm. The elements with higher BA% are also Pb, V, Zn, Ni and Cu. As, Cd and Cr exhibit both low BA% and low total concentration in the samples. A significantly higher bioaccessible amount was measured for V in the BV3 sample (17 ppm). Most importantly, despite very high concentration of Cr, relative to other elements, the bioaccessible fraction of Cr is below 1% for both samples.

Having in mind that amount of clay minerals in pharmaceutical formulations can typically vary between 10 and 20 %, the resulting amount of potentially ingested toxic

elements can be adjusted in a final product. Although the bioaccessibility assay was limited to gastric solutions, BA% in gastrointestinal solutions is usually lower for clayey materials (Roussel *et al*., 2010). In conclusion, provided that Benavila smectite is used in low amounts (~1 g/day), it can be considered nontoxic.

3.5. Effective Cation Exchange Capacity and Exchangeable Cations

The values of cation exchange capacity (CEC), measured for the three Benavila bentonite samples: BV3, BV4 and BV5 (<63 μm) are presented in Figure 27. The determined cation exchange capacities are quite low and range from 30-45 meq/100g, what can be linked with relatively high amounts of associated minerals (~26% - 32%). Whereas the typical CEC reported for montmorillonite ranges between 70 – 120 meq/100g (Bergaya *et al*., 2006), CEC of exemplary bentonite samples varies significantly from 20 – 130 meq/100g (Lorenz *et al*., 1999; Amman, 2003; Olsson *et al*., 2009). Rebelo, 2010, reports CEC of 73 and 20 meq/100g for two different Benavila bentonite samples. This suggests that Benavila clay deposit is quite inhomogeneous.

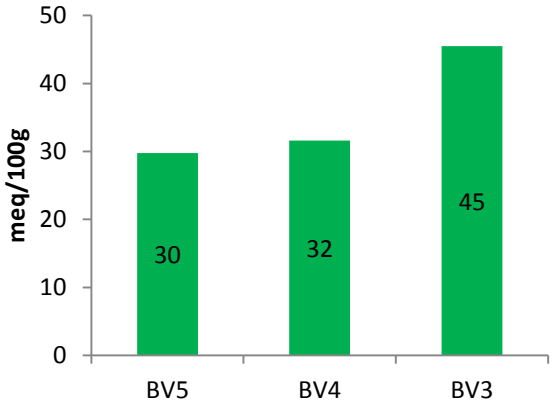

Figure 27. Effective cation exchange capacity of Benavila bentonite samples (<63 μm) measured by ammonium acetate method.

The main exchangeable cations present in the BV3 and BV5 samples (<63μm), measured by AAS, are presented in Figure 28. The dominant cation is Ca^{2+} and the second abundant Mg^{2+}. Concentrations of K^{+} and Na^{+} are minor. This suggests that the clay interlayer is composed of Ca^{2+} and Mg^{2+}.

However, according to Dohrman, 2006, minerals such as calcite and dolomite are highly prone to dissolution in contact with concentrated electrolytes alike ammonium acetate. As these mineral phases are abundant in the analyzed samples, the determined exchangeable cation composition may be biased. Additionally, the bentonite samples may contain certain amount of soluble salts. This issues might be also responsible for lowering the effective CEC, as Ca^{2+} and Mg^{2+} compete with NH_4^{+} to

be absorbed in the interlayer space of clay minerals. Measurements should be repeated after a removal of calcite and desalting by dialysis.

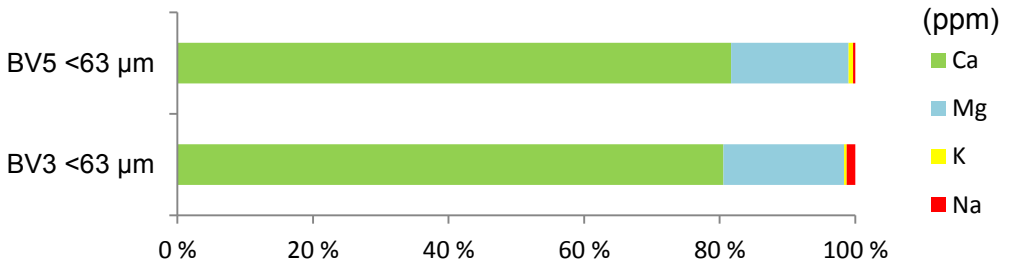

Figure 28. Exchangeable cations composition of Benavila bentonite samples (<63 µm).

3.6 Identification of Smectite Type

The first indication on what type of smectite is present in Benavila bentonite samples is provided by XRD. Dioctahedral and trioctahedral smectites can be distinguished on the basis of smectite (060) reflection's position. Usually, the peak position for trioctahedral smectites ranges from 1.54 to1.515 Å, whereas for dioctahedral ones (montmorillonite, beidelite), it ranges from 1.49 – 1.51 Å. For dioctahedral nontronite, which is Fe-rich smectite, the reflection's position is usually present at about 1.52 Å (Brindley & Brown, 1980).

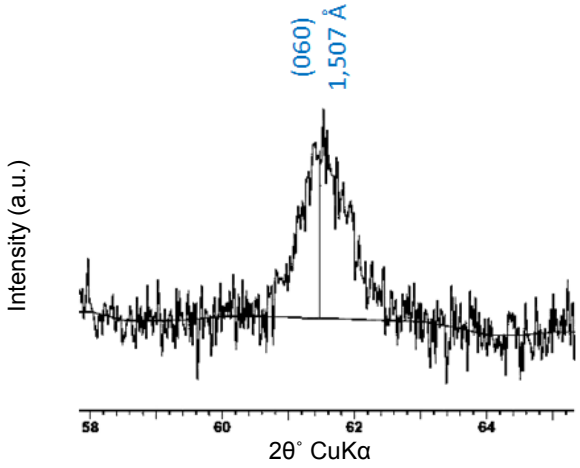

Figure 29. Benavila smectite (BV5 <2µm) high angle XRD diffraction pattern, with (060) smectite reflection.

The smectite type present in Benavila BV5 and BV3 bentonite is a dioctahedral one, since the (060) reflections' positions were measured at 1.507 Å and 1.505 Å, respectively (Fig. 29).

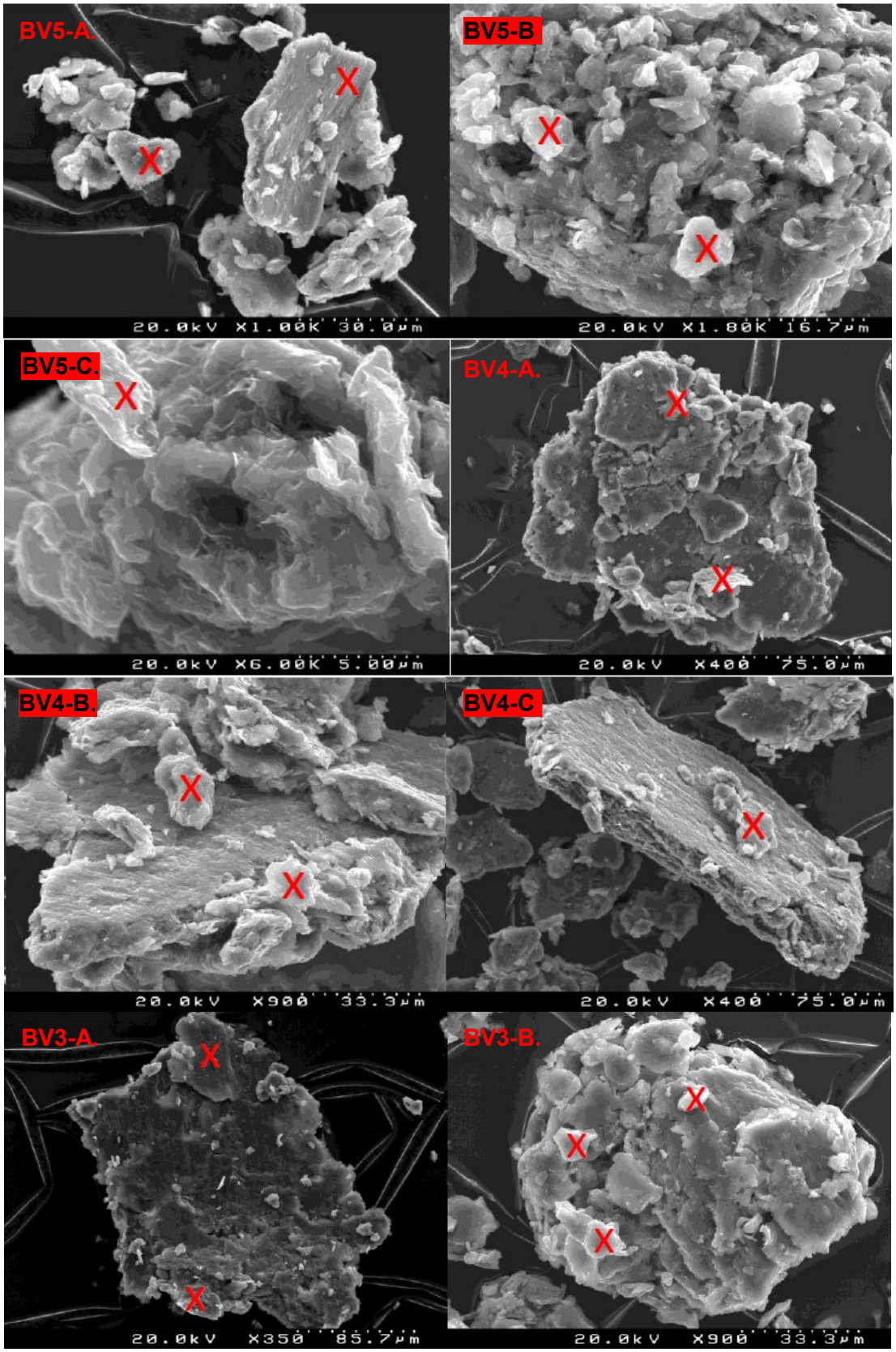

Figure 30. Benavila smectite SEM micrographs showing layered smectite aggregates and flaky smectite crystals morphology (BV5-C). Points used for SEM-EDS point chemical analyses are marked with a red cross. The SEM images were acquired at 20 kV and EDS was performed at 15 kV, no coating.

More detailed data is provided by SEM-EDS. Chemical composition of smectite may be determined by point chemical analyses. Figure 30 shows marked points used for the EDS measurement, performed for three Benavila clay mineral samples (BV3, BV4, BV5 <2 μm).

In addition, Figure 30-BV5.C depicts typical smectite morphology – flaky layers, exfoliated at edges. In this case smectite crystals adopt rose-shape morphology (Wieczorek *et al*., 2001).

The average, calculated structural formulas for the three samples, based on the point chemical analyses, are presented below:

BV5: $Na_{0.11}K_{0.1}Ca_{0.04}Mg_{0.01}(Al_{1.34}Mg_{0.34}Fe_{0.32})O_{10}(Si_{3.99}Al_{0.01})(OH)_2 \cdot nH_2O$

BV4: $Na_{0.06}Ca_{0.04}K_{0.02}(Al_{1.43}Mg_{0.36}Fe_{0.01})O_{10}(Si_{4,0})(OH)_2 \cdot nH_2O$

BV3: $Mg_{0.08}Ca_{0.08}Na_{0.04}K_{0.03}(Al_{1.18}Fe_{0.44}Mg_{0.38})O_{10}(Si_{3.99}Al_{0.01})(OH)_2 \cdot nH_2O$

According to these structural formulas, the smectite present in the three samples is montmorillonite – a dioctahedral smectite with an octahedral charge. The two samples – BV5 and BV3 have a high content of iron in the octahedral sheet, contrary to the BV4 sample which is depleted in iron. This is in a good agreement with the XRF chemical analysis for the three samples (Fe_2O_3 content: BV5 – 11.8%; BV4 – 1.5 %; BV3 – 9.0%). As these three samples are the neighboring ones from the same clay outcrop, there is also an observed corresponding change of color. Iron rich, external samples – BV5 and BV3 - are greenish, whereas the middle one – BV4 – is light grey. This discontinuity in chemical composition and color may be explained by the presence of a fault.

Interlayer cation composition differs for the three samples. For the BV5 and BV4 samples, the dominant cation is Na^+, whereas Mg^{2+} and Ca^{2+} are the most abundant in the case of BV3. According to other authors the main exchangeable cations in the interlayer of different Benavila montmorillonites are Ca^{2+} (Rebelo *et al*., 2010; Hajaji *et al*., 2013), Ca^{2+} and Mg^{2+} (Quintela *et al*., 2012) and Na^+ (Dias *et al*., 2004). The interlayer space occupancy should thus be verified using the exchangeable cations analysis for the clay fraction <2 μm.

Last but not least, clay mineral type can be identified with the aid of FTIR analysis (Fig. 31). The spectra of the two samples well agree with the literature data for montmorillonite (Madejova *et al*., 2001), which is in accordance with the SEM-EDS

results. The positions of the most pronounced bands in the spectra and their interpretation (Madejova *et al*., 2001; Prencipe *et al*., 2004) are listed in Table 6.

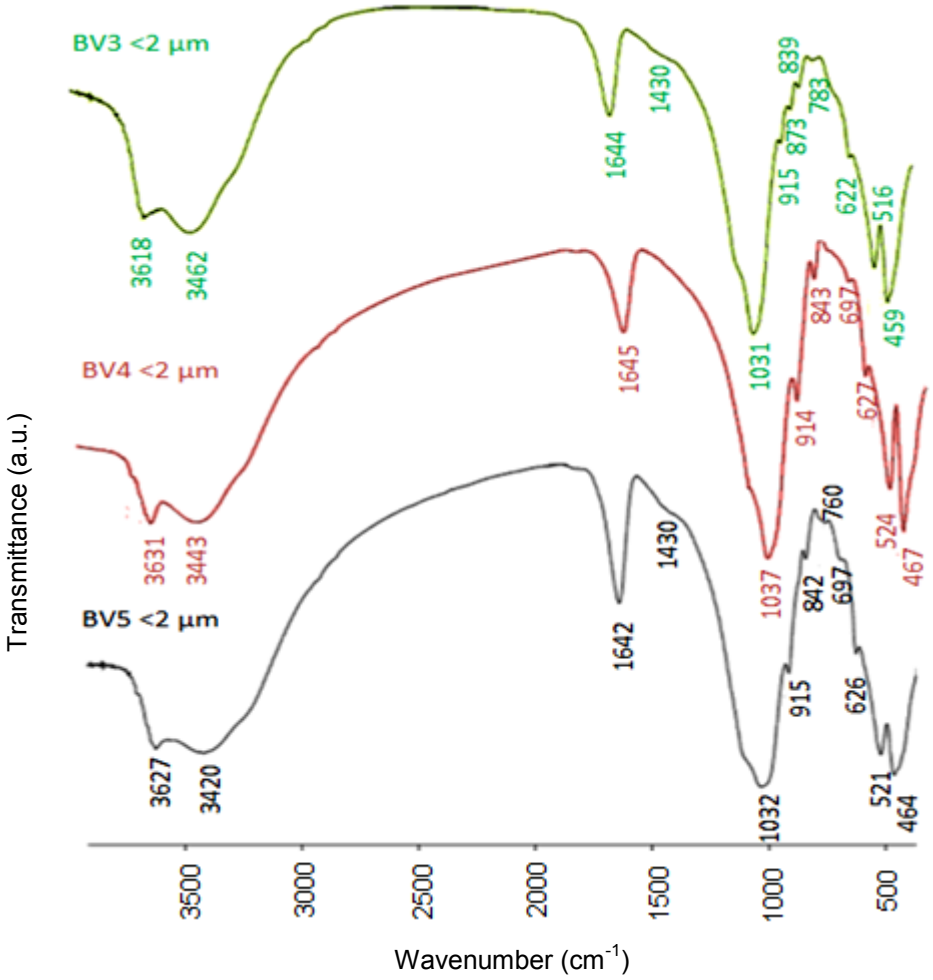

Figure 31. FTIR transmittance spectra of BV3, BV4 and BV5 <2µm samples.

Three main groups of vibrations can be evidenced: stretching and deformation vibrations (i) of water molecules associated with montmorillonite, (ii) of –OH structural groups and (iii) of other structural groups of the minerals. Stretching vibrations in the 3700 – 3000 cm^{-1}, associated with –OH structural groups of clay minerals and –OH in water molecules, vary significantly between various clay minerals and can aid their identification. The single peak in the region of structural –OH vibrations and the broad, significant feature connected with stretching vibrations of water molecules, are very typical for montmorillonite (Madejova *et al*., 2001). Additionally, FTIR can reveal mineral and organic impurities in the samples. In the case of Benavila smectite, there are minor silica and carbonate impurities. The first one is reflected by bands between 783 and 760 cm^{-1} for the three samples, respectively. The carbonate impurity can be associated with a very minor broad bump around 1430 cm^{-1} in both BV3 <2 µm and BV5 <2 µm samples. In detail, these bumps correspond to stretching vibrations of C-O

in calcite at 1420 cm^{-1} (Prencipe *et al*., 2004). Carbonate vibrations are not present in BV4 <2 μm, which correlates well with the XRD data.

FT-IR transmittance bands

wavenumber [cm^{-1}]	interpretation
3631-3618	stretching of -OH structural groups
3462-3420	stretching of -OH groups in water molecules
1645-1642	deformation of -OH groups in water molecules
1430	stretching of C-O in trace carbonate
1037-1031	stretching of structural Si-O
915 -914	deformation of AlAlOH
873	deformation of AlFeOH
842 - 839	deformation of AlMgOH
783-760	stretching of Si-O in silica
697	perpendicular Si-O vibration
627 - 622	out-of-plane vibration of Al-O and Si-O
524 - 516	deformation of Al-O-Si
467 - 459	deformation of Si-O-Si

Table 6. FTIR transmittance bands and their interpretation.

SEM-EDS measurements revealed the presence of Al, Mg, and Fe in both BV5 and BV3 montmorillonite clay minerals. On the basis of the structural formulae, recalculated from the SEM-EDS chemical analysis, these elements build octahedral sheets. The composition of octahedral sheets of clay minerals can be verified by FTIR, in the 1000 to 700 cm^{-1} wavenumber region. For the BV3 sample , bands at 873 cm^{-1} and 839 cm^{-1} reflect the presence of Fe and Mg, respectively. Mg is similarly evidenced in the octahedral composition of the BV5 and BV4 samples (AlMgOH deformation band at 842 cm^{-1}). There is Fe evidenced by FTIR for the BV4 sample. In the case of BV5 (high content of Fe evidenced by SEM-EDS), presence of iron for this sample is not obvious, as there isn't any well-pronounced band corresponding to AlFeOH deformation vibration. However, judging from a barely visible bump, around 870 cm^{-1}, one can expect the superimposition of the neighboring peaks.

3.7. Mechanical Properties – Plasticity

Plasticity of clay is a very important feature in clay-water systems. It is defined as "the property of a material which allows it to be repeatedly deformed without rupture when acted upon by a force sufficient to cause deformation and which allows it to retain its shape after the applied force has been removed" (Perkins, 1995). It means that the

more plastic the clay, it can deform to a greater extent without cracking. The clay plasticity depends on its water content, mineralogical composition, particle size distribution, type of exchangeable cations, presence of salts and organic materials (Andrade *et al*., 2010). Thus the clays with the highest swelling ability, especially montmorillonite, should exhibit the biggest plasticity.

The LL,PL and PI values were determined for the three Benavila samples <63 μm (BV5, BV4, BV3). The results (Tab. 7), show that all three clays have similar plastic characteristics and can be classified as very plastic (PI value above 50%). As these are not pure clay mineral samples, the obtained results correspond to the lower limits for montmorillonite (Mitchel & Soga, 2005). According to the Casagrande plasticity chart (Fig. 32), all three Benavila bentonite samples can be classified as very plastic clays. The BV5 sample has a little bit lower plasticity, as there is less clay in the <63 μm fraction. As the clay minerals are potential components of nanocomposites used in drug delivery, high plasticity of clays may have a beneficial effect on the preparation of different drug dosage forms, e.g. compressed tablets.

SAMPLE	BV5	BV4	BV3	montmorillonite (Mitchel & Soga, 2005)
LL (%)	82	92	91	100-900
PL (%)	28	35	34	50-100
PI (%)	54	57	57	50-800

Table 7. Plasticity characteristics of Benavila bentonite samples (<63 μm): LL- liquid limit, PL-plastic limit, PI- plasticity index and typical values for montmorillonite.

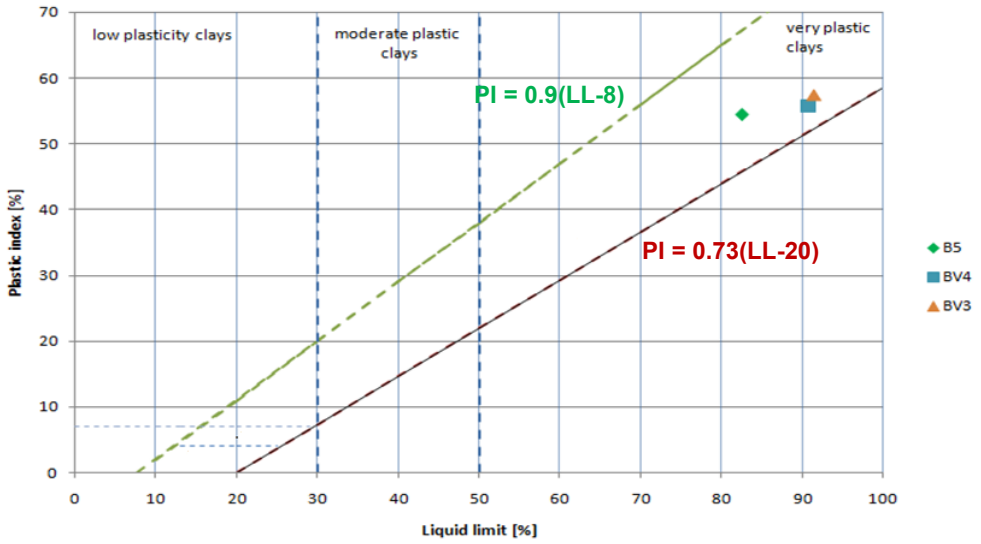

Figure 32. Plasticity of Benavila bentonite samples classified according to the Casagrande plasticity chart. Generally, the chart is used for assessment of soils' mechanical properties - the red line sets the upper limit for sandy and silty soils and the green line sets the upper limits for typical soils (adapted from Holtz, R.D. & Kovacs W.D., 1981).

4. Summary and Conclusions

Portuguese clay from a bentonite deposit in Benavila was collected from six sampling sites and characterized by the means of XRD and XRF. Three samples with the highest clay content (BV3, BV4, BV5) were subjected to a more detailed characterization, including physicochemical and mechanical properties. After separation of a clay fraction <2 μm, the smectite-rich samples were analyzed with respect to smectite type (XRD, FTIR, SEM-EDS), mineralogical (XRD) composition, chemical composition (major and minor elements) (XRF), and bioaccessibility of heavy metals. The smectite present in the ore is montmorillonite with varying Fe content.

The goal of this part of the thesis was fulfilled and the sample with best properties for a nanocomposite synthesis was chosen – BV3. The sample (BV3 <2 μm) exhibits the highest content (> 90%) of a clay mineral – Fe-rich montmorillonite, with trace amounts of chlorite and calcite. It possesses the highest cation exchange capacity (45 meq/100g for the fraction <63 μm). Compared with another montmorillonite-rich clay sample BV5 < 2μm, it has a smaller content of potentially toxic elements, especially chromium. Moreover, except for V, bioaccessibility of these elements is similar or lower than for the BV5 sample. These properties were the most important regarding a possible application of the clay mineral in a drug delivery formulation intended for ingestion.

Part III: Synthesis of Guar-Montmorillonite Nanocomposites

1. Aims

The main goal of this part of the thesis was to prepare and characterize guar gum-montmorillonite nanocomposites using commercially available reference clay from the Source Clay Repository, with known characteristics, and less a recognized Portuguese montmorillonite from the Benavila bentonite deposit.

2. Materials and Methods

2.1. Materials

Portuguese montmorillonite from the Benavila bentonite deposit (BV3) and the reference clay mineral, Sodium Wyoming Montmorillonite (SWy-2), were used to prepare guar gum-clay nanocomposites. SWy-2 was supplied from the Source Clay Repository (the Clay Minerals Society, USA) and has the following structural formula: $(Ca_{0.12}Na_{0.32}K_{0.05})[Al_{3.01}Fe(III)_{0.41}Mn_{0.01}\ Mg_{0.54}Ti_{0.02}][Si_{7.98}\ Al_{0.02}]O_{20}(OH)_4$ (The Clay Minerals Society; Source Clay Physical/Chemical Data).

Both clays were purified in order to separate a clay fraction <2μm (by a sedimentation procedure described in Part II, chapter 2.3). Subsequently, to enhance their swelling properties (Norish, 1954), montmorillonite samples were saturated with Na^+ according to a procedure adapted from Carrado *et al*., 2002 and Steudel *et al*., 2013. Typically, dry clay samples were dispersed in 1M NaCl solution and shaken for 24 h. After saturation, the samples were centrifuged at 3500 rpm for 5 min and the clear supernatant was decanted. The saturation procedure was repeated three times. Clay samples were washed with distilled water and recovered by centrifugation (10 000 rpm). After washing, dialysis was performed to remove excess salts (using dialysis membranes from Spectrum Laboratories Inc., MCWO 12,000 – 14,000) until no Cl^- was detected by $AgNO_3$ test. The samples were dried at 60°C and ground with an agate mortar and a pestle. Subsequent to sodium saturation, exchangeable cations were measured by the method described in Part II, chapter 2.7.

Neutral Guar Gum (NGG) was purchased from Sigma-Aldrich (USA). It is a beige powder with total ash content ≤ 1% and loss on drying ≤ 13 %. Cationic guar gum (gum guar 2-hydroxy-3-(trimethylammonio)propyl ether chloride, CGG) was purchased Spec-Chem Ind. (China). It is a yellow powder with N content ranging from 0.8 – 1.8 %. Both gums were used as received.

2.2. Synthesis of Neutral Guar Gum - Montmorillonite Nanocomposites

Neutral guar gum-montmorillonite nanocomposites, with a biopolymer : clay mineral ratio 6 : 1, were prepared by a solvent intercalation method adapted from Mansa & Detellier, 2013. Typically, 15 g of NGG were dispersed in 1.7 L of distilled water and mixed using a magnetic stirrer (1500 rpm). Subsequently, 2.5 g of sodium-saturated montmorillonite (Na^+-BV3 or Na^+-Swy-2) were added into NGG solution and stirred for two weeks at room temperature. Some part of the materials was recovered directly after synthesis for a characterization of unwashed products. Subsequently, the dispersions were centrifuged at 3500 rpm for 5 min to recover the products and supernatants were discarded. The remaining part of the materials were washed 3 times with distilled water and recovered by centrifugation (4000 rpm, 5 min). The washed and unwashed products were dried at 50°C and well ground with an agate mortar.

Due to high viscosity of dispersions, a control experiment was performed, where NGG-SWy nanocomposite was prepared using a more vigorous mechanical stirring (using Caframo RZR 50 stirrer; 2000 rpm), in comparison with magnetic stirring (Scilogex MS-H20-PRO; 1500 rpm).

Additionally, in a blank experiment 15 g of NGG were dissolved in 1.7 L of distilled water and stirred for two weeks at room temperature. The solution was centrifuged at 3500 rpm for 5 min to recover the product. The blank sample was then washed three times with distilled water, recovered by centrifugation (4000 rpm, 5 min), dried at 50°C and well ground with an agate mortar.

2.3. Synthesis of Cationic Guar Gum - Montmorillonite Nanocomposites

Cationic guar gum-montmorillonite nanocomposites, with a biopolymer : clay mineral ratio 4 : 1, were prepared by a solvent intercalation method using a modified procedure adapted from Mansa & Detellier, 2013. Prior to addition of CGG, 0.5 g of dry sodium-saturated montmorillonite (Na^+-BV3 or Na^+-Swy-2) were dispersed in 1L of distilled water to allow swelling. Subsequently, 2 g of CGG were added into the clay suspension and stirred for 3 days at 500 rpm, at room temperature. The materials were dried at 50°C and well ground with an agate mortar.

2.4. Characterization Techniques

2.4.1. X-ray Diffraction

X-ray diffractograms were collected using Philips PW 3710 diffractometer, with aCu Kα radiation (λ = 1,5405 Å), at 45 kV, 40 mA, and with a step size of 0,02°2θ, in 2-90° 2θ angle range. Randomly oriented powder samples were prepared by a back-loading method. Oriented XRD mounts were prepared by pipetting a small amount of suspension onto glass slides, which were then air dried.

2.4.2. Thermogravimetric Analysis

Thermogravimetric data (TG, DTG) was recorded using a TGA Q5000 instrument in a temperature range 25°C – 700°C or 25°C – 1000 °C and heating rate 10°C/min, under nitrogen atmosphere. Platinum-HT or alumina Al_2O_3 sample pans were used and the amount of a sample was ranging from ~2 mg – 15 mg.

2.4.3. Solid State Nuclear Magnetic Resonance

Solid state nuclear magnetic resonance spectra were collected using a Bruker AVANCE 200 spectrometer and a Bruker AVANCE 500 spectrometer for the Na^+-BV3 sample. ^{13}C CP- MAS and ^{23}Na MAS spectra were collected at spinning rates of 4500 Hz and 5000 Hz, respectively, and for one sample, Na^+-BV3, the spinning rate was 31.2 kHz. The ^{13}C CP-MAS spectra were calibrated with respect to glycine at 176.5 ppm. The ^{23}Na MAS spectra were referenced to sodium chloride at 0 ppm.

3. Results and Discussion

3.1. Na^+- saturated Clay Minerals

XRD of both montmorillonite samples, after separation of a fraction < 2μm and saturation with Na^+, are presented in Figure 33. The enhancement (Na^+-SWy) and appearance (Na^+-BV3) of a peak at 3.2 Å, which is typical for Na^+-saturated montmorillonite (Brindley & Brown, 1980), indicates that Na^+ is present in the interlayer of both clay minerals. Additionally, the diffractograms show that quartz (~10%[1]) is present as an impurity in the Na^+-SWy sample. In case of Na^+-BV3, there is a minor amount of calcite (~4%[1]) in the sample.

[1] According to XRD semi-quantification performed as described in the chapter 2.5.

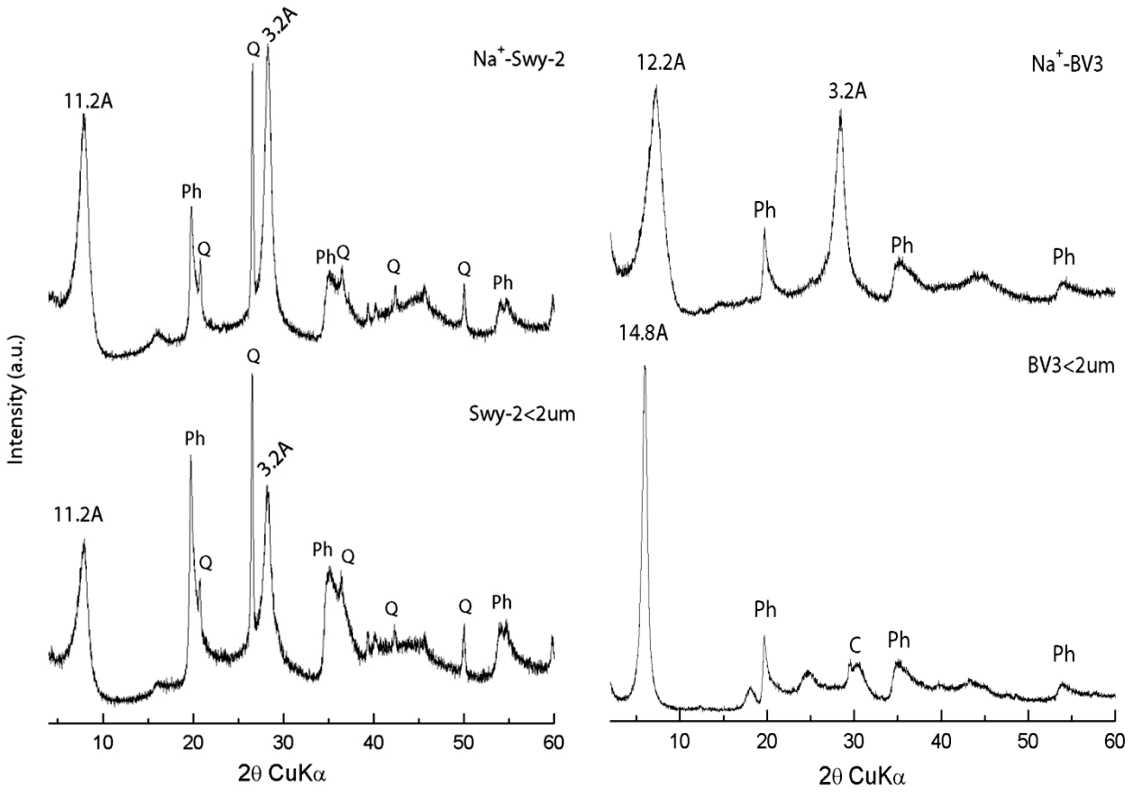

Figure 33. XRD powder diffractograms of the purified SWy-2 and BV3 montmorillonite samples after saturation with Na^+ (Ph – phyllosilicates, Q – quartz, C- calcite).

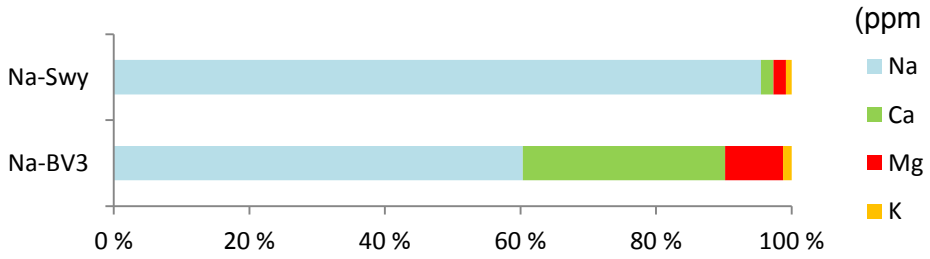

Figure 34. Exchangeable cations composition of sodium saturated montmorillonite measured by ICP-MS.

The main exchangeable cations, present in the sodium-saturated samples, are shown in Figure 34. The dominant cation in the Na^+-SWy interlayer is sodium, with minor amounts of Ca^{2+}, Mg^{2+} and K^+, which indicates that the saturation was efficient. In the case of Na^+-BV3 sample, the process was less effective - apart from Na^+, there is still a substantial amount of Ca^{2+} and Mg^{2+} present in the interlayer. Following the previous discussion, some part of Ca^{2+} may be due to dissolved calcite impurity (Dohrman, 2006). Effective CEC, calculated as a sum of exchangeable cations, is equal to 61 meq/100g (Na^+-SWy) and 111 meq/100g (Na^+-BV3).

3.2. Neutral Guar Gum-Montmorillonite Nanocomposites

3.2.1. X-ray Diffraction

The interaction of neutral guar gum with Na^+-SWy was principally assessed by XRD. Figure 35 shows enhancement of clay mineral's interlayer spacing from the initial 11.2 Å (Na^+-SWy), to 30 Å and 24 Å for the unwashed and washed NGG-SWy samples, respectively. Such an increase, clearly indicates that NGG is present in the clay mineral's interlayer and that nanocomposites with intercalated structures have been obtained.

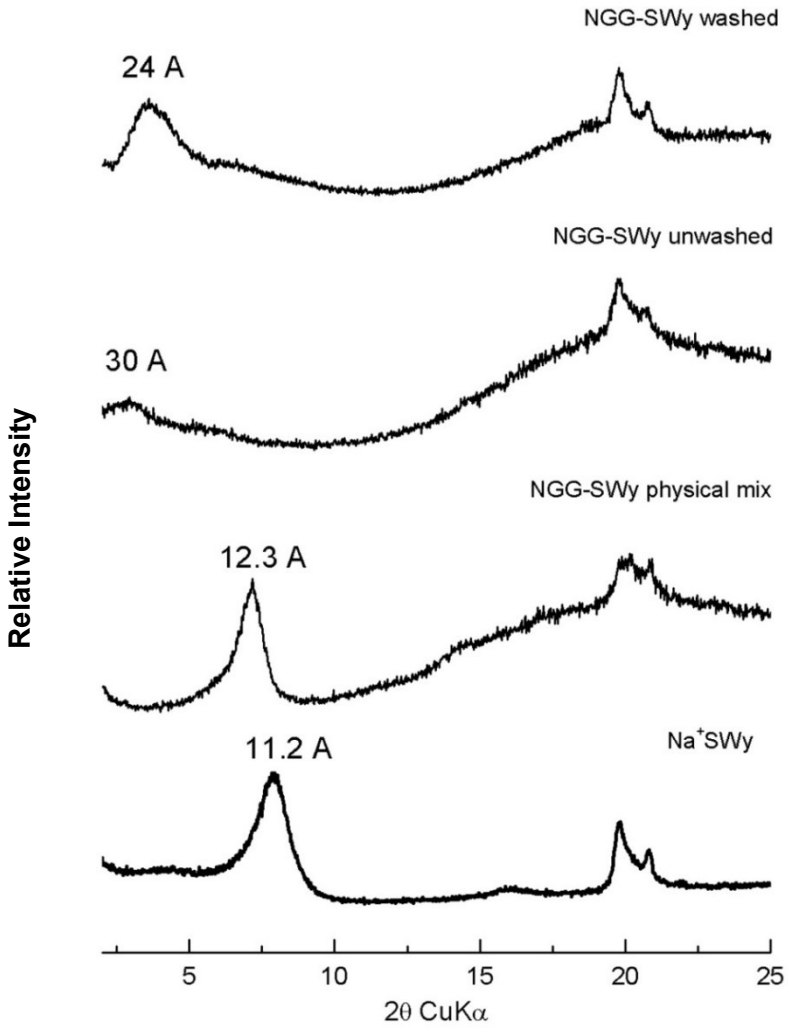

Figure 35. XRD powder diffractograms of Na^+-saturated SWy montmorillonite, physical mixture NGG and SWy, ratio 6:1, unwashed NGG-SWy nanocomposite, and washed NGG-SWy nanocomposite.

The (001) reflection for the unwashed NGG-SWy nanocomposite is broad and diffuse, suggesting a partial exfoliation of the clay mineral (Theng, 2012). However, this

substantial decrease in the peak's intensity may be also caused by other factors, e.g. low clay volume loading. To verify this, a physical mixture of neutral guar gum and Na^+-SWy (mass ratio 6:1) was prepared. The mixture's XRD pattern shows a well-defined (001) and a relatively intense reflection of the clay mineral, excluding the effect of clay dilution. A shift of the peak's position from 11.2 Å to 12.3 Å is probably due to different humidity conditions.

After three cycles of washing and centrifuging, the washed NGG-SWy nanocomposite with a more defined basal spacing of 24 Å was obtained. This suggests that upon centrifugation and simultaneous reduction of the polymer content, clay layers tend to reassemble. Similar behavior has been reported for other nanocomposites prepared with montmorillonite and uncharged polymers (Greenland, 1963; Lagaly, 1986; Theng, 2012). Due to strong interactions between polymer chains and the clay mineral, the latter may partially realign to form tactoids and thus producing intercalated, rather than exfoliated structures (Theng, 2012). A similar NGG-SWy nanocomposite with the d_{001} of 18.3 Å was synthesized by Mansa & Detellier, 2013. The broadness of the peak, along with a diffuse diffraction feature with an interlayer spacing of ~14 Å, was interpreted by the authors as due to coexisting bilayer (prevalent) and monolayer orientations of neutral guar gum. A further elucidation of the structure by TEM, revealed a presence of mixed morphology, comprised of exfoliated single clay layers and small clay tactoids. According to this previous work, the interlayer spacing of 24 Å, in case of the washed NGG-SWy nanocomposite, may correspond to average values of coexisting mixed morphologies (Mansa, 2011; Mansa & Detellier, 2013).

As neutral guar gum tends to form highly viscous solutions even at 1% concentration, two stirring methods were compared during the synthesis. Figure 36 presents the effect of magnetic stirring (1500 rpm) and more vigorous, mechanical stirring (2000 rpm) on the structure of the washed NGG-SWy nanocomposite. Mechanical stirring led to only a slight enhancement of d_{001} spacing of the nanocomposite.

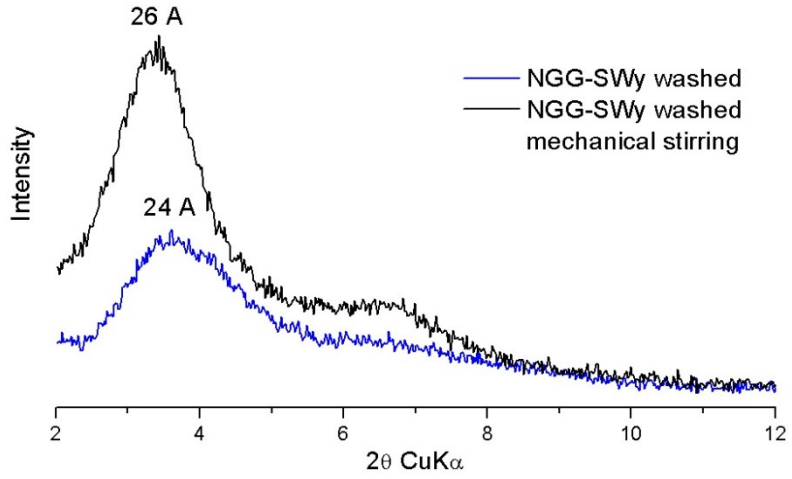

Figure 36. XRD powder diffractograms of SWy-NGG washed nanocomposite prepared by magnetic stirring (1500 rpm) and mechanical stirring.

In the case of Portuguese Benavila montmorillonite, similar unwashed and washed materials (NGG-BV3) have been prepared. According to XRD, both NGG-BV3 nanocomposites exhibit intercalated structures (Fig. 37). The interlayer spacing of Na^+-BV3 montmorillonite was enhanced from the initial 12.2 Å to 16.8 Å in the case of the washed NGG-BV3 sample. The diffraction pattern of the unwashed BV3-NGG sample shows a broad diffraction feature with two maxima around 32 and 17 Å.

Generally, although the interlayer spacing obtained for the NGG-BV3 washed nanocomposite was smaller than for the NGG-SWy sample, both materials exhibit a similar behavior. The poorly-defined (001) diffraction features for the unwashed nanocomposites are replaced by well-pronounced peaks, subsequent to washing, what again suggests a tendency of the clay mineral to realign in a polymer matrix. Many factors may impact the interaction of biopolymer and clay mineral, leading to a varied thickness of interlayer space, as in the case of NGG-BV3 and NGG-SWy nanocomposites. One possible hypothesis is a presence of carbonates in the BV3 sample, which promotes aggregation of clay crystals and can impede delamination of smectite clay minerals (Bergaya & Lagaly, 2013). Additionally, presence of Ca^{2+} and Mg^{2+} in the BV3 interlayer may diminish its ability to swell (Norrish, 1954).

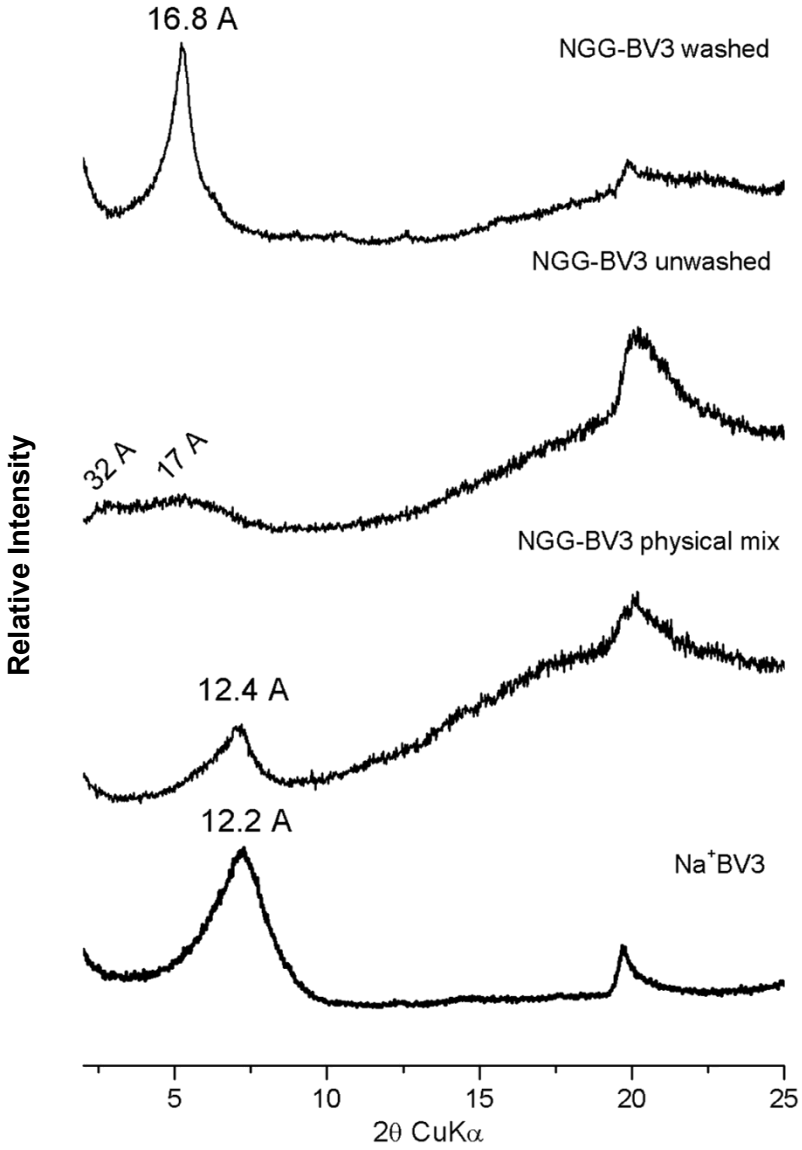

Figure 37. XRD powder diffractograms of Na^+-saturated BV3 montmorillonite, a physical mixture of NGG and BV3, ratio 6:1, unwashed NGG-BV3 nanocomposite, and washed NGG-BV3 nanocomposite.

Usually, the driving force for intercalation of neutral molecules, such as guar gum, into montmorillonite interlayer is a gain in entropy due to desorption of water (multiple water molecules are replaced by a single polymeric chain) (Zeng *et al*., 2005; Theng, 2012). Additionally, van der Waals forces and hydrogen bonding between biopolymer –OH groups and clay siloxane surface play a major role in stabilizing intercalated molecules (Ruiz-Hitzky *et al*., 2005).

3.2.2. Thermogravimetric Analysis

Interaction of clay minerals with neutral guar gum was further investigated by the means of thermal analysis, using TG and DTG traces.

TG and DTG results for Na^+-SWy and NGG-SWy samples are presented in Figure 38 and Figure 39. The total mass loss for Na^+-SWy montmorillonite reaches 9,9 % and involves loss of molecular water and dehydroxylation of the clay mineral (Rouquerol *et al*., 2013). Molecular water is lost between 25°C and 100°C, with a fastest loss at 56°C, and includes interlayer and surface-adsorbed water (Foldavari, 1991). Hydroxyl groups constitute a part of clay mineral structure and escape on heating up to higher temperatures (Roquerol *et al*., 2013; Foldavari, 1991). For Na^+-SWy dehydroxylation occurs between 540°C and 750°C.

Decomposition of neutral guar gum on pyrolysis takes place between ~200°C and 400°C, with a DTG peak centered at 304°C, subsequent to a ~10% mass loss due to adsorbed water. The total mass loss of NGG reaches 83.6% and in the case of the unwashed and washed NGG-SWy nanocomposites 70.9% and 60.7%, respectively. These values indicate that NGG content in the nanocomposite is still high after washing procedure.

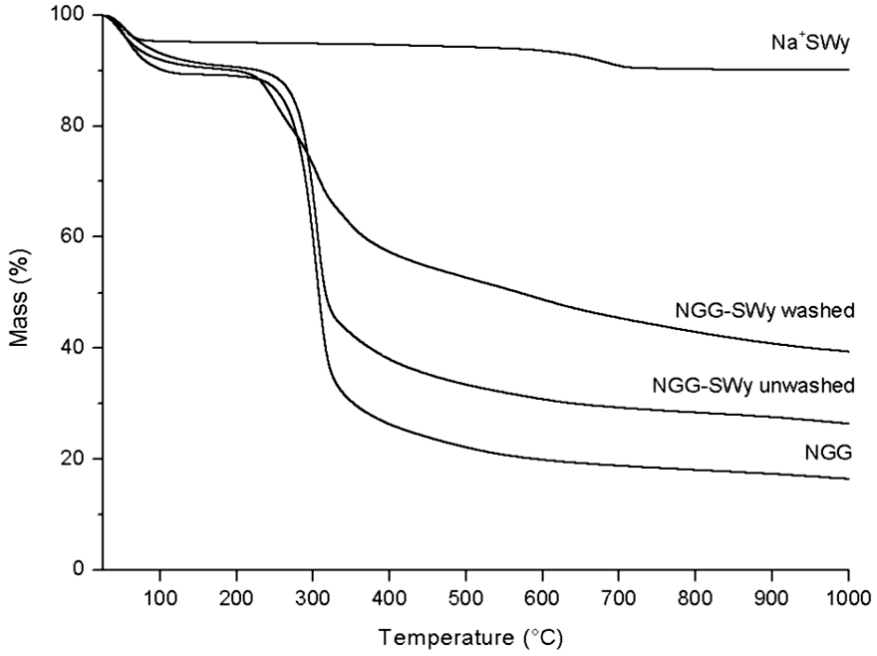

Figure 38. TG traces of Na^+-saturated SWy montmorillonite, NGG, unwashed, and washed NGG-SWy nanocomposites.

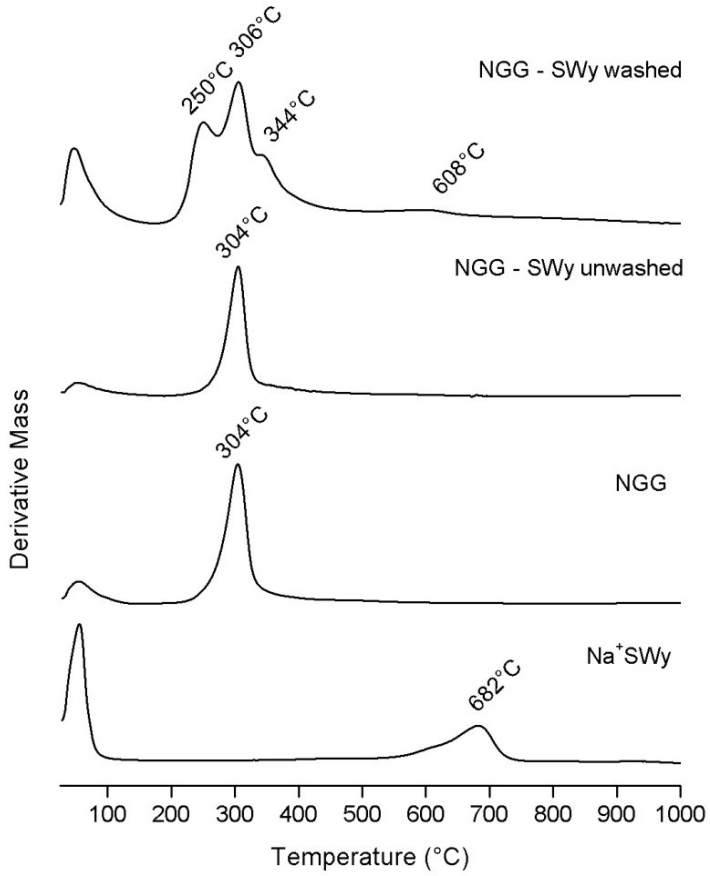

Figure 39. DTG traces of Na^+-saturated SWy montmorillonite, unwashed, and washed NGG-SWy nanocomposites.

The DTG trace of unwashed NGG-SWy is very similar to that of NGG. However, DTG trace of the washed NGG-SWy nanocomposite reveals a three-step decomposition of NGG with DTG peaks' maxima at 250°C, 306°C and 344°C. According to Mansa & Detellier, 2013, this altered behavior of NGG upon interaction with SWy may be interpreted as due to varied thermal stability of NGG adsorbed in different environments: externally (250°C) and in the interlayer space of SWy (344°C). The most intense DTG peak at 306°C would then correspond to the excess guar gum that is not in contact with the clay mineral.

Figures 40 and 41 show TG and DTG traces of Portuguese montmorillonite, Na^+-BV3, and NGG-BV3 nanocomposites.

Na^+-BV3 (14.7 %) exhibits a higher mass loss than Na^+-SWy, what can be explained by a ~5% higher water content for Na^+-BV3. The decomposition of calcite (~900°C; Mackenzie & Rahman, 1987) is not well evidenced in the DTG trace, suggesting a minor content of this mineral. Additionally, dehydroxylation of Na^+-BV3 occurs at lower temperatures, with a DTG peak's maximum at 603°C

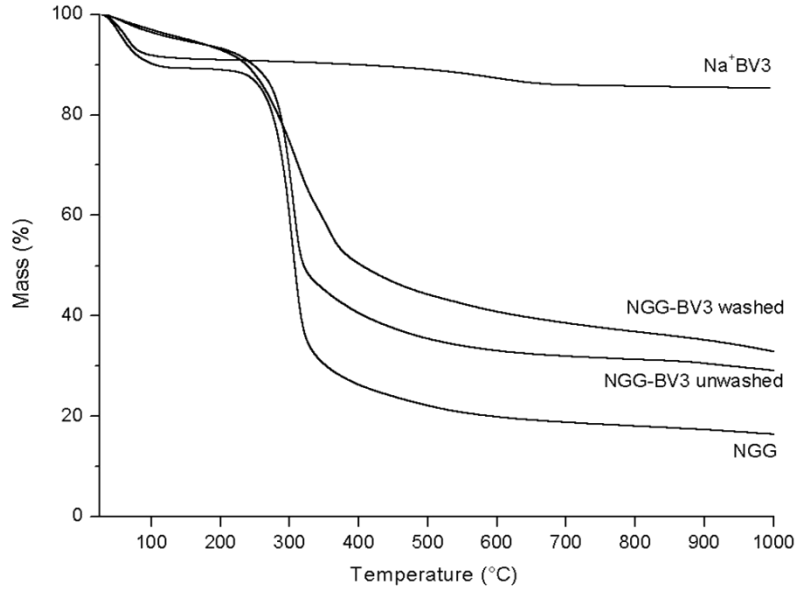

Figure 40. TG traces of Na^+-saturated BV3 montmorillonite, unwashed, and washed NGG-BV3 nanocomposites.

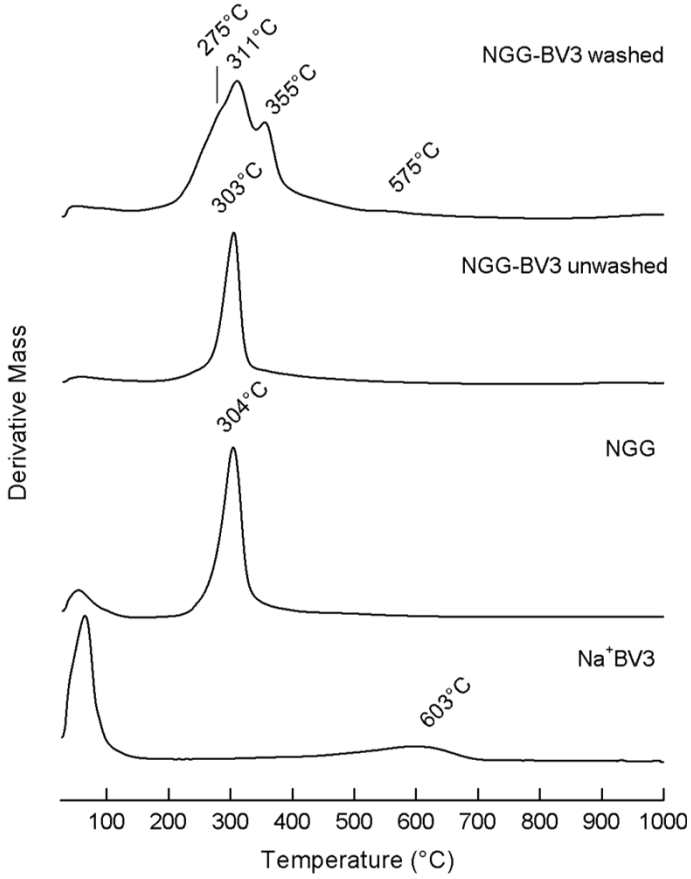

Figure 41. DTG traces of Na^+-saturated BV3 montmorillonite, unwashed, and washed NGG-BV3 nanocomposites.

The total mass loss of the unwashed and washed NGG-BV3 nanocomposites is equal to 70.9 % and 67.1%, respectively, suggesting that external NGG has been removed less efficiently than for NGG-SWy upon washing. The DTG traces show analogous behavior of the unwashed and washed sample. Whereas, NGG is pyrolysed in a single step for the former (DTG peak centered at 303°C), the latter shows a multiple step decomposition of NGG (DTG feature with two maxima at 311°C, 355°C and a shoulder at 275°C), like the washed NGG-SWy. Since the difference in a total mass loss is only 3.8%, indicating comparable organic content, this evident alteration of the pyrolysis pattern further suggests a reorganization of the nanocomposite structure upon washing and centrifugation. Noteworthy, the DTG traces of washed NGG-BV3 and NGG-SWy samples show a decrease of dehydroxylation temperature of the clay mineral components (a ~30°C- and ~70°C-decrease, respectively), which is typical in interactions of clay minerals with organic molecules (Mansa & Detellier, 2013).

3.2.3. Solid State Nuclear Magnetic Resonance Spectroscopy

^{13}C CP MAS NMR spectra (Fig. 42) further reflect the presence of neutral guar gum in the prepared materials. The spectrum of NGG shows four major peaks (at 102, 82, 73 and 63 ppm) that are the typical ^{13}C chemical shifts corresponding to the structure of this polysaccharide (Cheng & Neiss, 2012). However, the blank experiment (NGG residue), where NGG was subjected to a similar experimental procedure as the nanocomposites, reveals a presence of additional peaks that cannot be attributed to the structure of this biopolymer (174, 130, 40-20 ppm). According to Cunha *et al*., 2007, commercial neutral guar gum, supplied from Sigma, contains 13.1 % of impurities, which include glucose and arabinose impurities, proteins (3.6 %) and uronic acid (2.1%). Most likely, the peaks in 40-20 ppm range are due to protein contaminants, since these chemical shifts are typical for carbon-nitrogen bonds. In the same manner, a peak with a chemical shift of 174 ppm can be attributed to carboxylic functional groups in the structure of proteins or uronic acids. This indicates that upon centrifugation, impurities (probably due to their higher molecular weight) are concentrated in the remaining part of NGG, which was not discarded with a supernatant.

Spectra of both NGG-SWy and NGG-BV3 washed nanocomposites closely resemble each other and that of NGG residue, showing a range of peaks attributed to NGG and guar impurities. Similarly, as for NGG alone, the impurities are selectively accumulated in materials during centrifugation of nanocomposites. The substantial reduction of a peak at 40 ppm in the case of nanocomposites, which is a significant one

in the spectrum of NGG residue, suggests that clay minerals may further contribute to selective concentration of contaminating phases. Very similar NMR results were obtained for the neutral guar gum-montmorillonite nanocomposite by Mansa & Detellier, 2013.

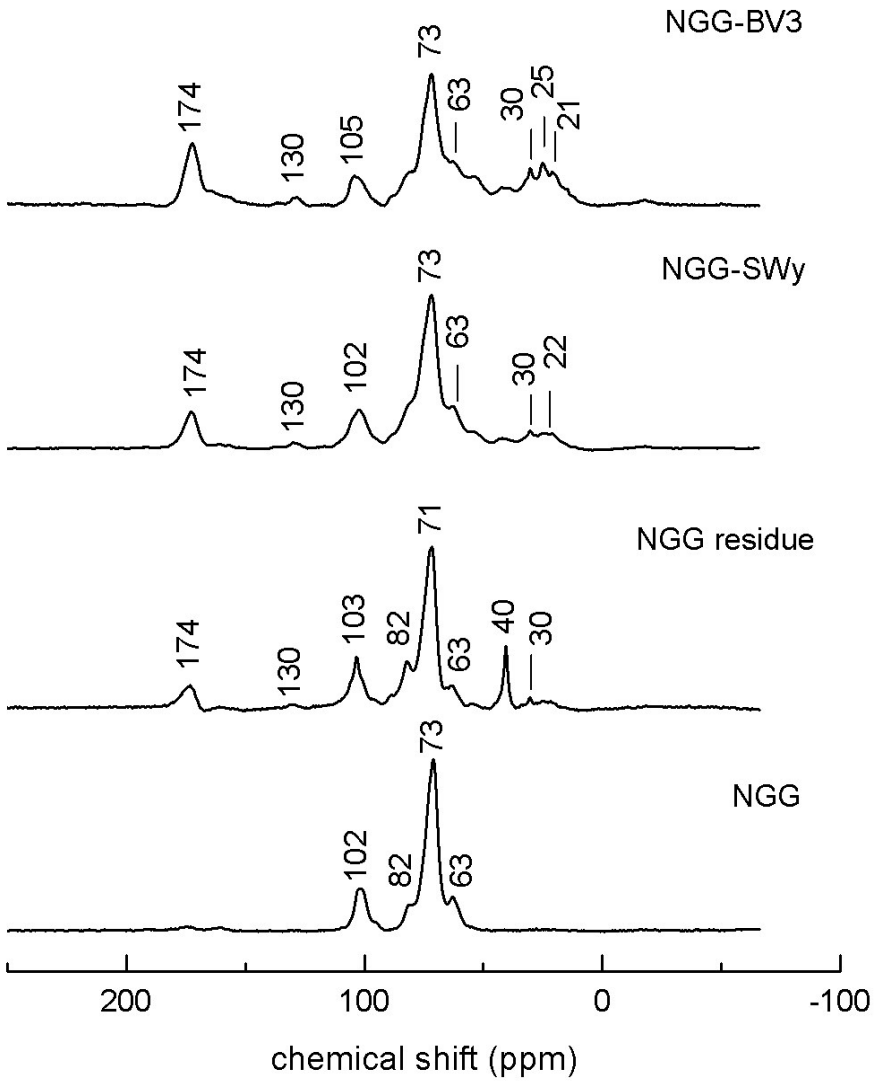

Figure 42. ^{13}C CP MAS spectra of NGG, NGG residue (blank experiment), and washed NGG-SWy and NGG-BV3 nanocomposites.

^{23}Na MAS spectra of sodium saturated montmorillonite samples (Na^+-SWy and Na^+-BV3) and washed NGG-SWy and NGG-BV3 samples are presented in Figure 43. Single peaks of starting clay minerals reveal a presence of sodium in the interlayer. These features are significantly diminished in the instance of the nanocomposites, what indicated that vast majority of sodium has been removed from the interlayer upon introduction of the biopolymer. According to Mansa & Detellier, 2013, ICP-ES results, for a similar NGG-SWy nanocomposite, indicate exchange of Na^+ by Ca^{2+} and K^+ cations that are associated with guar gum.

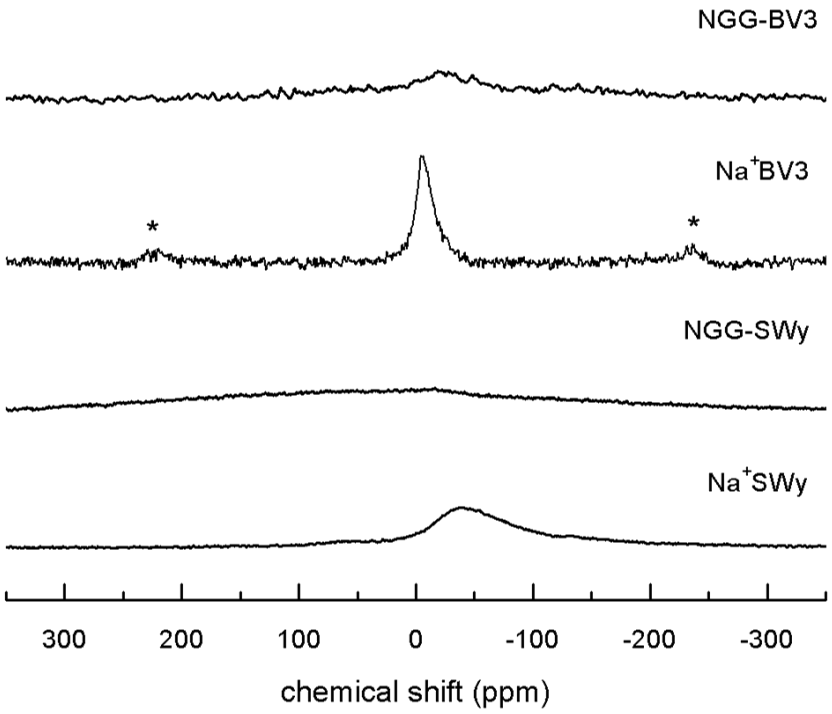

Figure 43. ^{23}Na MAS spectra of Na^+-SWy, Na^+-BV3 and washed NGG-SWy and NGG-BV3 nanocomposites.

3.3. Cationic Guar Gum-Montmorillonite Nanocomposites

3.3.1. X-ray Diffraction

Another series of materials were prepared with a cationic derivative of neutral guar gum (CGG). XRD served as a principal technique to determine if a synthesis of nanocomposites, using two different montmorillonite samples (Na^+-SWy and Na^+-BV3), was successful.

Figure 44 shows diffractograms of CGG-SWy and CGG-BV3 samples as compared to starting montmorillonite clay minerals – Na^+-SWy and Na^+-BV3, respectively. The interlayer spacing of Na^+-SWy (12.5 Å) and Na^+BV3 (12.9 Å) is typical for hydrated species with a water monolayer (Meunier, 2005). For both of them, a comparable enhancement of basal spacing have been observed – (001) reflection shifted to 14.5 Å in the instance of CGG-SWy and 14.3 Å for CGG-BV3. These values are in good accordance with literature data for a similar CGG-montmorillonite nanocomposite, with a CGG to clay mineral ratio 3:1 (Mansa, 2011; Mansa & Detellier, 2013). Additionally, XRD peaks of these two materials, exhibit a shoulder centered at lower 2θ values, which is more pronounced for the CGG-SWy sample. As such, XRD

indicated that cationic guar gum has been intercalated into both clay minerals. Given that a thickness of a single montmorillonite layer is approximately 9.5 Å, the interlayer space occupied by a biopolymer would be ~ 5Å (Meunier, 2005). This value, according to Mansa & Detellier, 2013, corresponds to a CGG monolayer.

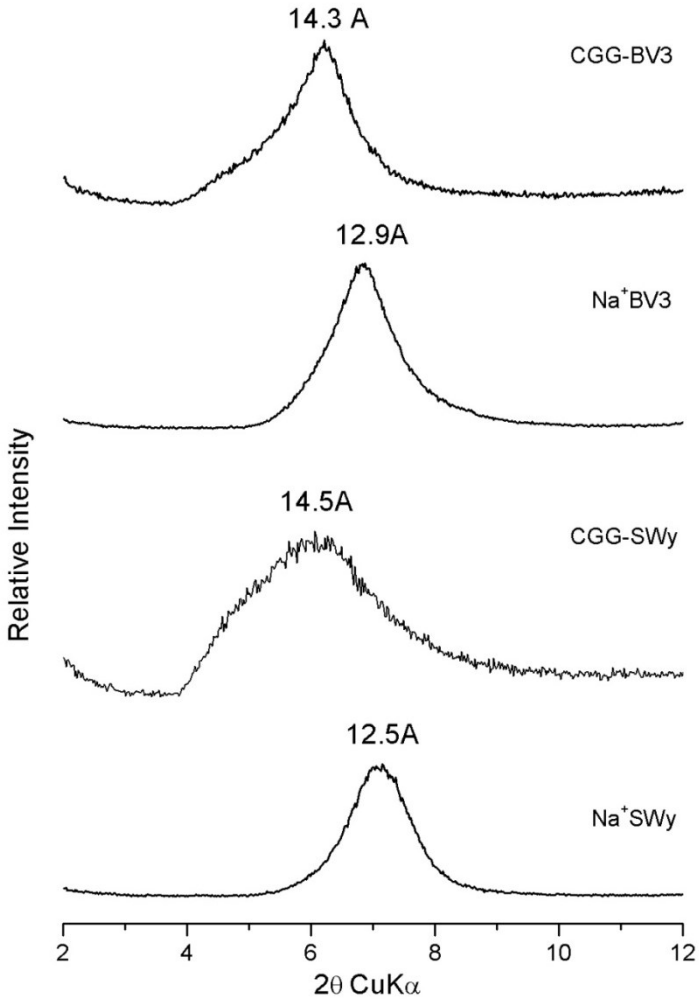

Figure 44. XRD diffractograms of Na^+-SWy and Na^+-BV3, CGG-SWy and CGG-BV3 samples with a biopolymer-clay ratio 4:1 (oriented mounts).

Contrary to nanocomposites prepared with NGG, an intercalated structure with a well-defined basal spacing was obtained for unwashed nanocomposites (subsequent to the synthesis, CGG-montmorillonite dispersions were dried without a further treatment). This behavior is due to electrostatic interaction of a positively charged biopolymer and a negatively charged clay mineral surface (Mansa & Detellier, 2013). Such interaction is a driving force for intercalation of CGG into clay minerals interlayer spaces (Ruiz-Hitzky *et al*., 2005).

3.3.2. Thermogravimetric Analysis

TG traces of Na^+-SWy, CGG-SWy, CGG-BV3 and CGG are shown in Figure 45. The weight loss of the nanocomposite samples: CGG-SWy (58.9%) and CGG-BV3 (70.7%) is intermediate between those of Na^+-BV3 (13.6%) and CGG (73.8%), indicating a prevalent amount of CGG in the nanocomposite (data up to 650°C). Additionally, uptake of CGG by CGG-BV3 is larger than for the CGG-SWy sample – the former has a 11.8% higher weight loss. Since the composites were dried directly after the synthesis, this may be due to a grinding step, when some part of the material is lost.

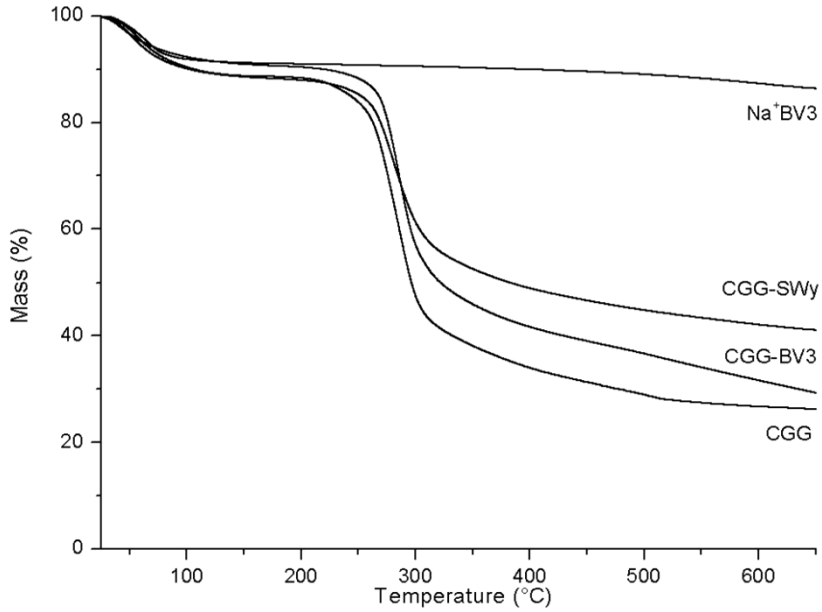

Figure 45. TG traces of Na^+- SWy montmorillonite, CGG , CGG-BV3, and CGG-SWy samples.

DTG traces of CGG and CGG nanocomposites (Fig. 46) closely resemble each other, without any distinct features. Pyrolysis of CGG occurs between ~200°C and 320°C in a single step, as indicated by peak centered at 286°C. In the DTG trace of CGG-BV3, pyrolysis is the fastest at the same temperature, and in the case of CGG-SWy the peak is centered at a slightly lower temperature: 280°C. This behavior is analogous to the unwashed NGG-montmorillonite nanocomposites, where pyrolysis of NGG occurred in a single step, as well. Since the CGG-clay samples exhibit a well-defined intercalated structure, the previous hypothesis regarding its influence on a multistep guar gum pyrolysis seems to be invalid. More likely, there is a high amount of externally adsorbed biopolymer, which prevents environments with different thermal stabilities, as well as a dehydroxylation step of clay minerals, from being distinguished.

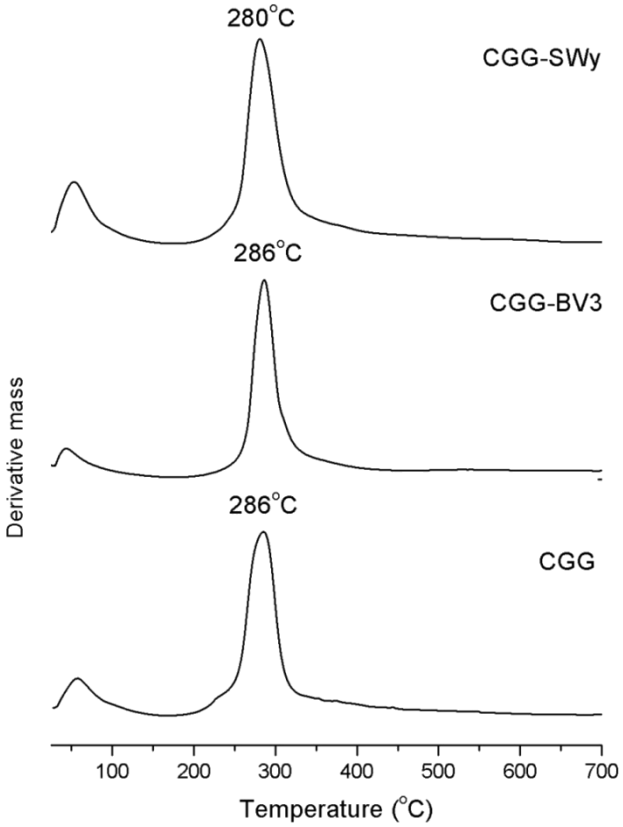

Figure 46. DTG traces of CGG, CGG-BV3 and CGG-SWy.

3.3.3. Solid State Nuclear Magnetic Resonance Spectroscopy

^{13}C CP MAS NMR spectra (Fig. 47) reveal the presence of cationic guar gum in the prepared materials. The peaks present in the spectrum of CGG can be attributed to guar gum structure (at 101, 95, 81, 72, and 64 ppm), as they are analogous to those present in NGG, and to ^{13}C in a grafted surfactant (hydroxypropyltrimonium) at 55 ppm. The spectra of both CGG-BV3 and CGG-SWy nanocomposites exhibit a series of peaks closely corresponding to CGG biopolymer, the integrity of which is not affected upon interaction with montmorillonite. A minor peak at ~172 ppm is present in the spectra of all materials, suggesting that CGG contains carboxylic acid impurities. As in the instance of NGG (chapter 3.2.2), these impurities are most probably due to presence of proteins from guar seed husks – a common contaminant of guar gum (Cunha *et al*., 2007). Due to a limited treatment of the CGG-nanocomposites (omitted centrifugation and washing steps), impurities are more diluted in the materials than for the NGG-composites, what is reflected by only a minor trace of them in the NMR spectra.

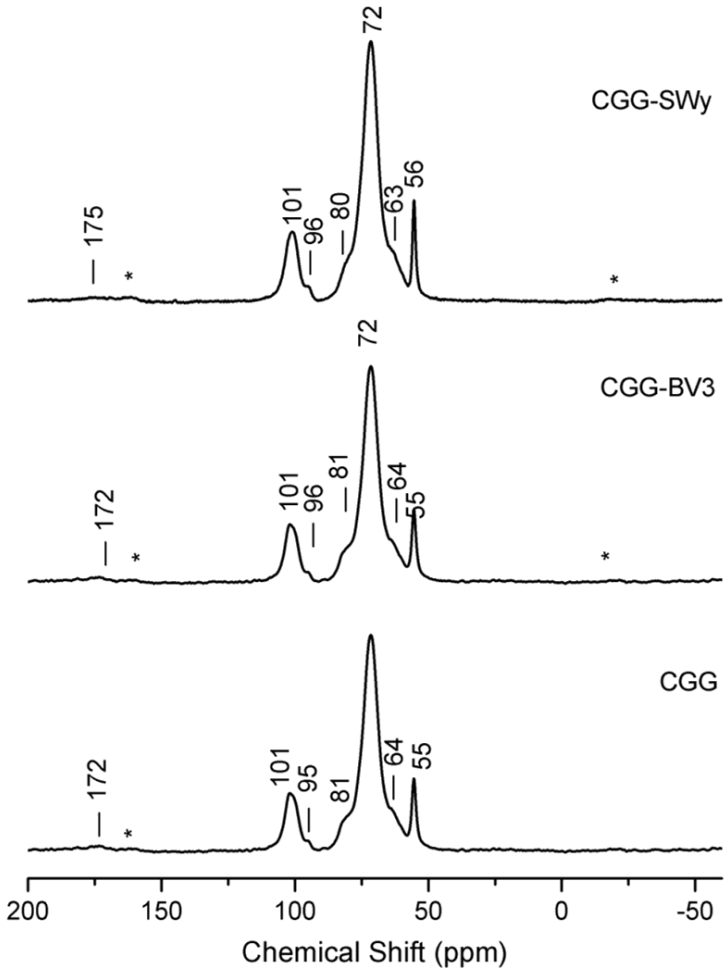

Figure 47. ^{13}C CP MAS spectra of CGG, CGG-BV3 and CGG-SWy nanocomposites.

4. Summary and Conclusions

Neutral guar gum-montmorillonite and cationic guar gum-montmorillonite nanocomposites have been successfully prepared using both the reference clay from the Source Clay Repository (SWy-2) and the Portuguese montmorillonite from the Benavila bentonite deposit.

The presence of biopolymers in the interlayer of clay minerals was evidenced by XRD. Intercalated structures with varied d_{001} spacings have been reported. In the case of NGG, interlayer spacings of 24 Å for Na^+-SWy and 17 Å for Na^+-BV3 were obtained for the washed samples. The nanocomposites prepared with CGG exhibited lower d_{001} values of ~14 Å. Whereas in the case of NGG, the structure of the nanocomposite depends on the clay mineral sample, the nanocomposites prepared with CGG exhibit

similar interlayer spacings for both clays. XRD also indicated that morphologies of the NGG-nanocomposites are altered upon centrifugation. Instead of broad diffraction features, which are present for the materials prior to washing, more defined basal spacings are obtained. TGA and NMR further confirm the presence of the polysaccharide in the prepared materials. DTG traces show changes of NGG stability upon interaction with both clay minerals. Such nanocomposites, with varying morphologies, will be tested as potential excipients for an anti-inflammatory drug Ibuprofen.

Part IV: Preparation of Drug-loaded Guar-Montmorillonite Nanocomposites

‘

1. Aims

In this part of the thesis, preparation of guar-montmorillonite nanocomposites, loaded with an anti-inflammatory drug Ibuprofen is described, and the obtained materials are characterized by XRD, TGA, and NMR.

The main goal was to find an efficient method of drug loading that yields nanocomposites with a relatively high Ibuprofen content. Such systems, where guar-montmorillonite nanocomposite acts as an excipient, are intended for application in modified drug delivery systems (MDDS). In general, due to possible side effects in the gastrointestinal tract caused by Ibuprofen, a decrease in a release rate, without affecting therapeutic level of the drug is desired. Nanocomposites prepared with NGG and CGG were loaded with Ibuprofen using two different methods and their potential as a MDDS was assessed. As far, to the best of my knowledge, there are no reports of guar gum-montmorillonite nanocomposites loaded with Ibuprofen in the literature data.

2. Materials and Methods

2.1. Materials

Clay minerals, and neutral and cationic guar gum, used to prepare drug-loaded nanocomposites, are described in Part II, chapter 2.1.

Ibuprofen (α-Methyl-4-(isobutyl)phenylacetic acid) sodium salt ≥98 %, with a molecular formula $C_{13}H_{17}O_2Na$ and molecular weight of 228.3 g/mol, was supplied from Sigma-Aldrich and used as received (Fig. 48).

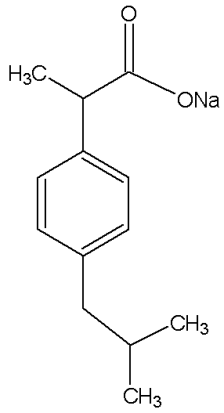

Figure 48. Schematic representation of Ibuprofen sodium salt structure.

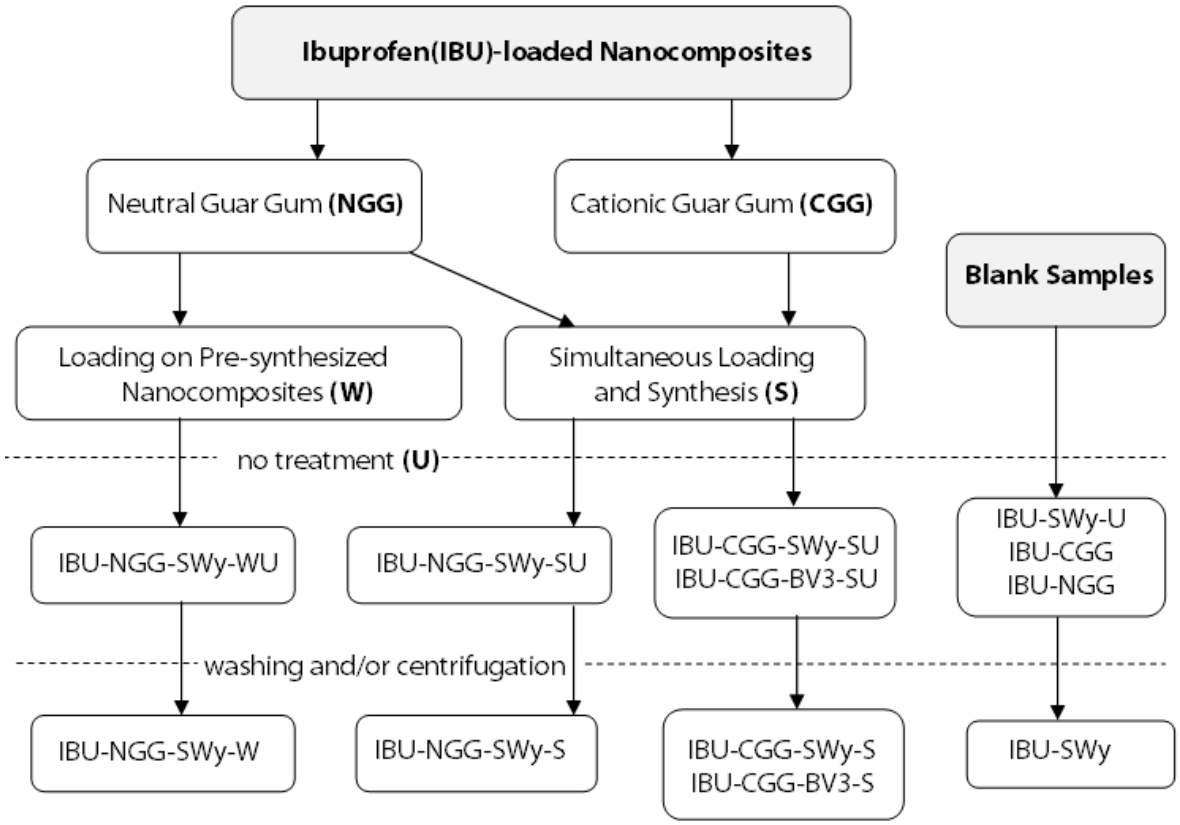

Figure 49. Scheme showing organization of prepared Ibuprofen-loaded materials (SWy - Na^+-saturated Wyoming montmorillonite, BV3 – Na^+- saturated Portuguese Benavila montmorillonite).

2.2. Preparation of Drug-loaded Neutral Guar Gum-Montmorillonite Nanocomposites

2.2.1. Loading of the Drug on a Pre-synthesized Nanocomposite

In this method, Ibuprofen was loaded subsequent to the synthesis of a neutral guar gum-montmorillonite nanocomposite. The chosen sample was a washed NGG-SWy nanocomposite, with an Ibuprofen to nanocomposite mass ratio of 3:1. Typically, 3 g of Ibuprofen sodium salt were dissolved in 500 mL of distilled water and 1 g of the washed NGG-SWy sample was added. The dispersion was stirred for 3 days on a magnetic stirrer at 500 rpm at room temperature. The product was recovered by centrifugation at 5000 rpm for 5 min and the supernatant was discarded. The sample (IBU-NGG-SWy-W) was dried at 50°C and ground using an agate mortar.

Additionally, a similar material has been prepared using the above procedure, where the centrifugation step was omitted and the sample was dried directly after the synthesis. This product is referred to as IBU-NGG-SWy-WU.

2.2.2 Simultaneous Synthesis and Drug Loading

In this 'one-pot' method, synthesis of guar gum-montmorillonite nanocomposites and Ibuprofen loading is simultaneous. Ibuprofen loaded NGG-SWy, CGG-SWy and CGG-BV3 nanocomposites were prepared using similar methods as previously (Part III, chapter 2.2), this time involving the addition of drug.

The NGG-SWy nanocomposite, having NGG : SWy : Ibuprofen mass ratio of 6 : 2 : 1 was prepared using the following procedure. 0.7 g of Na^+-SWy were dispersed in 600 mL of distilled water. Subsequently, 1.4 g of Ibuprofen sodium salt were added to the clay mineral dispersion, followed by addition of 4.2 g of NGG. The mixture was stirred magnetically (1500 rpm) at room temperature for 2 weeks. Some part of the material was removed at that point, dried at 50°C and ground with an agate mortar (labeled as IBU-NGG-SWy-SU). The remaining part of the sample was recovered by centrifugation at 5000 rpm for 5 min, supernatant was discarded, the sample was dried at 50°C and ground with an agate mortar (labeled as IBU-NGG-SWy-S).

The CGG-SWy and CGG-BV3 nanocomposites, having CGG : SWy : Ibuprofen mass ratio of 4 : 2: 1, were prepared using the following procedure. 0.5 g of Na^+-SWy or Na^+-BV3 were dispersed in 1L of distilled water prior to addition of 1.0 g of Ibuprofen sodium salt. After 30 min, 2.0 g of CGG were added to the dispersions and stirred 3 days at 500 rpm, at room temperature. The samples, labeled IBU-CGG-SWy-SU and IBU-CGG-BV3-SU were then dried at 50°C and ground with agate mortar. Subsequently, some part of the both materials was gently washed with water. Typically, ~1.5 g of samples were suspended in 200 mL of distilled water, shaken vigorously in a centrifuge bottle and centrifuged at 5000 rpm for 5 min. The samples were dried at 50°C and ground with an agate mortar. The resulting materials are referred to as IBU-CGG-SWy-S and IBU-CGG-BV3-S.

2.3 Preparation of Blank Samples

2.3.1 Preparation of an Ibuprofen - Montmorillonite Blank

The IBU-SWy blank was prepared keeping the previous Ibuprofen to montmorillonite ratio of 2 : 1, respectively. Typically 0.25 g of Na^+-SWy were dispersed in 0.5 L of distilled water, prior to addition of 0.5 g of Ibuprofen sodium salt. The suspension was stirred for 3 days using a magnetic stirrer (500 rpm) at room temperature. Subsequently, the product, labeled as IBU-SWy-U, was dried at 50°C and ground with an agate mortar.

Additionally, a similar material has been prepared using the above procedure, where prior to drying, the materials were centrifuged at 10 000 rpm for 5 min. The supernatant was discarded, and the recovered montmorillonite was dried at 50°C, ground with an agate mortar and labeled as IBU-SWy.

2.3.2. Preparation of Ibuprofen – Guar Gum Blank Samples

The blanks were prepared keeping the guar gum to Ibuprofen ratio from the previous experiments – 3:1 for the IBU-NGG blank and 2:1 for the IBU-CGG blank.

Typically, 200 mg of NGG and 66 mg of Ibuprofen sodium salt were dissolved in 100 mL of distilled water. Similarly, 200 mg of CGG and 100 mg of Ibuprofen sodium salt were dissolved in 100 mL of distilled water. Both samples were shaken for 3 days on a platform shaker (300 rpm) at room temperature. Subsequently, the samples were dried at 50°C and ground with an agate mortar.

2.4. Determination of Drug Loading

The content of Ibuprofen in the prepared materials was determined using a modified method adapted from Ribeiro *et al*., 2013 and Wang *et al*., 2009. Typically, 20.0 mg of a drug loaded material were placed in a plastic tube, which was ten filled with 50 mL of phosphate buffer (pH 7.4), prepared according to U.S. Pharmacopeia (Buffer Solutions). The tube was shaken for 3 days on a platform shaker (300 rpm), at room temperature. Subsequently, the solution was sonicated using a constant pulse program for 5 minutes. In the next step the solution was filtered using a qualitative paper filter. The tube was filled again with a known amount of fresh phosphate buffer in order to rinse it, and this solution was filtered, too. The experiment was performed in triplicate for each sample. The concentration of the Ibuprofen was measured in the collected filtrate using a Genesys10S UV-Vis Spectrometer and a quartz cuvette at λ_{max} = 222 nm. The filtrate samples required dilution (absorbance >1) and UV-Vis measurements were carried out in triplicate, as well. The error was expressed as a standard deviation.

Drug loading (DL) and drug loading efficiency (DLE) were calculated according to the following equations (Ambrogi *et al*., 2008):

$$\% \text{ DL} = \frac{mass\ of\ drug\ in\ the\ material\ (mg)}{mass\ of\ the\ material\ (mg)} * 100\%$$

$$\% \text{ DLE} = \frac{mass\ of\ drug\ loaded\ (=DL\ of\ the\ treated\ sample)\ (mg)}{total\ mass\ of\ drug\ added\ (=DL\ of\ the\ untreated\ sample)\ (mg)} * 100\%.$$

DL is an experimentally determined value. DLE is a simple recalculation of the DL parameter, and it is used to express how much drug is lost during centrifugation or washing.

2.5. Characterization Techniques

The prepared materials were characterized by the means of XRD, TGA and NMR techniques, which were described in the previous part of the thesis (Part III, chapter 2.4.).

2.5.1. UV-Vis Spectrometry

UV-Vis Spectrometry was performed using a Genesys10S UV-Vis single beam spectrometer. The measurements were carried out in an absorbance mode, in a wavelength range 200 – 300 nm, using a quartz cuvette. The resolution of a scan was 1 nm, and the scan speed was medium. The maximum absorbance of Ibuprofen was measured at λ = 222 nm, using pH 7.4 phosphate buffer (prepared according to U.S. Pharmacopeia) as a solvent.

The calibration curve was obtained using six solutions with a known Ibuprofen sodium salt concentration. The solutions were prepared using pH 7.4 phosphate buffer as a solvent. A stock solution with Ibuprofen concentration of 20 mg/100 mL was prepared and after a series of dilutions, the following Ibuprofen solutions were obtained: 2.0 mg/100 mL, 1.5 mg/100 mL, 1.0 mg/100 mL, 0.5 mg/100 mL, 0.25 mg/100 mL, 0.1 mg/100 mL. The background was collected using the pH 7.4 phosphate buffer as a reference before measurements.

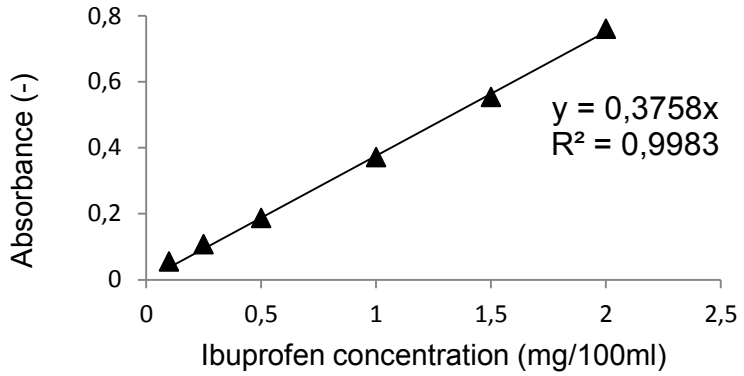

Figure 50. UV-Vis absorbance calibration curve for Ibuprofen in pH 7.4 phosphate buffer, measured at λ_{max} = 222 nm.

3. Results and Discussion

3.1. Drug Loading Determination

Figure 51 presents the drug loading (DL) and drug loading efficiency (DLE) for the prepared Ibuprofen-loaded samples. DL corresponds to mass % of Ibuprofen in the prepared materials and was determined for all the samples by the previously described dissolution test. DLE expresses the amount of the drug that remains in the samples after centrifugation or washing. Since the untreated samples did not undergo washing or centrifugation, their DLE is equal to 100%. On the basis of that, DLE for the treated samples can be recalculated from the experimentally determined DL values (Chapter 2.4).

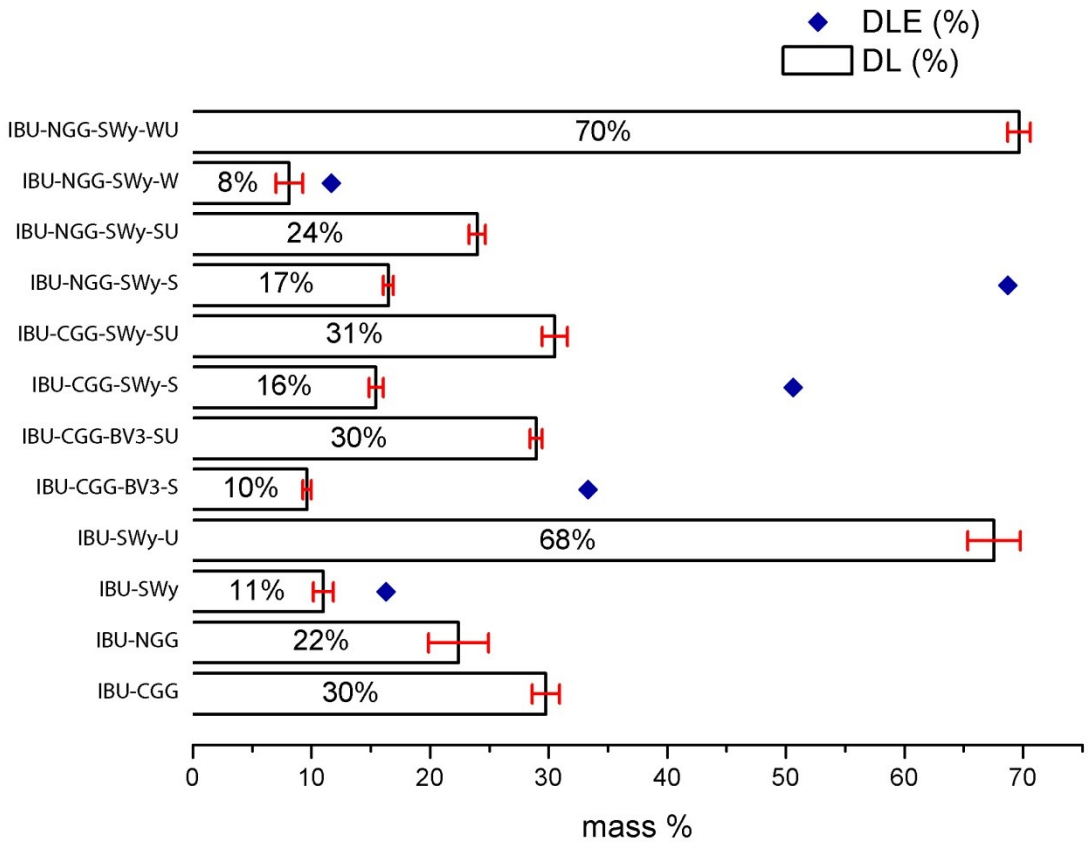

Figure 51. Determination of drug loading (DL %) and drug loading efficiency (DLE %) for the prepared materials.

The initial Ibuprofen content varied between samples prepared by the two different methods. When the drug was loaded subsequent to the synthesis of nanocomposite (W), Ibuprofen to nanocomposite ratio was equal 3:1. In the second method (simultaneous synthesis and loading - S), the drug to clay mineral ratio was 2:1. Despite the initial high content of Ibuprofen in the sample prepared by the first

method (IBU-NGG-SWy-WU), majority of the drug is lost upon centrifugation (~90%). In the second method of synthesis (S), the obtained DLE values are significantly higher. In spite of this, this way of preparing Ibuprofen-loaded materials would be suitable for future optimization. Desirably, the highest DLE values should be obtained by adjusting the contents of all the three components of nanocomposites. The DL and DLE results are discussed more thoroughly in the following chapters, when characterizing the obtained materials.

3.2. Ibuprofen – Montmorillonite Blank

Due to the high complexity of Ibuprofen-biopolymer-clay systems, it is vital to study an interaction of montmorillonite and Ibuprofen, first. XRD diffractograms IBU-SWy-U, and IBU-SWy blank samples are presented in Figure 52, and compared to the starting Na^+-SWy montmorillonite.

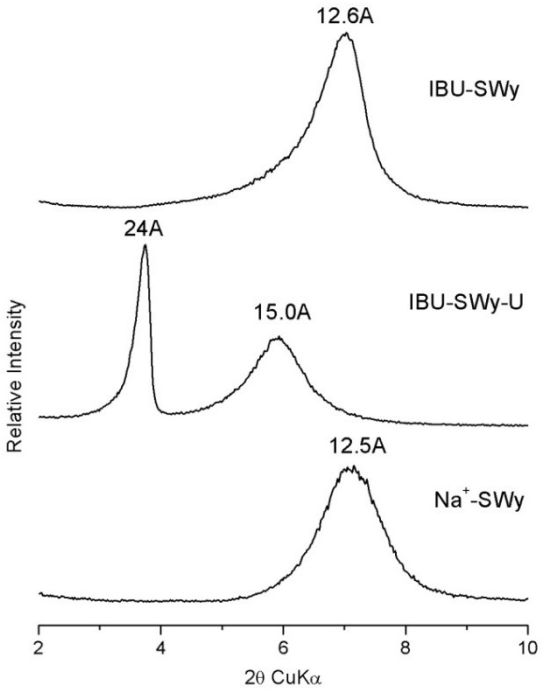

Figure 52. XRD diffractograms of Na^+- SWy montmorillonite, IBU-SWy-U, and IBU-SWy blank samples.

The untreated sample (IBU-SWy-U) shows a significant enhancement of d_{001} spacing from 12.5 Å to 15.0 Å, suggesting intercalation of Ibuprofen salt into the clay mineral interlayer. The intense peak at 24 Å is due to external Ibuprofen that crystallized on the clay mineral surface. However, after centrifugation, the (001) reflection of IBU-SWy is reduced to 12.6 Å, which corresponds to the starting clay mineral. This indicates that Ibuprofen adsorbed in the interlayer is easily replaced by water molecules. Additionally, a major part of crystalline Ibuprofen is also removed, as

the peak at 24 Å, which is typical for Ibuprofen sodium salt, disappears. Upon centrifugation, the amount of IBU is reduced from the initial 68% to 11%, showing DLE of 16% (Fig. 51). For the centrifuged sample, IBU is surface-adsorbed. Ibuprofen-intercalated montmorillonite complexes were also obtained by Zheng *et al*., 2007, where the clay interlayer spacing varied from 13.2 Å to 15.7 Å, depending on the initial Ibuprofen concentration.

The DTG traces of the untreated IBU-SWy-U, and centrifuged IBU-SWy samples are presented in Figure 53, in a reference to the DTG traces of Ibuprofen sodium salt (IBU), and a physical mixture of IBU and Na^+-SWy in a mass ratio 3:1. The corresponding TG traces are shown in Figure 54.

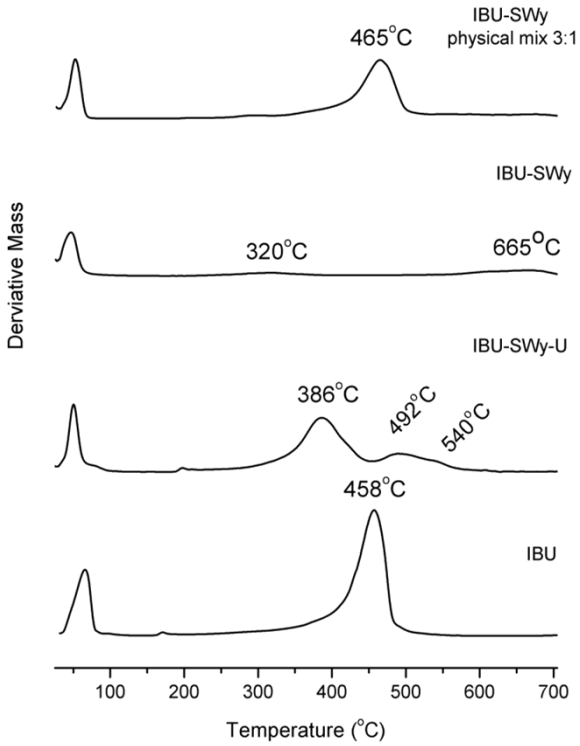

Figure 53. DTG traces of Ibuprofen sodium salt (IBU), IBU-SWY-U and IBU-SWy blank samples, and IBU-SWy physical mixture (3:1 mass ratio).

Thermogravimetric analysis revealed that pyrolysis of IBU is altered upon interaction with Na^+-SWy. Whereas IBU is pyrolysed between 300°C and 500°C, what is indicated by the single DTG peak centered at 458°C, the DTG trace of IBU-SWY-U shows two major DTG peaks with maxima at 386°C and 492°C, and a shoulder at 540°C. Knowing that some part of Ibuprofen underwent intercalation in IBU-SWY-U, one may attribute the higher thermal stability of IBU to this process. As such, the DTG peak at 386°C possibly corresponds to the externally absorbed part of IBU, which, on

the other hand, has a lower thermal stability comparing to the IBU blank. This may be further observed in the DTG traces of IBU-SWy and IBU-SWy physical mixture, where there are small, broad peaks, centered around 320°C. In the case of IBU-SWy physical mixture, a vast majority of IBU is pyrolysed at temperatures typical for the drug, showing no change in the drug crystallinity. In conclusion, a thermal stability of IBU may be increased or decreased upon interaction with montmorillonite, as in the case of IBU-NGG and IBU-CGG blank samples. The altered thermal stability of IBU may be also due to changes in the drug crystallinity upon its dissolution and drying (Dubernet *et al*., 1990).

Due to low IBU loading for the IBU-SWy sample (11%), a dehydroxylation step of montmorillonite is detectable (a broad DTG peak centered at 665°C).

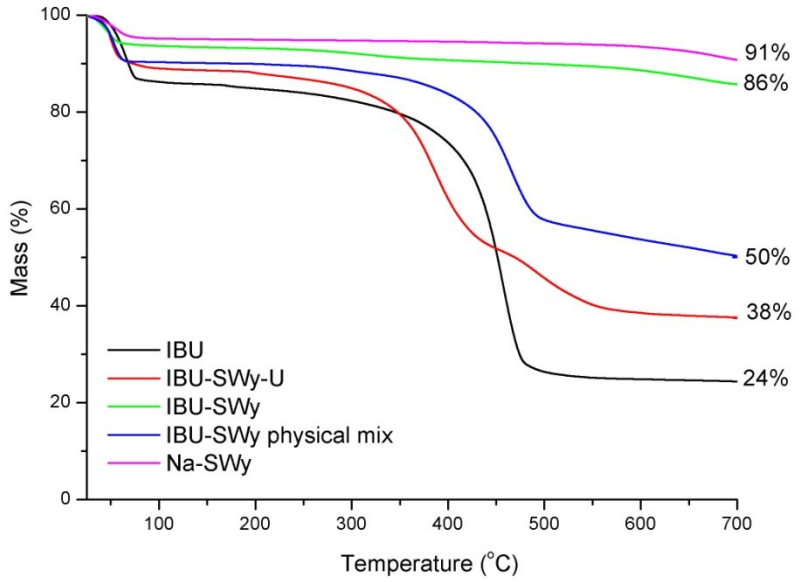

Figure 54. TG traces of Ibuprofen sodium salt (IBU), IBU-SWY-U and IBU-SWy blank samples, IBU-SWy physical mixture (3:1 mass ratio), and Na^+-SWy montmorillonite.

3.3 IBU-NGG and IBU-CGG Blank Samples

In the next step, interaction of NGG and CGG with IBU was analyzed by TGA for the IBU-NGG and IBU-CGG blank samples (Fig. 55).

The IBU-NGG and IBU-CGG systems are more complicated since they have two organic components. The DTG traces, compared to starting NGG, CGG, and IBU, show an altered behavior of both IBU and guar gum on pyrolysis. Starting NGG is

pyrolysed in a single step with the DTG peak centered at 304°C. In the instance of the IBU-NGG blank sample, there are three major weight loss steps (with DRG maxima at 242°C, 270°C and 587°C), apart from water loss at around 50°C. The absence of a major feature around 450°C, typical for IBU, suggests that the drug may be pyrolysed at lower temperatures (around 250°C), together with NGG, or at higher temperatures (around 580°C). Since the polymeric chains of NGG contain a large amount of –OH groups, the possible interaction of NGG and IBU may involve hydrogen bonding and weak van der Waals forces (Depan *et al*., 2008).

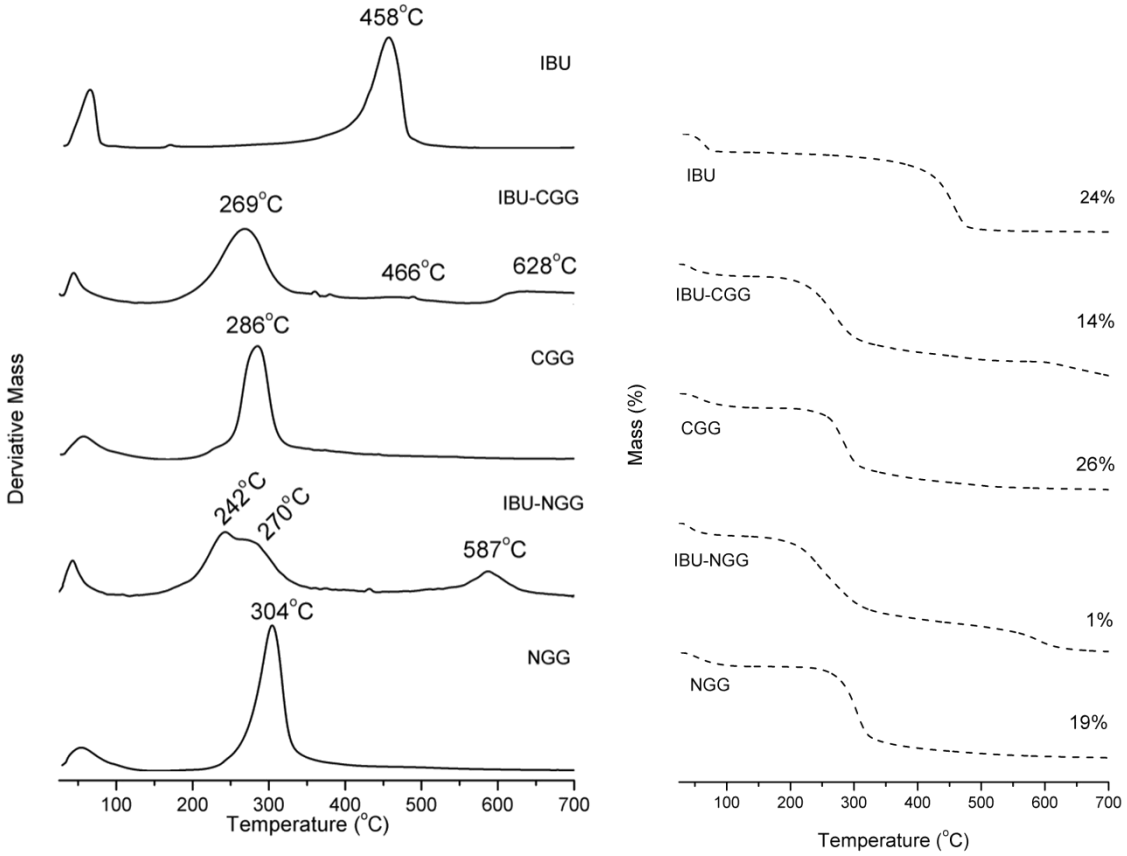

Figure 55. DTG traces (left) and TG traces (right) of IBU-NGG and IBU-CGG blank samples, compared to NGG, CGG, and Ibuprofen sodium salt (IBU).

The DTG trace of IBU-CGG reveals a similar situation – the DTG peak that is typical for CGG pyrolysis (centered at 286°C) is shifted to lower temperatures, and the additional, broad peak appears at around 630°C. In analogy with the IBU-NGG blank, IBU may be pyrolysed together with CGG at a lower temperature or at higher temperature, comparing to starting IBU. In the case of positively charged CGG, the interaction with IBU may also involve electrostatic interaction, as IBU, weak acid (pKa = 4.91; The DrugBank Database), dissociates to anionic species. However, the

most probable explanation for the altered behavior of IBU on pyrolysis is a change in its crystallinity. Apart from the fact that IBU may form different crystal polymorphs, upon interaction with polymers and porous solids, it can be present in an amorphous form or as molecular dispersion within a polymeric matrix (Dubernet *et al*., 1990; Saravanan *et al*., 2003; Azais *et al*., 2006).

The DTG peaks present at higher temperatures may as likewise correspond to thermal events arising from alteration of the earlier decomposition products. In conclusion, this complex behavior of IBU on pyrolysis may be influenced by a number of factors, e.g. drug crystallinity, interaction with guar gum, morphology of samples, degree of grinding, etc.

3.4. IBU-NGG-SWy-WU and IBU-NGG-SWy-W Nanocomposites

The first Ibuprofen-loaded samples (IBU-NGG-SWy-WU and IBU-NGG-SWy-W) were prepared using a pre-synthesized nanocomposite – the NGG-SWy washed sample. The XRD diffractograms of these samples are presented in Figure 56, and compared to the starting material.

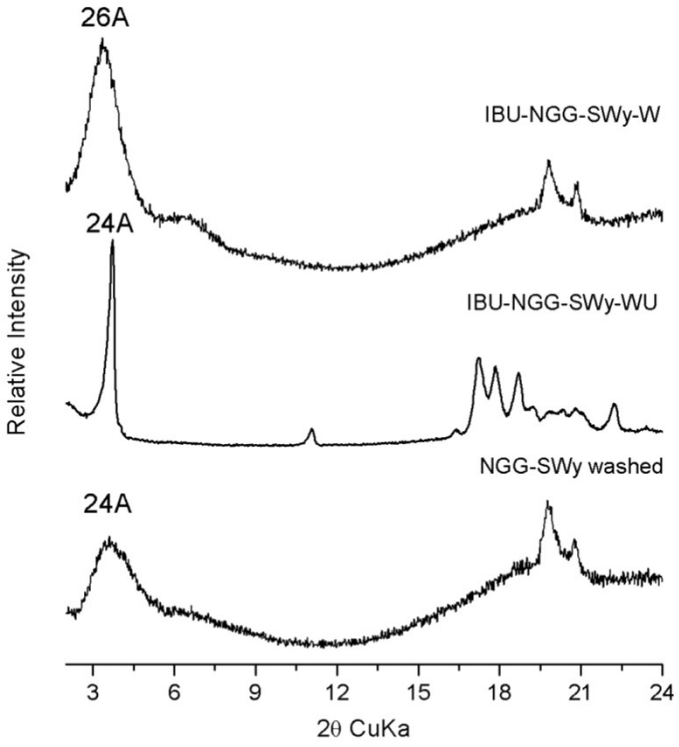

Figure 56. XRD powder diffractograms of IBU-NGG-SWy-WU and IBU-NGG-SWy-W in reference to the starting material – NGG-SWy washed nanocomposite.

The XRD pattern of the unwashed sample (IBU-NGG-SWy-WU) shows a number of diffraction peaks characteristic for crystalline IBU (the first two at 24 Å, 8 Å

and multiple reflections in 16-22°2θ range), what is associated with the high initial IBU loading (70%). The (001) plane reflection of Na^+-SWy is not evidenced as it most likely superimposed with the 24 Å IBU peak, or it may be not present due to possible exfoliation (Theng, 2012). The XRD pattern of the centrifuged, IBU-NGG-SWy-W sample exhibits a well-pronounced diffraction peak at 26 Å, and no peaks that could be associated with crystalline IBU. As there is a slight enhancement of d_{001} spacing in comparison with starting NGG-SWy, there is no evidence of significant NGG loss from the interlayer upon redispersion of the sample in distilled water during IBU loading. Additionally, it is not excluded that some part of IBU may be cointercalated with NGG in the interlayer space of montmorillonite.

Knowing that behavior of IBU on pyrolysis may be altered by interaction with both montmorillonite and guar gum (Fig. 53 and Fig. 55), one may expect even a greater complexity in the systems, where these three components are present. Figure 57 shows DTG traces and TG traces of IBU-NGG-SWy-WU and IBU-NGG-SWy-W in comparison with the starting washed NGG-SWy sample.

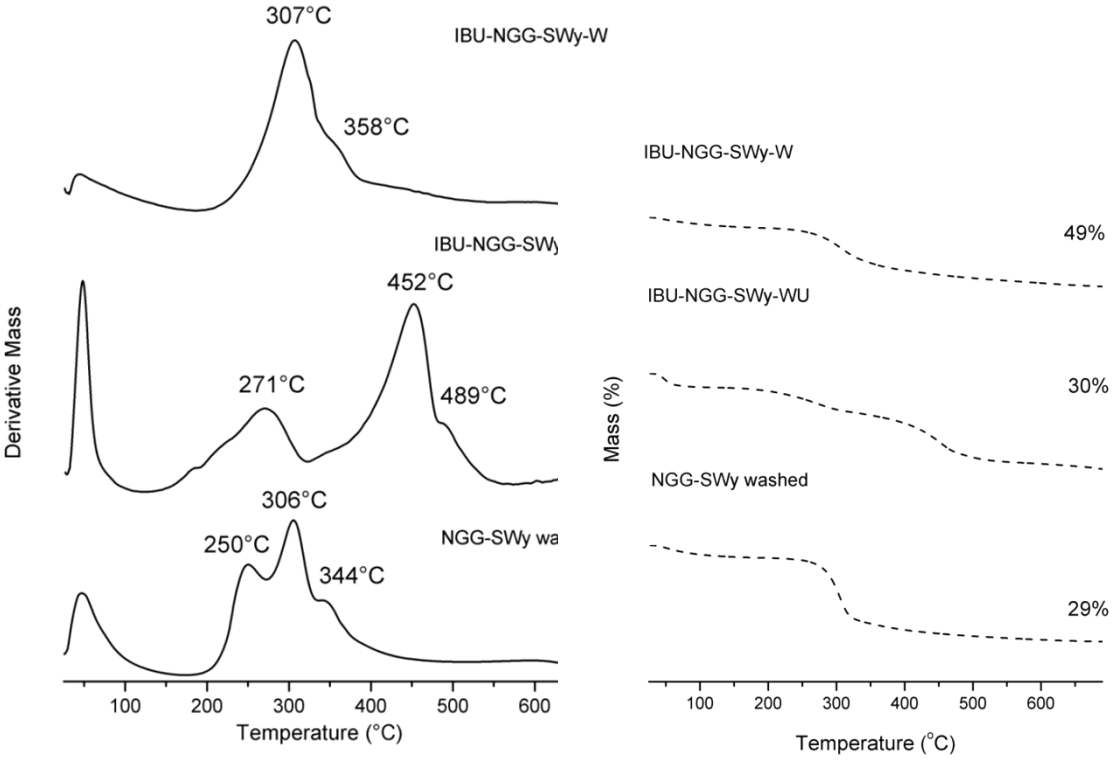

Figure 57. DTG traces (left) and TG traces (right) of IBU-NGG-SWy-WU and IBU-NGG-SWy-W compared to the starting material – the washed NGG-SWy nanocomposite.

The presence of a respectively high amount of externally crystallized IBU (as earlier evidenced by XRD) is also revealed by TGA for the IBU-NGG-SWy-WU

sample. The DTG peak centered at 452°C clearly corresponds to that of IBU (Fig. 55). The centrifuged IBU-NGG-SWy-W sample, with a lower IBU loading (8%), exhibits only a minor broad feature in that temperature region. The shoulder centered at 489°C in the DTG trace of IBU-NGG-SWy-WU may possibly indicate that some amount of IBU underwent intercalation in the montmorillonite interlayer space. This is suggested by a DTG peak at similar temperature, which was evidenced before for the IBU-SWy-U blank sample (Fig. 53).

Also the behavior of NGG on pyrolysis is altered. In the case of IBU-NGG-SWy-WU, one broad peak, centered at 271°C, replaced the three-step feature, characteristic for the unwashed NGG-SWy sample. This may be due to a change in morphology upon redispersion of the sample and interaction with IBU. The DTG trace of IBU-NGG-SWy-W reveals a presence of the major peak with a maximum at 307°C and the shoulder at 358°C. This feature most likely results from parallel pyrolysis of interacting NGG and IBU as in the case of the IBU-NGG blank, and a change in IBU crystallinity (Fig. 55) (Saravanan *et al*., 2003).

Overall, the prepared Ibuprofen-loaded IBU-NGG-SWy-W nanocomposite exhibits low drug loading (DL) of 8% and low drug loading efficiency (DLE) of 12%. DLE is lower than for Na^+-SWy alone, in which case it reaches 16%. This suggests that, due to presence of NGG adsorbed on the clay mineral surfaces, interaction of IBU with the clay mineral could be limited. Also the fact that the samples were redispersed from powder, suggests that a degree of grinding can strongly limit the surface area of nanocomposite, which is accessible for interaction of IBU.

3.5. IBU-NGG-SWy-SU and IBU-NGG-SWy-S Nanocomposites

Since, in the instance of the IBU-SWy-NGG-W sample, the obtained DLE was quite low (12%), another method of preparation drug-loaded nanocomposites was desired. The next set of samples was prepared by a ‘one-pot’ method, in which IBU was loaded on the nanocomposites, directly during their synthesis. The IBU-biopolymer-montmorillonite ratio was kept unchanged with respect to NGG-SWy 6:1 nanocomposites, to allow comparison of these materials.

The XRD diffractograms of the IBU-NGG-SWy-SU and IBU-NGG-SWy-S samples, obtained by this direct method, are presented in Figure 58, and compared to the diffraction pattern of crystalline IBU. In the case of IBU-NGG-SWy-SU, its XRD pattern closely resembles that of the IBU-NGG-SWy-WU sample, revealing peaks corresponding to IBU and a lack of montmorillonite’s (001) plane reflection. There is

a major amount of crystalline IBU, even though the initial IBU content was reduced from 70% to 24%, in comparison with the previous method of preparation. The presence of clay is evidenced by the peak typical for phyllosilicates at 4.49 Å, which is more pronounced in the XRD pattern of IBU-NGG-SWy-S. The increasing background, starting from ~13° 2θ is due to an amorphous NGG component.

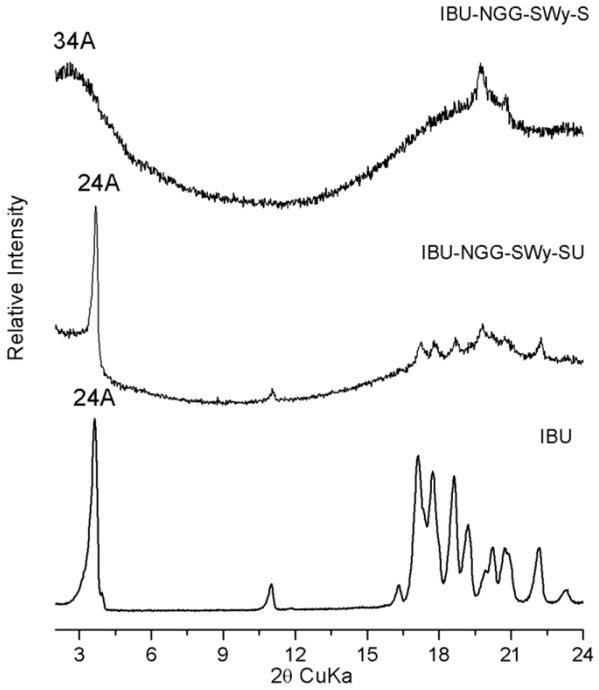

Figure 58. XRD diffractograms of IBU-NGG-SWy-SU and IBU-NGG-SWy-S compared to the Ibuprofen sodium salt diffraction pattern (IBU).

The interlayer spacing of the centrifuged IBU-NGG-SWy-S sample is not well defined, as the (001) plane reflection of that sample is very broad and present at low 2θ angle values. The estimated d_{001} value of 34 Å indicate that NGG was introduced into the interlayer space of Na^+-SWy and that a nanocomposite with the intercalated structure was obtained. Because the feature is broad and diffuse, the sample may exhibit some degree of exfoliation, too. Additionally, the high interlayer spacing may suggest that some part of IBU is intercalated together with NGG. The lack of peaks, typical for crystalline IBU, indicates that the excess of this salt was removed upon recuperation by centrifugation and the drug molecules are homogenously dispersed within the polymer matrix (Dubernet *et al*., 1990). Interestingly, IBU content was reduced only by 7% comparing to IBU-NGG-SWy-SU, and this sample exhibits the highest DLE of 70%. This indicates a higher efficiency of this method, where all three components are dispersed homogenously in the solvent during the synthesis, in contrast with the first method of preparation (W).

The presence of NGG and IBU in the IBU-NGG-SWy-SU and IBU-NGG-SWy-S samples was further confirmed by TG and DTG (Fig. 59). The decomposition of NGG was slightly shifted to lower temperatures, alike for the previously obtained materials (DTG peaks centered at 290°C and 295°C for the untreated and centrifuged samples, respectively).

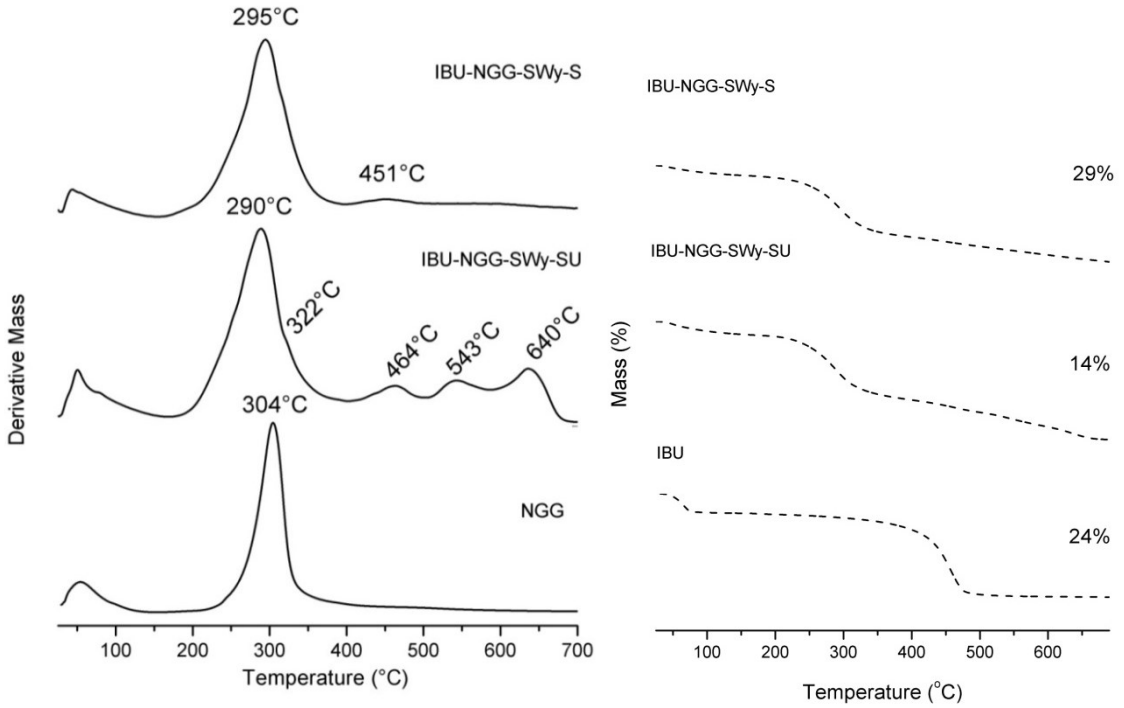

Figure 59. DTG traces (left) and TG traces (right) of IBU-NGG-SWy-SU and IBU-NGG-SWy-S compared to the starting biopolymer – NGG.

In the case of IBU-NGG-SWy-SU, the behavior of IBU on pyrolysis is complex. Apart from the DTG peak with a maximum at 290°C, there is a shoulder centered at 322°C and a series of three minor peaks with maxima at 464°C, 543°C and 640°C. Whereas, the peak at 464°C probably corresponds to crystallized IBU salt, the other features suggest that the drug is dispersed within polymer matrix, where it interacts with NGG and montmorillonite in varied environments, what affects its thermal stability (Dubernet *et al*., 1990; Saravanan *et al*., 2003).

The DTG trace of IBU-NGG-SWy-S reveals the presence of one major peak centered at 295°C and a minor, broad feature at around 451°C. The lack of features at 543°C and 640°C may suggest that they were due to IBU associated with excess NGG, which was then removed upon centrifugation. This is in accordance with the DTG trace of IBU-NGG, showing a peak centered at 587°C (Fig. 55). As there is also no peak that was associated before with intercalated IBU (IBU-SWy-U; Fig. 53), there

is probably no IBU in the interlayer space of montmorillonite. However, given that NGG occupies this space, IBU behavior may be further altered if it is intercalated together with the biopolymer. Finally, the DTG broad thermal event at ~450°C may be associated with some amount of crystalline IBU.

3.6. IBU-CGG-SWy-SU and IBU-CGG-SWy-S Nanocomposites

Another set of Ibuprofen-loaded materials was prepared with cationic guar gum and Na^+-SWy or Na^+-BV3 montmorillonite samples, by a solvent intercalation method with a simultaneous drug loading ('one-pot' method). The choice of CGG was motivated by the fact that its possible interaction with IBU will be stronger than for NGG. IBU is a weak acid that dissociates producing anionic species, which could interact with CGG electrostatically.

Figures 60 and 62 show enhancements of interlayer spacing of both IBU-CGG-SWy-SU (from 12.5 Å to 14.3 Å) and IBU-CGG-BV3-SU (from 12.9 Å to 14.3 Å), comparing to the starting SWy and BV3 montmorillonite (Fig. 44). This increase indicates that nanocomposites with intercalated structures were obtained. XRD diffractograms of the IBU-CGG-SWy-SU and IBU-CGG-SWy-S samples are presented in Figure 60, and compared to the CGG-SWy sample with the same biopolymer to clay ratio. In spite of IBU presence, during preparation of the nanocomposites, IBU-CGG-SWy-SU exhibits a very similar interlayer spacing to CGG-SWy (14.5 Å and 14.3 Å, respectively), suggesting that only CGG underwent intercalation between montmorillonite layers. After washing treatment, the IBU-CGG-SWy-S sample retained the interlayer spacing of 14.7Å, showing that the nanocomposite is stable and CGG in not easily removed by washing with distilled water.

The peaks at 8.0 Å present for both IBU-loaded sample, correspond to crystalline IBU, what suggests that the washing was not efficient for the IBU-CGG-SWy-S sample. However, the powder diffractogram of IBU-CGG-SWy-S (Fig.61) reveals that the amount of crystalline IBU has been significantly reduced in comparison with the unwashed IBU-CGG-SWy-SU nanocomposite.

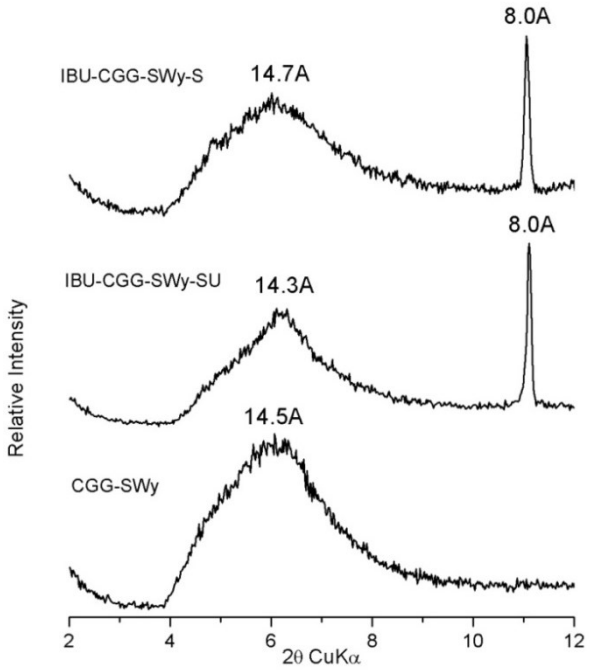

Figure 60. XRD diffractograms of IBU-CGG-SWy-SU and IBU-CGG-SWy-S in comparison to the CGG-SWy nanocomposite (oriented mounts).

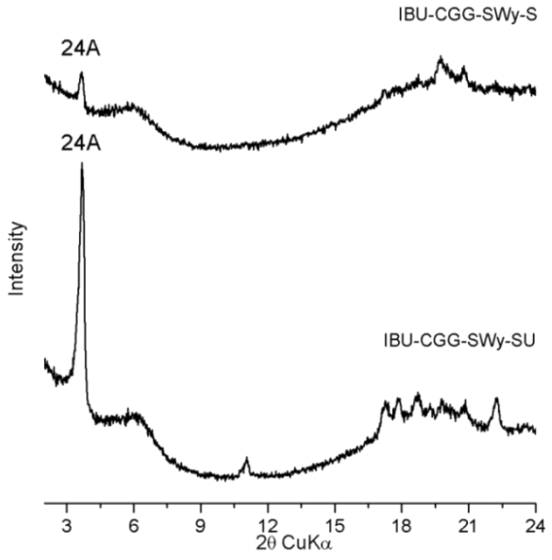

Figure 61. XRD powder diffractograms of IBU-CGG-SWy-SU and IBU-CGG-SWy-S.

The DTG traces and TG traces for IBU-CGG-SWy-SU and IBU-CGG-SWy-S are presented in Figure 62, and compared with CGG-SWy.

The dominant DTG peak for each trace is centered at around 280°C. According to the CGG-SWy trace, this peak corresponds to decomposition of CGG. However, as discussed earlier in the instance of the CGG-IBU blank sample (Fig. 55), a certain part of IBU may be also pyrolysed in this temperature range. In the case of IBU-CGG-

SWy-SU, the relatively small DTG peak with a maximum at 458°C may be attributed to decomposition of crystalline IBU, similarly as for other samples (IBU-NGG-SWy-WU and IBU-NGG-SWy-SU). The unwashed sample IBU-CGG-SWy-S, exhibits only a very minor and broad feature in this temperature range. This is in accordance with XRD data, showing that the prevalent amount of crystalline IBU was removed from the sample (Fig. 61). Apart from that, there are only minor features in the DTG traces that can be attributed to pyrolysis of IBU (centered at 565°C for the unwashed sample and at around 590°C for the washed one). This further suggests that a certain part of dispersed, amorphous IBU is pyrolysed at lower temperatures as the DL is only reduced from 31% to 16% upon washing.

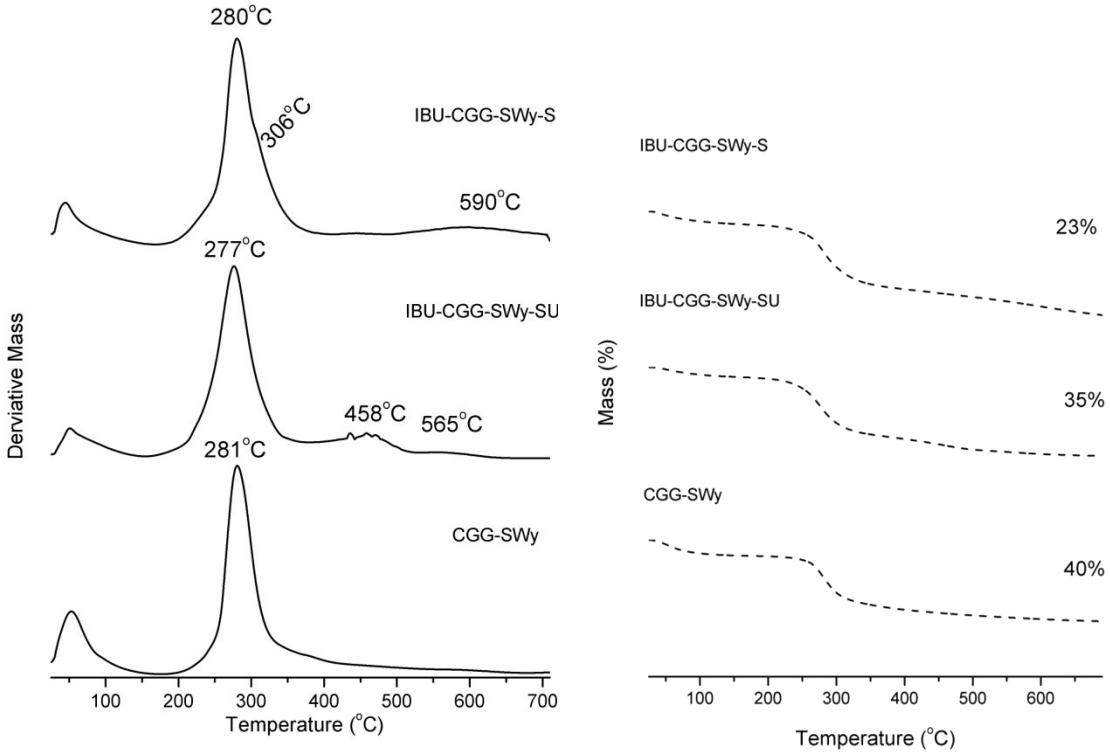

Figure 62. DTG traces (left) and TG traces (right) of IBU-CGG-SWy-SU and IBU-CGG-SWy-S compared to the CGG-SWy nanocomposite.

3.7. IBU-CGG-BV3-SU and IBU-CGG-BV3 Nanocomposites

Ibuprofen-loaded CGG composites, were also prepared with the Portuguese montmorillonite from the Benavila deposit – BV3.

XRD diffractograms of the IBU-CGG-BV3-SU and IBU-CGG-BV3-S samples are presented in Figure 63, along with the reference sample (CGG-BV3). XRD reveals

a similar enhancement of BV3 interlayer spacing in case of the Ibuprofen-loaded nanocomposite, as for the CGG-BV3 sample (14.3 Å for both samples). The washed sample, IBU-CGG-BV3-S , also exhibits a similar d_{001} value (14.3 Å), indicating that in the case of Portuguese montmorillonite, the nanocomposite is as well stable upon washing with water and centrifuging (Fig. 63).

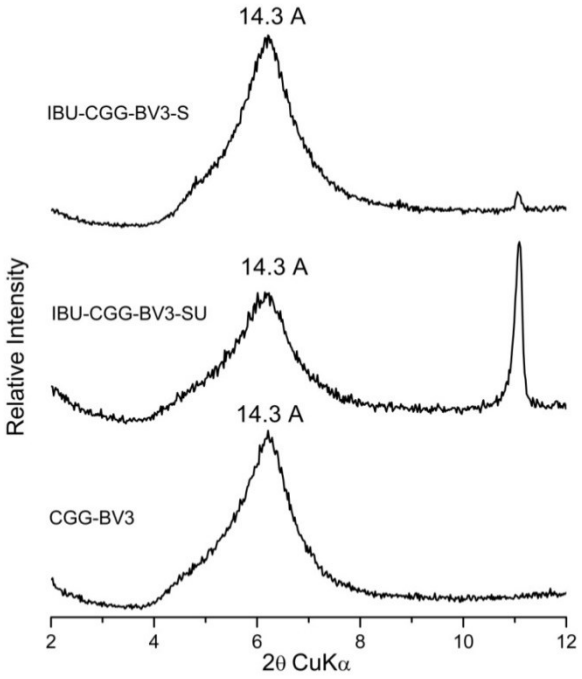

Figure 63. XRD diffractograms of IBU-CGG-BV3-SU and IBU-CGG-BV3-S, compared to the CGG-SWy nanocomposite (oriented mounts).

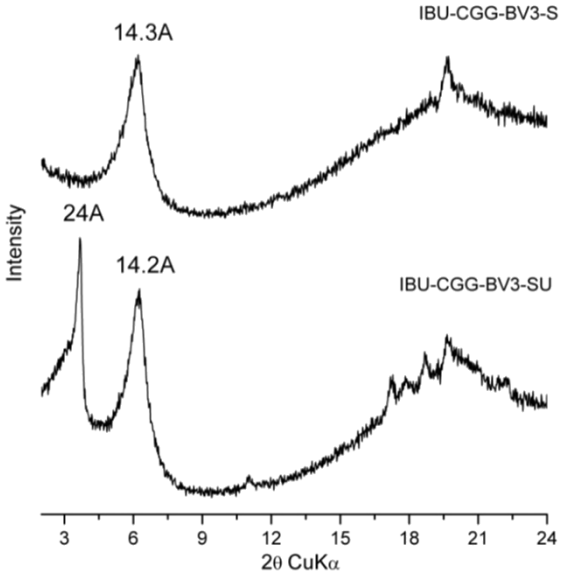

Figure 64. XRD powder diffractograms of IBU-CGG-BV3-SU and IBU-CGG-BV3-S.

Whereas the diffraction pattern of powdered samples (Fig. 64) suggests that there is no surface crystallized IBU present, in the case of washed sample (no peak at 24 Å), the oriented mounts still reveal its minor amount (presence of the peak at 8.0 Å) (Fig. 63).

Repeatability of the obtained interlayer spacing for both montmorillonite samples in the CGG-nanocomposites results from a strong electrostatic interaction between cationic biopolymer and the negatively charged clay surface, which may affect the ordering of clay layers in the polymeric matrix (Mansa & Detellier, 2013). Since Ibuprofen is present in the solution as anionic species, there is a preference to uptake CGG in the interlayer by clay minerals. As such, Ibuprofen is most likely dispersed in a polymeric matrix, interacting with both clay mineral layers and polymeric chains.

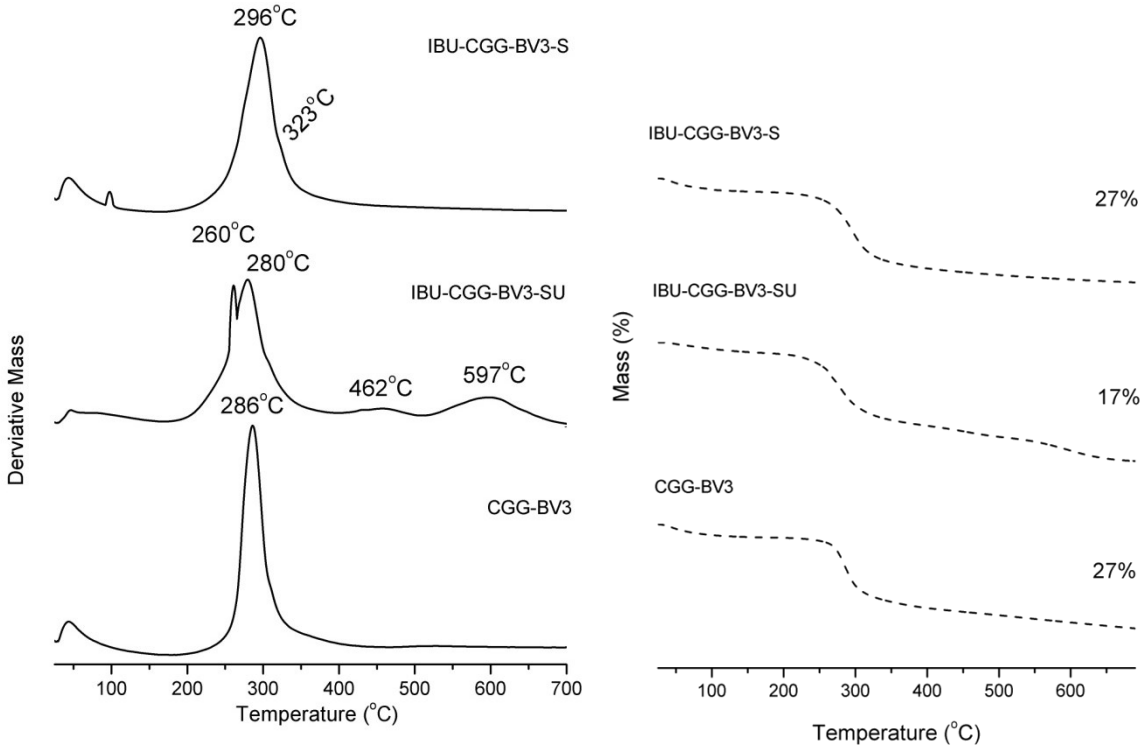

Figure 65. DTG traces (left) and TG traces (right) of IBU-CGG-BV3-SU and IBU-CGG-BV3-S compared to the CGG-BV3 nanocomposite.

The DTG traces and TG traces for IBU-CGG-BV3-SU and IBU-BV3-SWy-S are presented in Figure 65, and compared with CGG-BV3. The pyrolysis of CGG occurs between 250°C and 350°C, what is reflected by the DTG maximum at 286°C, for the reference CGG-BV3 sample. Upon addition of IBU, DTG traces are altered, confirming the uptake of IBU.

The DTG trace of IBU-CGG-BV3-SU resembles the trace of the similar sample prepared with the reference SWy montmorillonite (IBU-CGG-BV3-SU), except for one unexpected peak, centered at 260°C. The feature centered at 462°C can be associated with pyrolysis of crystalline IBU, in accordance with IBU DTG trace (Fig. 55). The presence of another broad peak, with a maximum at 597°C again suggests a complex interactions of IBU and CGG on heating. The most intense peak, centered at 280°C, corresponds to pyrolysis of CGG together with some part of IBU, as discussed before (Fig. 55). Its feature is broader and slightly shifted towards lower temperatures, comparing to CGG-BV3. The unexpected peak at 260°C may be associated with IBU pyrolysis, however, this was not evidenced for any of the other samples and suggests an experimental artifact.

The DTG trace of the washed IBU-CGG-BV3-S sample also resembles the trace of its counterpart prepared with Na^+-SWy (IBU-CGG-SWy-S). However, in the case of Portuguese montmorillonite, the major peak, with a maximum at 296°C and a shoulder at 323°C, is shifted towards higher temperatures. As there is no other feature than can be associated with pyrolysis of IBU (DL of 10%), both CGG and IBU are pyrolysed around 300°C.

DLE for the samples prepared with the cationic guar gum was quite high. For IBU-CGG-SWy-S, it reached 51 %, and for the nanocomposite with the Portuguese clay, IBU-CGG-BV3-S, it was lower and reached 33%. In general, the nanocomposites prepared with CGG show a lower DLE than the IBU-NGG-SWy-S sample, prepared by a similar method with NGG. However, these samples are not directly comparable, as the CGG-nanocomposites were washed with water and the biopolymer content was higher in the case of NGG (67 % initially, compared to 57% for CGG).

3.8 Solid State Nuclear Magnetic Resonance Spectroscopy

NMR spectra of the centrifuged, Ibuprofen-loaded samples are presented in Figure 66 and compared to IBU spectrum. The main goal of NMR experiments was to confirm the uptake of both Ibuprofen and guar gum in the prepared materials and assure structural integrity of the drug, upon interaction with biopolymers and montmorillonite.

The spectrum of IBU reveals sharp lines that can be assigned to C atoms in the drug molecule structure. The peaks in the range 143 – 130 ppm and 45 – 17 ppm can be attributed to phenyl and alkyl groups, respectively. The line at 185 ppm is assigned to carboxylic groups (Azais *et al*., 2006; Carignani *et al*., 2011).

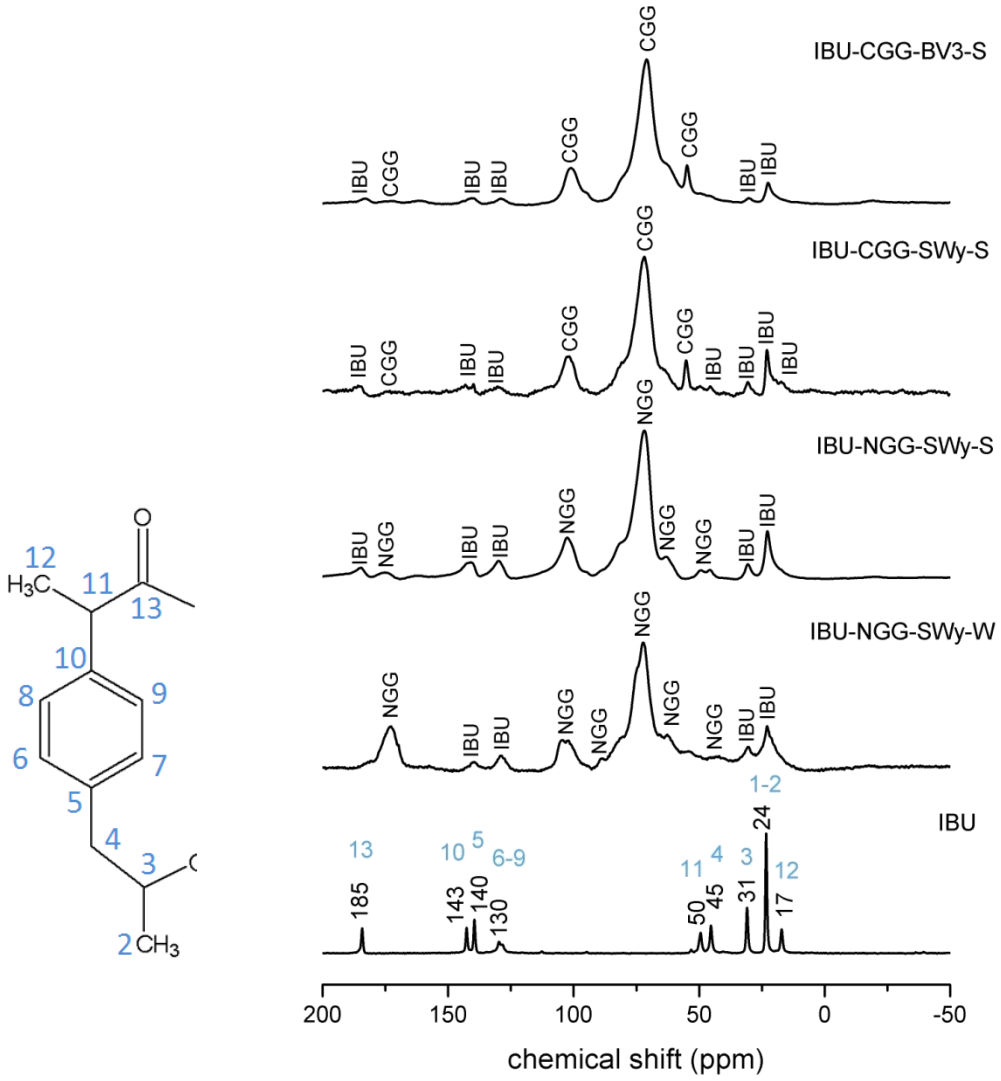

Figure 66. ^{13}C CP MAS spectra of Ibuprofen sodium salt (IBU) and Ibuprofen-loaded samples: IBU-NGG-SWy-W, IBU-NGG-SWy-S, IBU-CGG-SWy-S, and IBU-CGG-BV3-S. Scheme of an Ibuprofen sodium salt molecule is shown on the left and chemical shifts for each carbon atom is assigned, according to Carignani et al., 2011.

In the case of all prepared samples, series of NMR lines, which are typical for both guar gum and IBU, are present in the spectra and were appropriately assigned. The peaks attributed to NGG and CGG are in good accordance with the spectra of the previously synthesized nanocomposites, with no IBU loaded (Fig. 42 and Fig. 47). Despite low resolution of the spectra, no additional lines were evidenced, that would suggest any alteration in the structures of the biopolymers and/or the drug.

4. Summary and Conclusions

In this chapter, interaction of Ibuprofen with montmorillonite, neutral and cationic guar gum, and montmorillonite-guar gum nanocomposites have been characterized by XRD, TGA and NMR. XRD indicated that intercalation complexes of montmorillonite and Ibuprofen, with the interlayer spacing of 15 Å, were obtained. However, they were not stable upon centrifugation. TGA traces of montmorillonite and biopolymers loaded with IBU, suggested alteration of Ibuprofen crystalline state and interaction with both materials.

Ibuprofen-loaded nanocomposites were prepared by two methods. The first method involved loading of the drug on pre-synthesized neutral guar gum-montmorillonite nanocomposite. The resultant drug-loaded nanocomposite exhibited a slightly higher interlayer spacing in comparison with the starting material (26 Å and 24 Å, respectively). However, the material exhibited low drug loading (8%) and low drug loading efficiency (11%). In the second 'one-pot' method, Ibuprofen was loaded directly during the synthesis of the nanocomposite. This strategy was used to prepare three sets of samples using neutral guar gum, cationic guar gum, and Na^+-SWy and Na^+-BV3 montmorillonite samples. The successful synthesis of nanocomposites with intercalated structures were confirmed by XRD. The sample prepared with neutral guar gum and Na^+-SWy exhibited a high interlayer spacing, evidenced by a broad and diffuse feature at approximately 30Å, suggesting a large delamination. Both nanocomposites prepared with cationic guar gum and two different montmorillonite samples exhibited a similar interlayer spacing of 14 Å, which was also evidenced for the materials without Ibuprofen loaded. The materials obtained by the second method showed a higher drug loading (between 10 to 17%) and exhibited a higher drug loading efficiency (between 33 and 70%). The sample with the highest DL and DLE was IBU-NGG-SWy-S. TGA traces of the nanocomposites indicated altered behavior of IBU on pyrolysis, suggesting its dispersion in the polymeric matrix, changes in crystallinity, and interaction with both polymer and clay minerals. NMR further indicated presence of biopolymers and Ibuprofen in the prepared nanocomposites, with no evidence of loss in their structural integrity.

In conclusion, Ibuprofen-loaded nanocomposites obtained by two methods, using two biopolymers and two different montmorillonite samples were obtained. These materials will be further tested in an *in vitro* drug release system.

Part V: *In Vitro* Drug Release Experiments

1. Aims

The main goal of this part of the thesis was to test the prepared, Ibuprofen-loaded nanocomposites as drug delivery systems with potentially improved properties. The performance of materials was assessed *in vitro,* using a membrane diffusion method as a dissolution testing strategy.

Ibuprofen is a non-steroidal, anti-inflammatory drug. It is typically applied in the symptomatic treatment of osteoarthritis and rheumatoid arthritis and it has analgesic and antipyretic properties (The Drug Bank Database). However, treatment with Ibuprofen frequently leads to side effects, due to reported gastrointestinal toxicity of this drug (Lichtenstein *et al*., 1995). Ibuprofen contributes to topical injuries of the gastric mucus, what decreases its resistance to acidic environment, pepsin and some exogenous factors, such as the drug itself (Wolfe *et al*., 1999). Additionally, Ibuprofen has an adverse systemic effect on gastric, mucosal protective agents, what may lead to ulceration and gastric bleeding (Schoen & Vender, 1989). Another problematic issue is connected with fast absorption of the drug (maximum blood concentration levels of Ibuprofen are reached within 1-2 h) and its rapid elimination from the plasma (~2 h) (Wilson *et al*., 1989; The DrugBank Database).

Due to this short half-life and adverse gastrointestinal side effects, modified drug delivery systems for Ibuprofen are desired. Such systems should exhibit sustained release of the drug to: decrease dosing frequency, prevent reaching toxic concentration of drug in the body, hinder unsteady release, and minimize occurrence of side effects (Wilson *et al*., 1989; Arida *et al*., 1999). Several authors report modified Ibuprofen delivery systems, based on polymers (Arida *et al*., 1999; Das *et al*., 2006; Pang *et al*., 2011; Abdeen & Salahuddin, 2013;), clay minerals (Zheng *et al*., 2007), LDH (Rojas *et al*., 2012), and polymer-clay nanocomposites (Depan *et al*., 2008; Campbell *et al*., 2010). However, to the best of my knowledge, there are no such systems based on guar gum-montmorillonite nanocomposites.

2. Materials and Methods

2.1. *In Vitro* Release Experiments

In vitro release experiments were performed using a modified membrane dissolution method, adapted from Marchal-Heussler *et al*., 1990 and Shen & Burgess, 2013.

The majority of experiments was carried out, using simulated intestinal fluid (SIF) - phosphate buffer pH =7.4, as a release medium. The buffer was prepared according to U.S. Pharmacopeia by mixing 250 mL of 0.2M KH_2PO_4, 195.5 mL 0.2 M NaOH and adding distilled water to 1L volume. Cellulose dialysis membranes, with MCWO 12,000 – 14,000, were supplied from Spectrum Laboratories Inc. Prior to release experiments, the membranes were immersed in distilled water for 2h to remove preservative, rinsed thoroughly with water and immersed in the SIF, to equilibrate for 1h. Subsequently, the dialysis bag was filled with 6 mL of the release medium. Afterwards, the carefully weighed amount of a powdered material, that contains approximately 20 mg of IBU, was placed inside the membrane. The bag, sealed with plastic clips, was shaken and immediately immersed in the 300 mL of the release medium, which was pre-heated to 37°C in order to simulate body conditions. The experiments were performed using a magnetic stirrer (100 rpm), during a 6h-interval. The aliquots of 9 mL (3x 3mL) were withdrawn after 5, 10, 20, 30, 45, 60, 90,120, 180, 240, 300 and 360 min and replaced with 9 mL of a fresh release medium each time. The concentration of Ibuprofen was measured by UV-Vis Spectroscopy at λ_{max} = 222 nm. The measurement was performed in triplicates. A few experiments were carried out using simulated gastric fluid (SGF) – hydrochloric acid buffer pH = 1.2 as a release medium, during a 2h-interval. SGF was prepared according to to U.S. Pharmacopeia by mixing 250 mL of 0.2 M KCl, 425 mL of 0.2 M HCl and adding distilled water to 1L volume.

The UV-Vis measurements were performed as described in Part II, chapter 2.5.1. Additionally, Ibuprofen concentration was determined in hydrochloric acid buffer, for the release experiments performed in SGF. The calibration curve was prepared in the same manner as for the phosphate buffer. Before each measurement, including the calibration curve preparation, 0.1 mL of 2 M NaOH was added per 3 mL of sample to assure total dissolution of Ibuprofen.

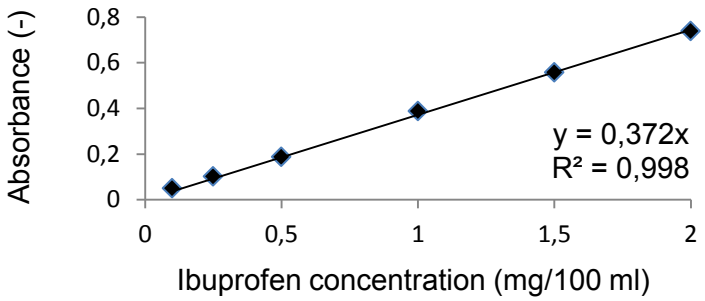

Figure 67. UV-Vis absorbance calibration curve for Ibuprofen in pH 1.2 hydrochloric acid buffer, measured at λ_{max} = 222 nm.

Cumulative amount of Ibuprofen (CR_{IBU} %), that was released during the experiment, was calculated according to the equation below (Pang *et al*., 2011):

$$CR_{IBU}\ (\%) = \frac{amount\ of\ Ibuprofen\ released\ at\ a\ time\ interval\ \ t\ (mg)}{total\ amount\ of\ Ibuprofen\ loaded\ (mg)} * 100\%$$

The UV-Vis measurement error was expressed as a standard deviation from three measurements. The total error (ΔCR), when calculating cumulative amount of released Ibuprofen was calculated as a combined error of two independent errors due to a drug loading determination (ΔDLD) and UV-Vis measurements (ΔUV) , according to the formula (Hogan, 2006):

$$\Delta CR = \sqrt{(\Delta DLD)^2 + (\Delta UV)^2}\ ,$$

where ΔDLD and ΔUV are expressed as standard deviations.

2.2. Drug Release Kinetics

Drug release kinetics was determined by fitting data, obtained from the drug release experiments, to three kinetic models: zero-order, first-order and Higuchi release model. The models' equations, according to Costa & Lobo, 2001, are presented in the table below:

Zero-Order	$Q_t = Q_0 + K_0 t$
First-Order	$\ln Q_t = \ln Q_0 + K_1 t$
Higuchi	$Q_t = K_H \sqrt{t}$

Table 8. Mathematical models used to fit drug dissolution profiles, Q_t – amount of the drug released at time t (%), Q_0 – initial amount of drug in the material (100%), K – zero order, first order and Higuchi rate constants; t – release time (h); (adapted from Costa & Lobo, 2001).

3. Results and Discussion

3.1. Ibuprofen Blank Release Profiles

In vitro release is a very simplified approach to simulate body conditions upon drug's dissolution and availability for absorption. Generally, in an oral administration route, a drug is subjected to three main environments: buccal, gastric and intestinal, that significantly differ in pH. Usually, the gastric empting time (low pH) is

approximately 2h (Hellmig *et al*., 2006), whereas intestinal transit time reaches tens of hours and pH is progressively more alkaline, up to 8 (O'Donnell *et al*., 1990).

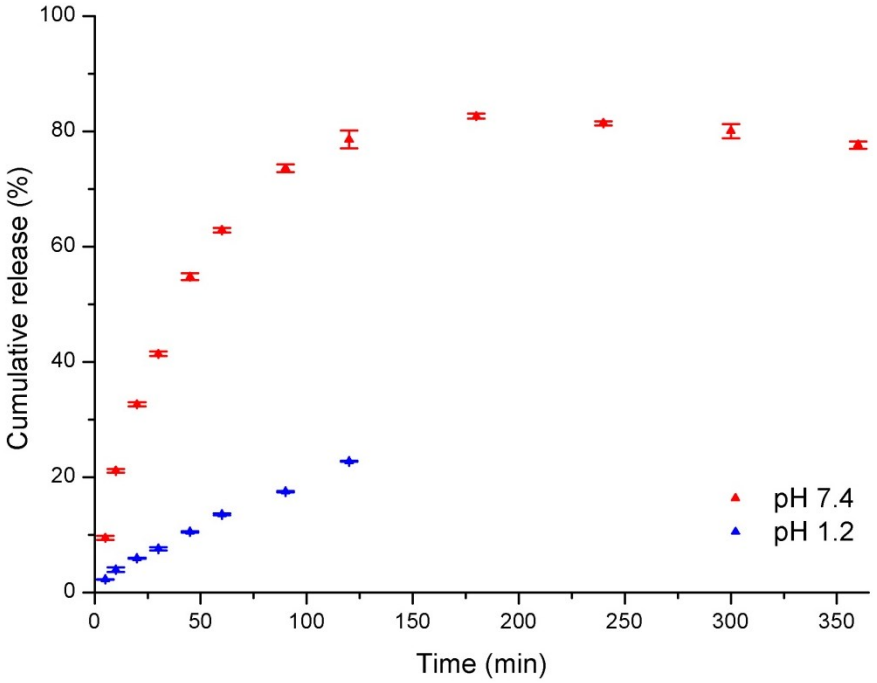

Figure 68. Cumulative release of Ibuprofen blank sample in pH 1.2 hydrochloric acid buffer and in pH 7.4 phosphate buffer.

Initially, behavior of pure Ibuprofen sodium salt (IBU blank), during release in pH 1.2 hydrochloric acid buffer (simulated gastric fluid, 2h) and in pH 7.4 phosphate buffer (simulated intestinal fluid, 6h), was examined (Fig. 68). Ibuprofen is a weak acid with pKa value of 4.91 (The DrugBank Database). Due to that, it has low solubility in an acidic medium, what is reflected by the release profile in pH 1.2 hydrochloric acid buffer. Only 23% of the drug is released within 2h. On the other hand, Ibuprofen is released rapidly at higher pH, reaching 80% cumulative release in the pH 7.4 phosphate buffer, within the first 2h. After this time, the concentration of the drug, within the dialysis bag and outside it, became equilibrated. In spite of this, Ibuprofen release was studied mainly in a pH 7.4 phosphate buffer.

3.2. Ibuprofen Release Profiles in Phosphate Buffer pH = 7.4

3.2.1. IBU-SWy-U and IBU-SWy Blank Samples

In the next step, release of Ibuprofen from the blank montmorillonite samples (IBU-SWy-U and centrifuged IBU-SWy) was studied in a phosphate buffer solution pH 7.4 (Fig. 69).

The untreated IBU-SWy-U sample exhibits a very similar Ibuprofen release pattern as the blank pure Ibuprofen sample. Despite the fact that some part of Ibuprofen is intercalated within montmorillonite layers (Fig. 51), the high drug loading of this sample (68 %) hinders any potential effect on sustained release of the drug that could result from its interaction with the clay mineral.

In the instance of the centrifuged Ibuprofen-loaded sample (IBU-SWy), there is a strong decrease of the drug's release rate. Approximately 20% of Ibuprofen is released within the first hour, followed by a very slow desorption of the drug from the sample. This indicates that Na^+-SWy montmorillonite can strongly interact with Ibuprofen, and this effect is enhanced when a drug loading is small (11 %). Since Ibuprofen, as a weak acid, exists prevalently in anionic form at pH 7.4, one possible mechanism of this interaction may be hydrogen bonding between COO^- groups of Ibuprofen and –OH groups on montmorillonite's surface (Xu *et al*., 2006; Zheng *et al*., 2007). A decreased release rate of Ibuprofen from similar complexes have been reported before, where depending on a drug's loading, approximately 40% of Ibuprofen was released over 10 hours (Zheng *et al*., 2007). However, a major disadvantage of such systems may be a too strong interaction of drug and clay mineral, which can prevent from reaching the therapeutic levels of drug in the plasma (Carreterro *et al*., 2013).

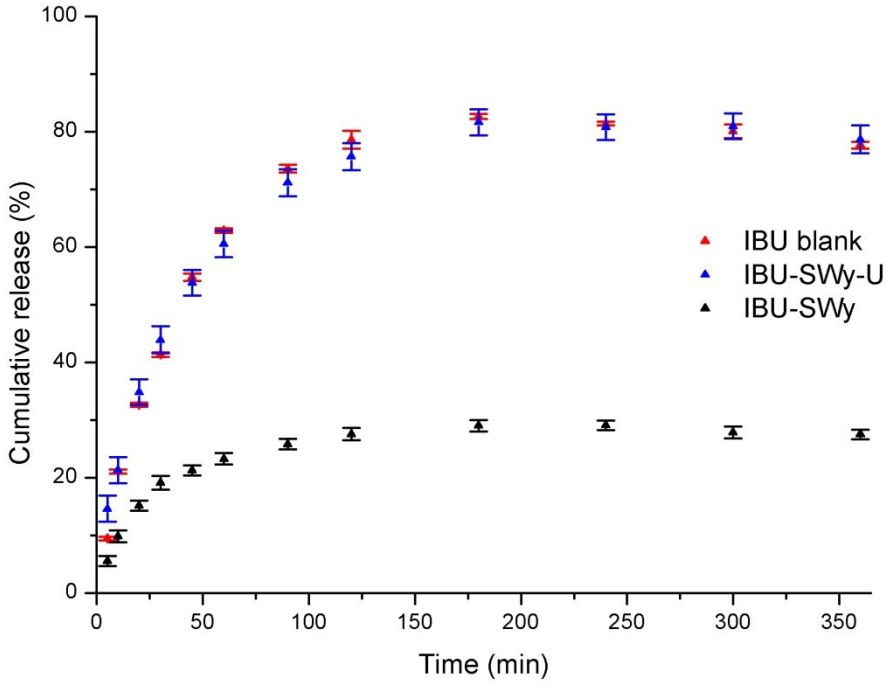

Figure 69. Cumulative release profiles of Ibuprofen sodium salt blank sample (IBU blank), IBU-SWy-U and IBU-SWy blank samples in pH 7.4 phosphate buffer.

3.2.2. IBU-NGG and IBU-CGG Blank Samples

Prior to release experiments, performed with the prepared guar gum-montmorillonite nanocomposites, it was important to determine behaviors of both NGG and CGG loaded with Ibuprofen (Fig. 70). These blank samples were prepared by following a similar method, as in the case of nanocomposites (Part IV, chapter 2.3.2.).

Figure 70 is showing a minor effect on Ibuprofen release kinetics for both NGG and CGG, as compared to pure IBU. Despite certain possible interaction of NGG and the drug (e.g. hydrogen bonding involving –OH groups of the polymer and carboxyl oxygens of IBU; Depan *et al*., 2008), Ibuprofen is released quickly, within the first 2h. Also in the case of positively charged CGG, which could interact more strongly with the ionized drug, there is no evidence of sustained drug release. Because the samples are simply used in a ground powder form in the release experiments, the very high fast swelling of biopolymers is not controlled in any way. As such, Ibuprofen can quickly diffuse through the swollen polymer matrix into the release media (Krishnaiah *et al*., 1998; Das *et al*., 2006).

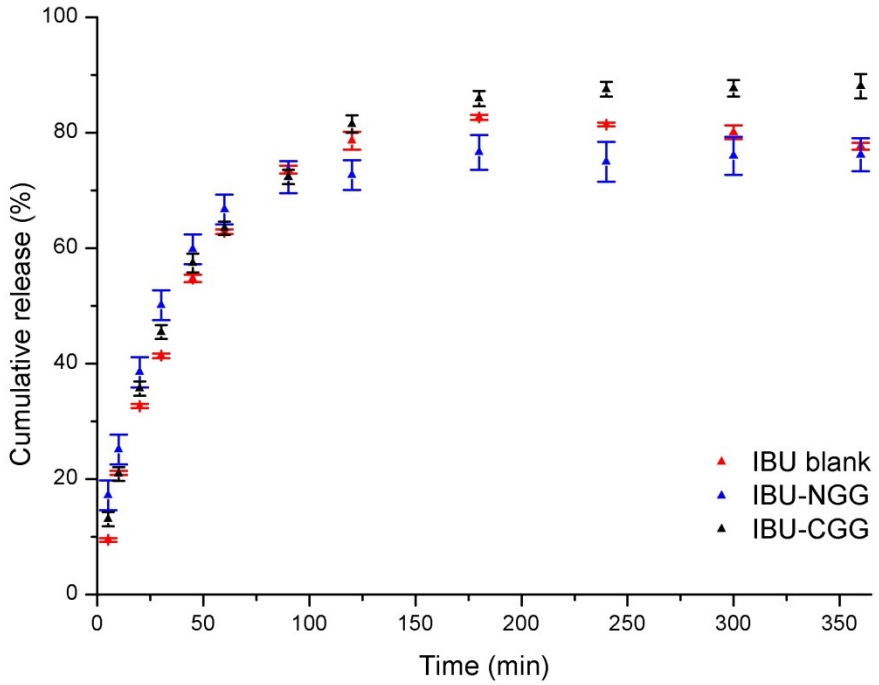

Figure 70. Cumulative release profiles of Ibuprofen sodium salt (IBU blank), IBU-NGG and IBU-CGG blank samples in pH 7.4 phosphate buffer.

3.2.3. IBU-NGG-SWy-WU and IBU-NGG-SWy-W

Being aware of the interaction of IBU with montmorillonite or biopolymers alone, the drug release experiments were performed using the prepared

nanocomposites. To begin with, the IBU-NGG-SWy-WU and IBU-NGG-SWy-W samples, prepared by loading Ibuprofen on the pre-synthesized biopolymer-clay nanocomposites, were tested (Fig. 71).

The untreated IBU-NGG-SWy-WU sample with DL of 70 % and a high amount of crystalline IBU (evidenced by both XRD and TGA), exhibits an unaltered release profile in comparison with the blank IBU sample. As in the instance of IBU-SWy-U, a very high drug loading prevents from evidencing any effect of the nanocomposite on controlled drug release.

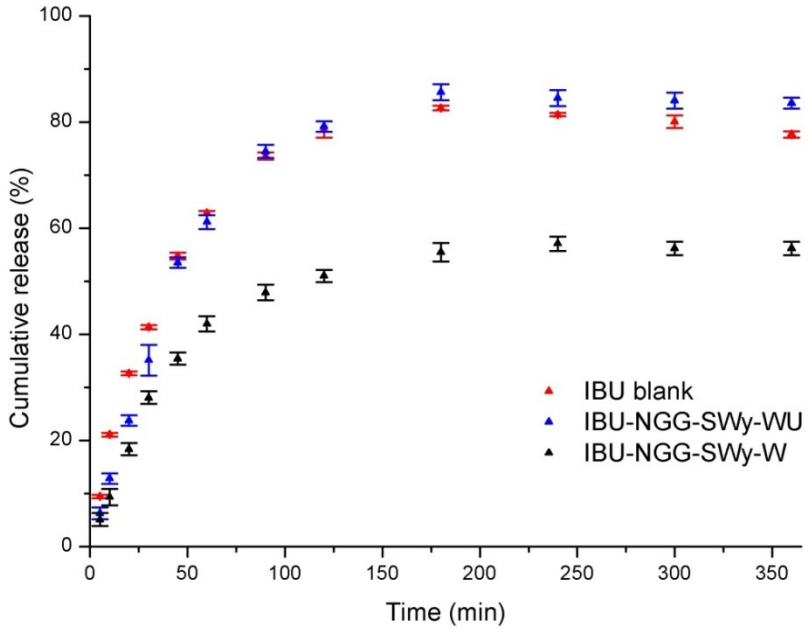

Figure 71. Cumulative release profiles of Ibuprofen sodium salt IBU blank), and nanocomposites prepared by loading IBU on pre-synthesized materials - IBU-NGG-SWy-WU (untreated sample) and IBU-NGG-SWy-W (centrifuged sample), in pH 7.4 phosphate buffer.

Such effect is however present for the centrifuged IBU-NGG-SWy-W sample with a lower drug content (8 %). According to XRD patterns (Fig. 56), there is no crystalline IBU evidenced, what suggests that the drug is dispersed in the nanocomposite matrix (Pang *et al*., 2011). The initial release rate is slightly lower than the pure IBU, and about 20% less drug than for the blank is released within the first hour. The release rate is further reduced and becomes very slow at the moment when about 50% of the drug has diffused through the membrane. This second stage of release is similar as for the IBU-SWy blank sample. Possibly in the first hours, Ibuprofen dispersed in the surface NGG matrix is released, followed by the desorption of the clay-associated drug molecules. The major disadvantage of such profile may be

a still present burst release of Ibuprofen, followed by a period of very slow release, what could cause a sudden drop of drug available for absorption (Saravanan *et al*., 2003).

3.2.4. IBU-NGG-SWy-SU and IBU-NGG-SWy-S

In spite of previous observations, nanocomposites with lower initial drug loading were prepared using the direct synthesis method (Part IV, chapter 2.2.2.). The as obtained IBU-NGG-SWy-SU and IBU-NGG-SWy-S samples have the DL of 24 % and 17 %, respectively. The latter additionally exhibits a high drug loading efficiency (70%), what is a desired feature (Zhang *et al*., 2012).

The Ibuprofen release profiles of these two samples were presented in Figure 72, and compared to the profile of a physical mixture of NGG, IBU, and Na^+-SWy, prepared in the same ratio as the untreated IBU-NGG-SWy-SU sample (6 : 2 : 1).

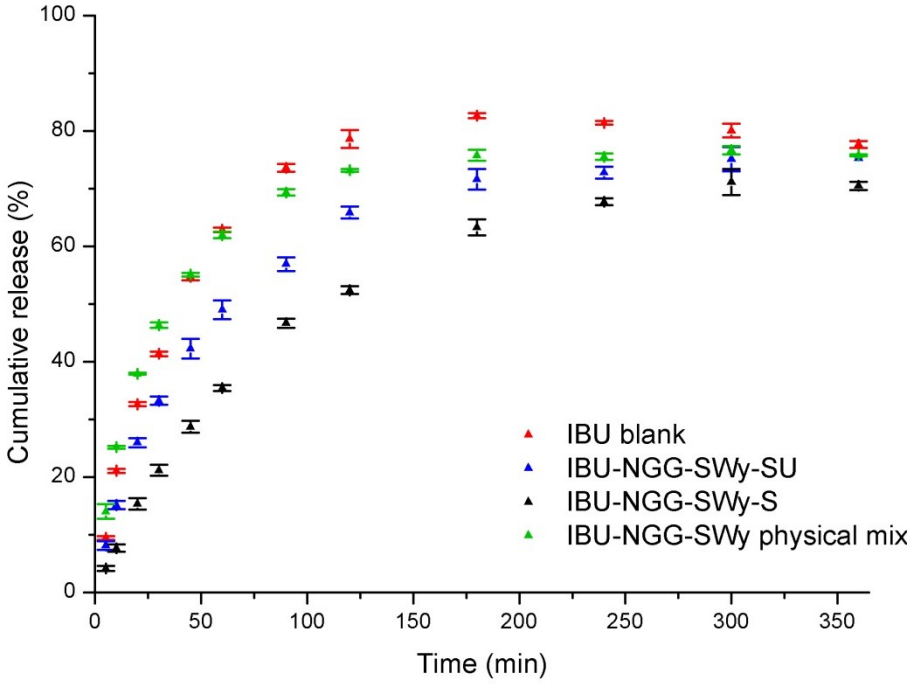

Figure 72. Cumulative release profiles of Ibuprofen sodium salt (IBU blank), physical mixture of IBU, NGG and SWy, and nanocomposites prepared by a direct synthesis - IBU-NGG-SWy-SU (untreated sample) and IBU-NGG-SWy-S (centrifuged sample), in pH 7.4 phosphate buffer.

The plots indicate that a slight sustained release-effect is observed even for the untreated sample in comparison with the behavior of the physical mixture. The effect is further enhanced for the centrifuged IBU-NGG-SWy-S sample. This indicates that the sustained release effect is induced by the nanocomposite. The major advantage, over the previous systems prepared by an indirect IBU loading, is that the initial burst

release is reduced to a greater extent. Moreover, the release rate of IBU is steadier, especially for the centrifuged sample, without a sudden drop of the rate after 1 hour.

Most probably, the improved release characteristics of these systems are due to more homogenous dispersion of IBU in the nanocomposite matrix than previously and its increased interaction with NGG and montmorillonite. Additionally, because of the interaction with clay layers and the presence of NGG in the interlayer space of the clay mineral, the extent of biopolymer's swelling may be reduced, what can also control IBU release (Saravanan *et al*., 2003; Viseras *et al*., 2008). Clay-mediated reduced swelling has been proposed as the dominant mechanism that sustains drug release in several systems (Wang *et al*., 2009; Liu *et al*., 2008). These interactions possibly prevent IBU from fast diffusion as which was observed in the case of IBU-NGG blank. The removal of excess crystalline IBU in the case of the centrifuged nanocomposite, and possible presence of IBU in amorphous form, as suggested by XRD and TGA (Fig. 58 and Fig. 59) further contribute to reduction of IBU release rate.

3.2.5. IBU-CGG-SWy-SU and IBU-CGG-SWy-S

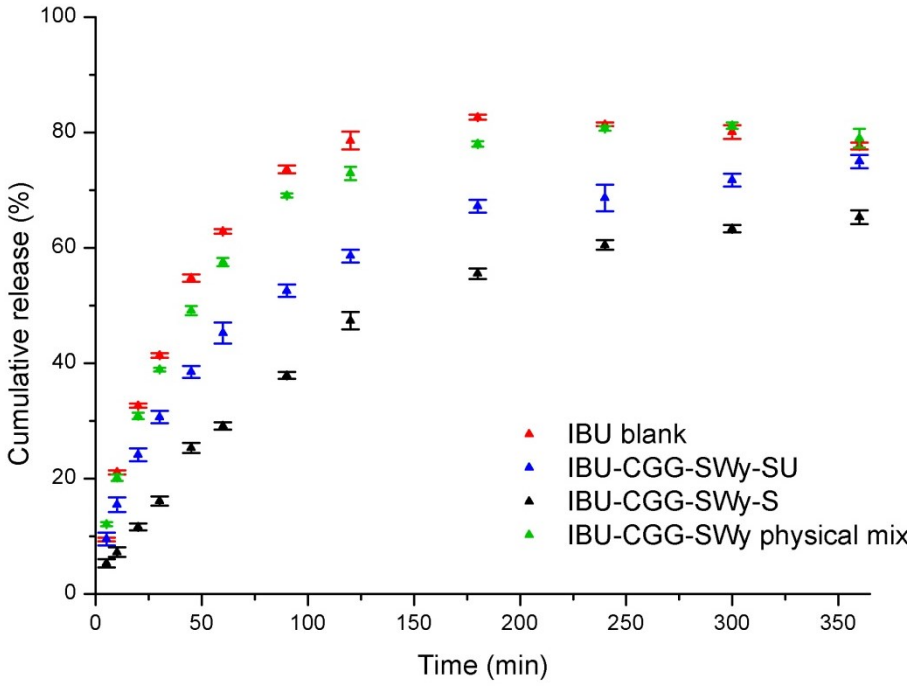

Figure 73. Cumulative release profiles of Ibuprofen sodium salt (IBU blank), physical mixture of IBU, CGG and SWy, and nanocomposites prepared by direct synthesis - IBU-CGG-SWy-SU (untreated sample) and IBU-CGG-SWy-S (washed sample), in pH 7.4 phosphate buffer.

On the basis of a possible electrostatic interaction of ionized IBU and a positively charged biopolymer, another set of Ibuprofen-loaded nanocomposites was prepared with CGG and Na^+-SWy (Part IV, chapter 2.2.2.). The Ibuprofen release profiles of the untreated IBU-CGG-SWy-SU and washed IBU-CGG-SWy-S samples are presented in Figure 73, and compared to a physical mixture of CGG, IBU and Na^+-SWy (4 : 2 : 1 ratio, respectively).

As in the case of the previous similar nanocomposite but prepared with NGG (IBU-NGG-SWy-SU, the reduced release rate of IBU is observed even for the untreated sample (U), as compared to the release pattern of the physical mixture. Again, upon removal of prevalent amount of crystalline IBU (Fig. 61 and Fig. 62), the release is more sustained for the washed IBU-CGG-SWy-S sample. The IBU release profile of this nanocomposite exhibit significantly reduced initial burst release effect. After 90 minutes, 36 % less IBU is released from this sample in comparison to the IBU blank. The nanocomposite exhibits also very steady release of IBU, which is desirable in modified drug delivery systems (Viseras *et al*., 2008). The fact that release rate is reduced with time to a less extent than for IBU-NGG-SWy-W, may be due to the fact that IBU is more homogenously dispersed in the nanocomposite, and there are different path lengths for diffusion of the drug into the release medium (Saravanan *et al*., 2003). Moreover, even more reduced swelling of CGG, due to a better defined intercalated structure of the nanocomposite than for the IBU-NGG-SWy-S, may contribute to further improvements of release parameters.

3.2.6. IBU-CGG-BV3-SU and IBU-CGG-BV3-S

Because of the most pronounced sustained release-properties for the nanocomposites prepared with CGG, similar materials were synthesized using the Portuguese montmorillonite, BV3. The release profiles of the untreated IBU-CGG-BV3-SU and washed IBU-CGG-SWy-S samples are presented in Figure 74.

Release rate of IBU was also noticeably reduced, when CGG-nanocomposites were prepared with the Portuguese montmorillonite BV3. The initial burst effect is also minimized for the washed sample, IBU-CGG-BV3-S.

In the case of the untreated sample (IBU-CGG-BV3-SU) , the release is less sustained as for its counterpart prepared with Na^+-SWy montmorillonite. Reduction of release rate can be observed only after 30 min, comparing to the IBU blank, whereas for IBU-CGG-SWy-SU it was almost immediate. As these two samples have a

comparable drug loading (~30%), and were prepared by the same method, it can be concluded that IBU-CGG-SWy-SU has a slightly better performance.

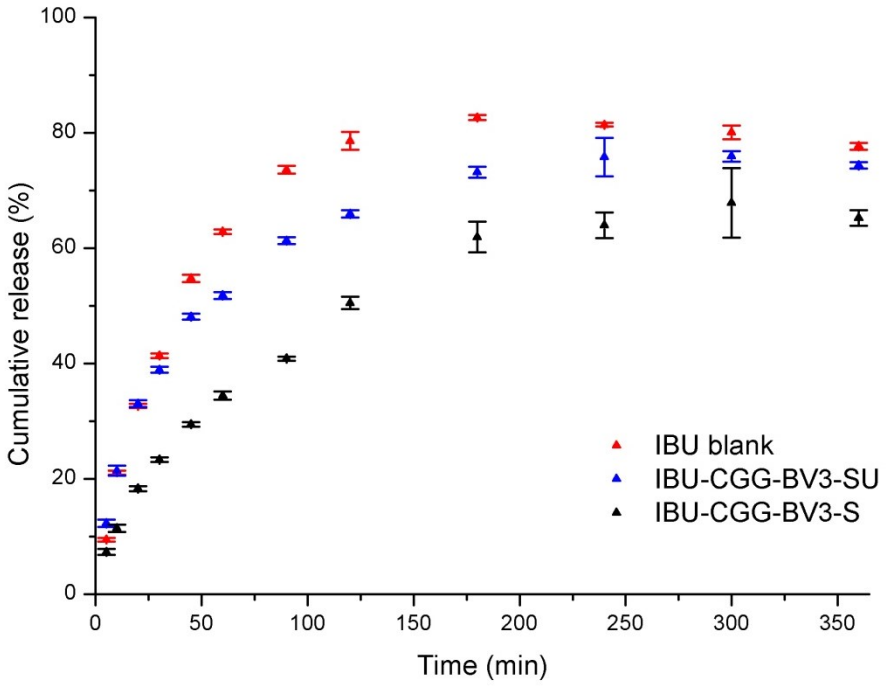

Figure 74. Cumulative release profiles of Ibuprofen in pH 7.4 phosphate buffer for: Ibuprofen sodium salt (IBU blank) and nanocomposites prepared by direct synthesis with Portuguese clay - IBU-BV3-SWy-SU (untreated sample) and IBU-CGG-BV3-S (washed sample),

The IBU release profiles of the two washed samples, prepared with Na^+-SWy and Na^+-BV3 are very similar, both showing a significant controlled release properties. This further indicates that nanocomposites prepared with CGG and having a well-defined intercalated structure exhibit a better performance. However, these samples are not directly comparable as the drug loading of the IBU-CGG-BV3-S sample is 6% lower than for IBU-CGG-SWy-S (DL 16%).

All in all, the significantly improved properties have been demonstrated for similar materials using two different montmorillonite samples, indicating utility of Portuguese montmorillonite in this application.

3.2.7. Comparison of Release Profiles

The release profiles of all centrifuged or washed nanocomposites were compared in Figure 75. All the samples showed a significant decrease of IBU release rate, as compared to the IBU blank. Both nanocomposites prepared with CGG and the IBU-NGG-SWy-S sample exhibit the best release patterns, what is reflected by a

minimized initial burst release effect (the first 2 h), followed by steadier release, in comparison with IBU-NGG-SWy-S. Additionally, IBU-NGG-SWy-S has the highest drug loading efficiency (70%).

Noteworthy, since the nanocomposites were used in a ground powder form, a further enhancement of the observed controlled release effect can be easily achieved by preparing compressed formulations, films or cross-linked beads (Cojocariu *et al*., 2012; Depan *et al*., 2009; Rao *et al*., 2014; Krishnaiah *et al*., 2002).

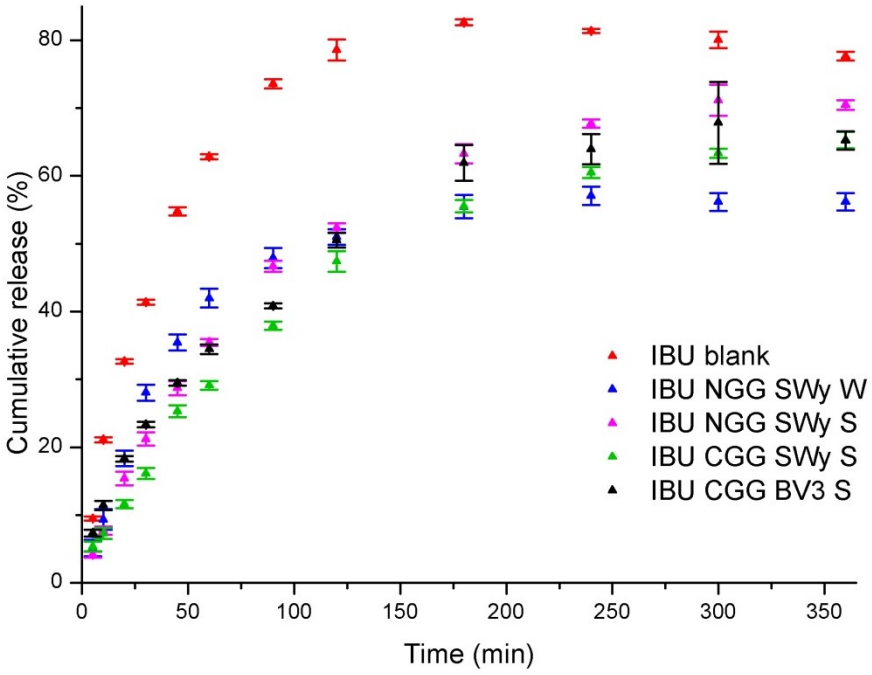

Figure 75. Comparison of cumulative release profiles of Ibuprofen in pH 7.4 phosphate buffer for the best samples.

3.3. Ibuprofen Release Profiles in Hydrochloric Acid Buffer pH = 1.2

Due to the fact that clay minerals may undergo partial degradation, when exposed to acidic solutions (Carreterro *et al*., 2013), a release in simulated gastric fluid with a pH 1.2, for 2h, was performed for the sample with best release parameters (IBU-CGG-SWy-S).

3.3.1. IBU-CGG-SWy-S

The release profile of the IBU-CGG-SWy-S in hydrochloric acid buffer pH 1.2 is presented in Figure 76 and compared to the IBU blank. Because of low solubility of IBU in acidic pH (pKa = 4.91), cumulative release for the pure drug is low and reaches

23% within 2h. In the case of the nanocomposite, the release rate is slightly lower and 5 % less IBU was released after this time.

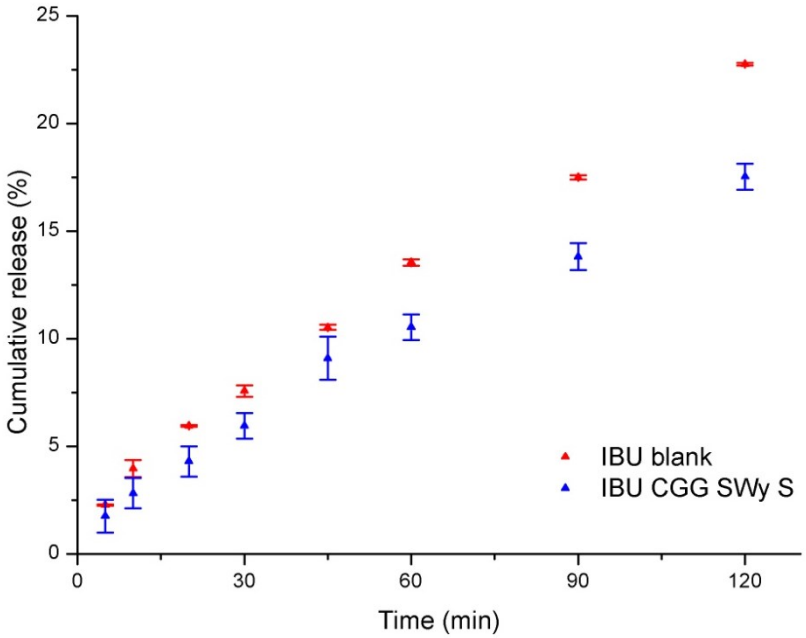

Figure 76. Cumulative release of Ibuprofen from the IBU blank sample and IBU-CGG-SWy-S nanocomposite in pH 1.2 hydrochloric acid buffer.

The XRD pattern of the nanocomposite, after the release in acidic pH is shown in Figure 77. In comparison with the starting material, a broader XRD feature is present at approximately 14 Å, suggesting a partial degradation of the nanocomposite structure. The observation of an interlayer spacing of 14 Å indicates however that some part of the nanocomposite remains intact.

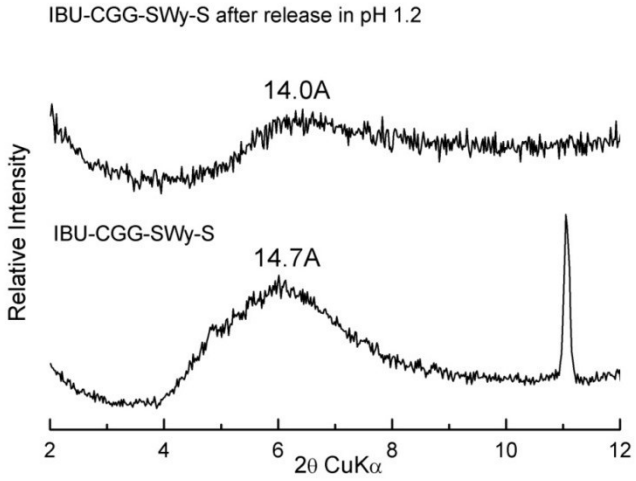

Figure 77. XRD diffraction pattern of the IBU-CGG-SWy-S nanocomposite before and after Ibuprofen release experiment in hydrochloric acid buffer pH 1.2 (simulated gastric fluid).

3.4. Drug Release Kinetics

Sample	Model	
	Zero-Order Kinetics	
	Equation	R^2
IBU-NGG-SWy-W	$Q_t = 12.50\ t + 18.28$	0.741
IBU-NGG-SWy-S	$Q_t = 13.59\ t + 14.95$	0.873
IBU-CGG-SWy-S	$Q_t = 10.45\ t + 14.18$	0.870
IBU-CGG-BV3-S	$Q_t = 12.21\ t + 16.85$	0.890

Sample	Model	
	First-Order Kinetics	
	Equation	R^2
IBU-NGG-SWy-W	$\ln(Q_t-Q_0) = -0.200\ t + 4.404$	0.817
IBU-NGG-SWy-S	$\ln(Q_t-Q_0) = -0.252\ t + 4.475$	0.952
IBU-CGG-SWy-S	$\ln(Q_t-Q_0) = -0.180\ t + 4.471$	0.934
IBU-CGG-BV3-S	$\ln(Q_t-Q_0) = -0.221\ t + 4.447$	0.951

Sample	Model	
	Higuchi Release	
	Equation	R^2
IBU-NGG-SWy-W	$Q_t = 31.84\ t^{-1/2} + 2.425$	0.900
IBU-NGG-SWy-S	$Q_t = 36.71\ t^{-1/2} - 3.963$	0.975
IBU-CGG-SWy-S	$Q_t = 30.62\ t^{-1/2} - 2.654$	0.969
IBU-CGG-BV3-S	$Q_t = 32.76\ t^{-1/2} + 0.114$	0.980

Table 9. Parameters of the three kinetic model equations (zero-order, first-order and Higuchi release) applied to the data obtained from drug release experiments for four nanocomposites; R^2 – regression coefficient, Q_t – amount of the drug released at time t (%), Q_0 – initial amount of drug in the material (100%), t – release time (h).

The chosen drug release data was fitted to three kinetic models: zero-order, first-order and Higuchi release model to assess a possible mechanism of drug release from the nanocomposites (Table 9).

The zero-order kinetics describes systems, in which drug release is very slow and dosage forms do not undergo disintegration (Costa & Lobo, 2001). The release rate of drug is constant and does not depend on its concentration. There is a low correlation of the release data fitted to this model for all the four nanocomposites. This is indicated by low R^2 regression coefficients that vary from 0.741 to 0.890.

The first-order kinetic model is generally applicable for the systems in which the amount of the drug released is proportional to its content remaining in the dosage. As such, the drug release rate decreases with time. The model is often used to describe the release of water soluble drugs from porous matrices (Costa & Lobo, 2001). There is a higher correlation with this model observed for the release data of nanocomposites, except for the IBU-NGG-SWy-W sample. This is reflected by R^2 regression coefficient ranging from 0.934 (IBU-CGG-SWy-S) to 0.952 (IBU-NGG-SWy-S). Indeed, IBU release rate from all the four nanocomposites is depended on drug content remaining in material, and decreases with time.

However, the best fit for all four nanocomposite samples were obtained for the Higuchi release model, which is indicated by the highest regression coefficients R^2. The IBU release rate is proportional to a square root of time. Generally, the simplified Higuchi model is applicable when drug is released from semi-solid and solid matrices and the release is diffusion controlled (Costa & Lobo, 2001; Saravanan *et al*., 2003). In the case of nanocomposites, this would indicate that IBU release depends on its diffusion through swollen polymer matrix and upon progressing diffusion the release rate is decreasing. For the three samples, with the best fit (IBU-NGG-SWy-S, IBU-CGG-BV3-S and IBU-CGG-SWy-S) the K_H release rate constants are 36.7, 32.8 and 30.6, respectively, what is in agreement with the fact that for the IBU-CGG-SWy-S, the release is the slowest.

4. Summary and Conclusions

The treatment with Ibuprofen may lead to gastric irritation and the drug itself has a short biological half-life. In spite of this, materials which exhibit sustained release of Ibuprofen are desired. In this part of the thesis, the performance of novel Ibuprofen-

loaded guar gum-montmorillonite nanocomposites was assessed *in vitro,* using a membrane diffusion method as a dissolution testing strategy.

The majority of the experiments was carried out in simulated intestinal fluid (pH 7.4 phosphate buffer). The best improvement of IBU release behavior has been observed for three nanocomposite samples, prepared by the direct Ibuprofen loading method. The release profiles of these samples indicate a minimized initial burst release effect and slower release rate in comparison with pure Ibuprofen. Both samples, prepared with cationic guar gum and two different clay samples (Na^+-SWy and Na^+-BV3), exhibited slightly better release properties than the one prepared with neutral guar gum, despite lower drug loading efficiency. In their case, the sustained release effect was observed even for the unwashed samples.

To check if the controlled release effect was caused by nanocomposite or just by its components alone, several blank experiments were performed. Ibuprofen loaded on cationic guar gum and on neutral guar gum was released as fast as pure IBU. This was also the case for physical mixture of the drug, biopolymers and montmorillonite, indicating superior properties of nanocomposites. In the instance of the drug loaded on pure montmorillonite sample, there was a very strong drug adsorption, which could potentially prevent from reaching a therapeutic level of the drug (less <25 % of IBU released within 6h).

The release from the nanocomposites was fitted to different kinetic models, among which the simplified Higuchi model has shown the highest correlation. As such, the release rate of drug was proportional to a square root of time and the possible mechanism of release was diffusion through a swollen, polymeric matrix. As clay-mediated reduced swelling may be an important mechanism of drug release, further studies of the nanocomposites' swelling behavior are suggested.

Due to the fact that the release experiments were performed using powdered samples, an additional improvement of sustained release properties can be easily achieved using another type of drug dosage (e.g. compressed tablets, cross-linked beads).

General Conclusions

Clay minerals offer remarkable potentials in the field of material science that are only beginning to be explored. Among others, polymer-clay nanocomposites exhibit striking properties and are extensively researched across disciplines. Whereas the ability of clay minerals to interact with multitude of organic molecules is well-established, the studies are often limited to commercially available clay mineral products. In this thesis, a less recognized montmorillonite from the Portuguese bentonite ore has been thoroughly characterized and its utility for the preparation of biopolymer-clay nanocomposites was demonstrated.

Widely recognized therapeutic properties of montmorillonite and guar gum suggest plenty of opportunities for their medicinal use. The prospect of merging these two non-toxic materials is especially attractive for drug-delivery applications. Modern advanced modified drug delivery systems are based on diverse materials that, through versatile interaction with drug molecules, can adjust release in a desired way. Ibuprofen is a common anti-inflammatory drug that has a short biological half-life and may cause severe gastrointestinal injuries. In spite of this, ingested pharmaceutical formulations that are able to decrease release rate of Ibuprofen are highly sought.

In this thesis novel neutral guar gum-montmorillonite and cationic guar gum-montmorillonite drug-loaded nanocomposites have been prepared and their ability to control the release of Ibuprofen was presented. These materials exhibit a reduced initial burst effect and sustained release up to several hours in a pH 7.4 simulated intestinal fluid. Blank experiments suggest the nanocomposite-mediated action. Improved properties were demonstrated for two different clay minerals: SWy-2 from the Source Clay Repository and Portuguese montmorillonite from the Benavila bentonite deposit. Additionally, montmorillonite, which is known to be an efficient gastrointestinal protector, can minimize the hazard of gastric irritation due to Ibuprofen ingestion.

The prepared novel nanocomposite materials have a great potential in drug delivery and there are further avenues that need exploring. As the materials were tested in a ground powder form, the sustained release action can be further improved by changing the dosage form, e.g. into compressed tablets or cross-linked beads. Future work involve also studying the release as a function of clay mineral content and pH.

References

Abdeen R. & Salahuddin N. (2013). *Modified Chitosan-Clay Nanocomposite as a Drug Delivery System Intercalation and In Vitro Release of Ibuprofen*. Hindawi Publishing Corporation Journal of Chemistry, Volume 2013, Article ID 576370.

Alam N.H., Meier R., Schneider H., Sarker S.A., Bardhan P.K., Mahalanabis D., Fuchs G.J., Gyr N. (2000). *Partially Hydrolyzed Guar Gum–Supplemented Oral Rehydration Solution in the Treatment of Acute Diarrhea in Children.* Journal of Pediatric Gastroenterology and Nutrition 31: 503–507.

Alemán J.V, Chadwick A.V., He J., Hess M., Horie K., Jones R.G., Kratochvíl P., Meisel I., Mita I., Moad G., Penczek S., Stepto R.F.T. (2007). *Definitions of terms relating to the structure and processing of sols, gels, networks, and inorganic-organic hybrid materials (IUPAC Recommendations 2007)*. Pure and Applied Chemistry, 79, pp. 1810, 1813.

Altaf S.,A., Yu K., Parasrampuria J., Friend D.,J. (1998). *Guar Gum-Based Sustained Release of Diltiazem*. Pharmaceutical Research 15, 8, 1196-1201.

Ambre A.H., Katti K.S., Katti D.R. (2010). *Nanoclay Based Composite Scaffolds for Bone Tissue Engineering Applications.* Journal of Nanotechnology in Engineering and Medicine 1, 031013.

Ambrogi V., Perioli L., Ricci M., Pulcini L., Nocchetti M., Giovagnoli S., Rossi C. (2008). Eudragit® and hydrotalcite-like anionic clay composite system for diclofenac colonic delivery. Microporous and Mesoporous Materials 115, 405–415.

Amman L. (2003). *Cation exchange and adsorptionon clays and clay minerals*. Dissertation, University of Kiel.

Andrade F.A, Al-Qureshi H.A., Hotza D. (2011). *Measuring the plasticity of clays: A review*. Applied Clay Science 51, 1–7.

Anzelmo J.A, Lindsay J.R. (1987). *X-ray Fluorescence Spectrometric Analysis of Geologic Materials. Part 1. Principles and Instrumentation*. Topics in Chemical Instrumentation Vol. 64, 8, A183 – A185.

Arida A.I., Amoro B., Jaghbir M., Elalem M., Sabri R., Abuzeid R. (1999). *Development of sustained-release ibuprofen microspheres using solvent evaporation technique*. Archiv der Pharmazie 332, 405–407.

Averous L., Pollet E. (2012). *Environmental Silicate Nano-Biocomposites*. Green Energy and Technology. Springer-Verlag.

Azais T., Tourne-Peteilh C., Aussenac F., Baccile N., Coelho C., Devoisselle J.-M., Babonneau F. (2006). Solid State Study of Ibuprofen Confined in MCM-41 Material. Chemistry of Materials 18 (26), 6382 – 6390.

Aznar, A.J., Ruiz-Hitzky, E. (1988). *Arylsulphonic resins based on organic/inorganic macromolecular systems*. Molecular Crystals Liquid Crystals Including Nonlinear Optics 161, 459–469

Bae H.J., Park H.J., Hong S.I., Byun Y.J., Darby D.O., Kimmel R.M., Whiteside W.S. (2009*). Effect of clay content, homogenization RPM, pH, and ultrasonication on mechanical and barrier properties of fish gelatin/montmorillonite nanocomposite films*. LWT-Food Science and Technology 42,1179–1186.

Baekeland L.H. (1909). *The Synthesis, Constitution, and Uses of Bakelite*. Industrial and Engineering Chemistry 1(3), 149 – 161.

Baldock, J.A., Oades, J.M., Waters, A.G., Peng, X., Vassallo, A.M., Wilson, M.A. (1992). *Aspects of the chemical-structure of soil organic materials as revealed by solid-state C13 NMR-spectroscopy.* Biogeochemistry 16, 1–42.

Barge, 2010 http://www.bgs.ac.uk/barge/docs/BARGE_UBM_DEC_2010.pdf

Belo G.M.S, Diniz A.S., Pereira A.P.C. (2008). *Effect of partially hydrolyzed guar gum in the treatment of functional constipation among hospitalized patients*. The Journal Arquivos de Gastroenterologia, 45(1), 93-95.

Bergaya F., B.K.G. Theng G. Lagaly (2006). *Handbook of clay science, 1st Edition*. Elsevier.

Bergaya F. & Lagaly G. (2011). *Intercalation processes of layered minerals, in Layered Minerals Structures and Their Application in Advanced Technologies* (Eds. M. F. Brigatti & A. Mottana). European Mineralogical Union Notes in Mineralogy, vol. 11, pp. 259–284. Mineralogical Society, London.

Bergaya F., Jaber M., Lambert J.F. (2012). *Clays and clay minerals as layered nanofillers for (bio)polymers, in Environmental Silicates Nano-Biocomposites, Green Energy and Technology* (Eds.

Bergaya F. & Lagaly G. (2013). *General introduction: Clays, Clay Minerals and Clay Science, in Handbok of Clay Science, 2nd edition.* Elsevier B.V.

Brindley, G.W., Brown G. (1980). *Crystal Structures of Clay Minerals and their X-ray Identification*. Mineralogical Society, 41 Queen's Gate, London SW7 5HR, 1980. pp. 495

Brown M.E. (1998). *Handbook of thermal Analysis and Calorimetry*. Volume 1, Principles and Practice. Chapter 1, pp. 1-9. Elsevier Science B.V

Butt M.S, Shahzadi N., Sharif M.K., Nasir M. (2007). *Guar Gum: A Miracle Therapy for Hypercholesterolemia, Hyperglycemia and Obesity*. Critical Reviews in Food Science and Nutrition, 47:389–396.

Campbell K. T., Craig D. Q., McNally T. (2010). *Ibuprofen-loaded poly (ε-caprolactone) layered silicate nanocomposites prepared by hot melt extrusion.* Journal of Materials Science: Materials in Medicine 21(8), 2307-2316.

Camus P.J. (2002). Management of Mineral Resources: *Creating Value in the Mining Business*. Society for Mining, Metallurgy, and Exploration.

Carreterro M.I., Pozo M. (2009). *Clay and non-clay minerals in the pharmaceutical industry. Part I: Excipients and medical applications*. Applied Clay Science, Vol. 46, 73-80.

Carreterro M. I., Gomes C. S. F., Tateo F. (2013). *Clays, Drugs and Human Health, in Handbook of Clay Science, 2nd edition* (Eds. F. Bergaya & G. Lagaly). Elsevier B.V.

Chaurasia M., Chourasia M.K., Jain N.K., Jain A., Soni V., Gupta Y., Jain S.K. (2006). *Cross-Linked Guar Gum Microspheres: A Viable Approach for Improved Delivery of Anticancer Drugs for the Treatment of Colorectal Cancer.* AAPS PharmSciTech 7, (3), article 74.

Cheng H.N., Neiss T.G. (2012). *Solution NMR Spectroscopy of Food Polysaccharides*. Polymer Reviews 52, 81-114.

Chenu, C. (1993). *Clay- or sand-polysaccharide associations as models for the interface between micro-organisms and soil: water related properties and microstructure*. Geoderma 56, 143–156.

Chourasia M.K. & Jain S.K. (2004). *Potential of Guar Gum Microspheres for Target Specific Drug Release to Colon*. Journal of Drug Targeting, 12 (7), 435–442.

Cojocariu A. Profire L., Aflori M., Vasile C. (2012*). In vitro drug release from chitosan/Cloisite 15A hydrogels*. Applied Clay Science 57, 1–9.

Costa P. & Lobo J. M.S. (2001). *Modeling and comparison of dissolution profiles.* European Journal of pharmaceutical sciences 13(2), 123-133.

Crystallography Open Database (http://www.crystallography.net/).

Cunha P.R.L., de Paula R.C.M., Feitosa J.P.A. (2007). *Purification of Guar Gum for Biological Applications*. International Journal of Biological Macromolecules 41, 324 – 331.

Das A., Wadhwa S., Srivastava A.K. (2006). *Cross-Linked Guar Gum Hydrogel Discs for Colon Specific Delivery of Ibuprofen: Formulation and In Vitro Evaluation.* Drug Delivery 13:2, 139-142.

Dawson J.I. & Oreffo R.O.C. (2013). *Clay: New Opportunities for Tissue Regeneration and Biomaterial Design.* Advanced Materials 25, 4069–4086.

Denys S., Caboche J., Tack K., Rychen G., Wragg J., Cave M., Jondreville C., Feidt C. 2012. *In Vivo Validation of the Unified BARGE Method to Assess the Bioaccessibility of Arsenic, Antimony, Cadmium, and Lead in Soils. Environmental Science and Technology* 46 (11), 6252–6260.

Depan D., Kumar A. P., Singh R. P. (2009). *Cell proliferation and controlled drug release studies of nanohybrids based on chitosan-g-lactic acid and montmorillonite*. Acta Biomaterialia 5(1), 93-100.

Detellier C & Letaief S. (2013). *Kaolinite-Polymer Nanocomposites*, *in Handbook of Clay Science, 2nd edition* (Eds. F. Bergaya & G. Lagaly). Elsevier B.V.

Dias M., Suarez Barrios M., Prates S. (2004). *Bentonites from Benavila (Portugal). Mineralogical characterization and properties*. Geogaceta, 35 (2004), 99-102, ISSN:0213683X.

Dohrman, R. (2006). *Problems in CEC determination of calcareous clayey sediments using the ammonium acetate method*. Journal of Plant Nutrition and Soil Science169, 330–334.

Droy-Lefaix M.T, Tateo F. (2006). *Clays and Clay Minerals as Drugs, in Handbook of Clay Science, Developments in Clay Science Vol. 1* (Eds. F. Bergaya, B.K.G. Theng, G. Lagaly). Elsevier Ltd.

Dubernet C., Benoit J. P., Peppas N. A., Puisieux F. (1990). Ibuprofen-loaded ethylcellulose microspheres: release studies and analysis of the matrix structure through the Higuchi model. Journal of microencapsulation 7(4), 555-565.

Dupont C., Vernisse B. (2009). *Anti-diarrheal effects of diosmectite in the treatment of acute diarrhea in children: a review.* Paediatric Drugs 11, (2):89-99.

Dutta P.K; Dutta J. (2013). *Multifaceted Development and Application of Biopolymers for Biology, Biomedicine and Nanotechnology*. Springer, Vol. 254.

EMEA, European Food Safety Authority (2008) Safety of aluminium from dietary intake[1] - Scientific Opinion of the Panel on Food Additives, Flavourings, Processing Aids and Food Contact Materials (AFC) Accessed on January 22/2012 at [http://www.efsa.europa.eu/en/efsajournal/pub/754.htm].

Endres H.-J. & Siebert-Raths A. (2011). *Engineering Biopolymers. Markets, Manufacturing, Properties and Applications*, pp. 2-17. Hanser Publications.

Ensminger L.E., Gieseking J.E. (1941). *The adsorption of proteins by montmorillonitic clays and its effect on base-exchange capacity*. Soil Science 51, 125–132.

Fafard J., Detellier C. (2015). *Intercalation of a block co-polymer in kaolinite*. Journal of Colloid and Interface Science 450:361-5.

Foldvari M. (1991). *Measurement of different water species in minerals by means of thermal derivatography. In W. Smykatz-Kloss & S.S.J Warne (Eds.) Thermal Analysis in the Geosciences. Lecture Notes in Earth Sciences Volume 38, pp. 84-100.*

Forteza M., Galan E., Cornejo J. (1989). Interaction of Dexamethasone and Montmorillonite –Adsorption – Degragation Process. Applied Clay Science, 4, 437 – 448.

Friedlander H.Z. & Frink C.R. (1964). *Organized polymerization III. Monomers intercalated in montmorillonite*. Journal of Polymer Science Part B: Polymer Letters 2, 4, 475–479.

Friel J.J. (2003). X-*ray and image analysis in electron microscopy, 2nd Edition*, pp. 1-63. Princeton Gamma-Tech.

Gaharwar A., Schexnailder P.J., Kline B.P., Schmidt G. (2010*). Assessment of using Laponite cross-linked poly(ethylene oxide) for controlled cell adhesion and mineralization*. Acta Biomaterialia 7, 568–577.

Gamal-Eldeen A.M., Amer H., Helmy W.A. (2006). *Cancer chemopreventive and anti-inflammatory activities ofchemically modified guar gum*. Chemico-Biological Interactions 161, 229–240.

Gauglitz G. (2001). *Ultraviolet and visible spectroscopy*, in *Handbook of Analtyical Techniques (Eds.* H. Gunzler & A. Williams). Wiley-VCH Verlag, Germany.

Gil A., Korili S.A., Trujillano R., Vicente M.A. (2011). *A review on characterization of pillared clays by specific techniques.* Applied Clay Science 53, 97–105.

Gomes, C.F. 1988 *Argilas: o que são e para que servem. Lisboa: Fundação Calouste Gulbenkian,* 1988. pp. 457.

Greenland D.J. (1963). *Adsorption of polyvinyl alcohols by montmorillonite*.Journal of Colloid Science 18(7), 647-664.

Guggenheim S., Martin R.T. (1995). *Definition of clay and clay mineral: joint report of the AIPEA nomenclature and CMS nomenclature committees*. Clays and Clay Minerals 43, 255 – 256.

Haines P. (2002). *Introduction, in Principles of Thermal Analysis and Calorimetry*, pp. 1-9. The Royal Society of Chemistry, UK.

Hajjaji, W.; Ganiyu, S. O.; Tobaldi, D. M. (2013). *Natural Portuguese clayey materials and derived TiO_2-containing composites used for decolouring methylene blue (MB) and orange II (OII) solutions*. Applied Clay Science 83-84, 91-98.

He B. B. (2009). *X-ray Source and Optics*, in *Two-dimensional X-ray Diffraction* (Ed. B.B. He). John Wiley & Sons, Inc., Hoboken, New Jersey.

Heal G.R. (2002). *Thermogravimetry and Derivative Thermogravimetry.* In P. Haines (Ed.) *Principles of Thermal Analysis and Calorimetry*. The Royal Society of Chemistry, UK.

Hellmig S., Von Schöning F., Gadow C., Katsoulis S., Hedderich J., Fölsch U. R., Stüber E. (2006). *Gastric emptying time of fluids and solids in healthy subjects determined by 13C breath tests: influence of age, sex and body mass index.* Journal of gastroenterology and hepatology 21(12), 1832-1838.

Henao L.J., Mazeau K. (2009). *Molecular modelling studies of clay-exopolysaccharide complexes:soil aggregation and water retention phenomena*. Material Science and Engineering C 29, 2326–2332.

Hogan R. (2006). *How to combine errors*. http://www.met.rdg.ac.uk/~swrhgnrj/combining_errors.pdf, retrieved in August, 2015.

Holtz R.D. & Kovacs W.D. (1981). *An introduction to Geotechnical Engineering*. Prentice-Hall.

ISO/TS 17892-12:2004: *Geotechnical investigation and testing - Laboratory testing of soil - Part 12: Determination of Atterberg limits.*

ISO/TS 17892-6/12: *Geotechnical investigation and testing - Laboratory testing of soil - Part 6: Fall cone test.*

IUPAC. (1997). *Compendium of Chemical Terminology, 2nd ed. (the "Gold Book").* Compiled by A. D. McNaught & A. Wilkinson. Blackwell Scientific Publications, Oxford.

Jaber M., Komarneni S., Zhou C.-H. (2013). *Synthesis of Clay Minerals, in Handbook of Clay Science, 2nd edition* (Eds. F. Bergaya & G. Lagaly). Elsevier B.V.

Jain S. & Datta M. (2014). *Montmorillonite-PLGA nanocomposites as an oral extended drug delivery vehicle for venlafaxine hydrochloride*. Applied Clay Science 99, 42–47.

Jenkins, R. (1999). *X-Ray Fluorescence Analysis, in X-ray Characterization of Materials* (ed E. Lifshin), Wiley-VCH Verlag GmbH, Weinheim, Germany.

Kaushik D., Dureja H. (2014). *Recent Patents and Patented Technology Platforms for Pharmaceutical Taste Masking*. Recent Patents on Drug Delivery & Formulation, 8, 37-45.

Keller, W.D. (1970). *Environmental aspects of clay minerals.* Journal of Sedimentary Petrology 40, 798–813.

Kogure T. (2013). *Electron microscopy, in Handbook of clay science, 2nd edition (Eds.* F. Bergaya & G. Lagaly). Elsevier B.V.

Krishnaiah Y.S.R., Satyanarayana S., Rama Prasad Y.V., Narasimha Rao S. (1998). *Evaluation of guar gum as a compression coat for drug targeting to colon.* International Journal of Pharmaceutics 171, 137–146.

Krishnaiah Y.S.R., Karthikeyan S.R, Gouri Sankar V., Satyanarayana V. (2002). *Three-layer guar gum matrix tablet formulations for oral controlled delivery of highly soluble trimetazidine dihydrochloride.* Journal of Controlled Release 81, 45–56.

Kuo D.-C., Hsu S.-P., Chien C.-T. (2009). *Partially hydrolyzed guar gum supplement reduces high- fat diet increased blood lipids and oxidative stress and amelioratesFeCl3-induced acute arterial injury in hamsters.* Journal of Biomedical Science16:15.

Lagaly G. (1986). *Smectitic clays as ionic macromolecules*. Development of Ionic Polymers 2, 77-140.

Lal S. & Datta S. (2015). *In vitro prolonged gastric residence and sustained release of atenolol using novel clay polymer nanocomposite*. Applied Clay Science 114, 412–421.

Lambert J.F., Bergaya F. (2013). *Smectite-polymer* nanocomposites, in *Handbook of Clay Science, 2nd edition* (Eds. F. Bergaya & G. Lagaly). Elsevier B.V.

Laye P.G. (2002). *Differential Thermal Analysis and Differential Scanning Calorimetry, in Principles of Thermal Analysis and Calorimetry* (Ed. P. Haines). The Royal Society of Chemistry, UK.

Lenz R.W. (1993) *Biodegradable Polymers, in Biopolymers I* (Eds. N.A Peppas & R.S. Langer). Springer-Verlag.

Leszczynska A., Njuguna J., Pielichowski K., Banerjee J.R. (2007). *Polymer/montmorillonite nanocomposites with improved thermal properties. Part II: Thermal stability of montmorillonite nanocomposites based on different polymeric matrices.* Thermochimica Acta, 454, 1, 1-22.

Lichtenstein D.R., Syngal S., Wolfe M.M. (1995). Nonsteroidal anti-inflammatory drugs and the gastrointestinal tract: the double-edged sword. Arthritis & Rheumatism 38,5-18.

Liu K. H., Liu T. Y., Chen S. Y., Liu D. M. (2008). *Drug release behavior of chitosan–montmorillonite nanocomposite hydrogels following electrostimulation*. Acta biomaterialia 4(4), 1038-1045.

Liu B., Luo J., Wang X., Lu J., Deng H., Sun R. (2013). *Alginate/quaternized carboxymethyl chitosan/clay nanocomposite microspheres: preparation and drug-controlled release behavior*. Journal of Biomaterials Science, Polymer Edition,24:5, 589-605.

Lorenz R., Kahr G. (1999). *Determination of the CEC of clay minerals using the complexes of copper (II) ion with triethylenetetramine and tetraethylenepentamine*. Clays and clay minerals 41, 3, 386-388.

MacKenzie J.D, Smith M.E. (2002). *Multinuclear Solid-State NMR of Inorganic Materials*, Chapter 1, pp. 1-18. In R.W. Cahn (Ed.) Pergamon Materials Series Volume.

Mackenzie R.C & Rahman A.A. (1987). *Interaction of kaolinite with calcite on heating. I. Instrumental and Procedural Factors for One Kaolinite in Air and Nitrogen*. Thermochimica Acta, 121, 51-69.

Madejova J., Komadel P. 2001. *Baseline Studies of the Clay Minerals Society Source Clays: Infrared methods*. Clays and Clay Minerals 49, 5, 410-432, 2001.

Mahdavinia G.R., Ettehadi S., Aminia M., Sabzib M. (2014). *Synthesis and characterization of hydroxypropyl methylcellulose-g- poly(acrylamide)/ LAPONITE®RD nanocomposites as novel magnetic- and pH sensitive carriers for controlled drug release*. RSC Advances 5, 44516.

Mansa R. & Detellier C. (2013). *Preparation and Characterization of Guar-Montmorillonite Nanocomposites*. Materials 6, 5199-5216.

Mansa R. (2011). *Preparation and Characterization of Novel Montmorillonite Nanocomposites.* Master Thesis, Departament of Chemistry, Faculty of Graduate and Postdoctoral Studies, University of Ottawa, Canada.

Marchal-Heussler L., Maincent P., Hoffman M., Spittler J., Couvreur P. (1990). *Antiglaucomatous activity of betaxolol chlorhydrate sorbed onto different isobutylcyanoacrylate nanoparticle preparations*. International journal of pharmaceutics 58(2), 115-122.

Marin E., Briceno M.I., Caballero-George C. (2013). *Critical evaluation of biodegradable polymer rs used in nanodrugs*. International Journal of Nanomedicine 8, 3071–3091.

Martins V, Dubert J, Jouanneau J M, Weber O, Silva EF, Patinha C. (2007). *A multiproxy approach of the Holocene evolution of selfslope circulation on the NW Iberian Continental Shelf.* Marine Geology, pp 1–18.

Mathur N.K. (2012). *Industrial Galactomannan Polysaccharides*. CRC Press, Taylor & Francis Group.

McGinity J.W., Lach J.L. (1977). *Sustained-release Applications of Montmorillonite Interaction with Amphetamine Sulfate*. Journal of Pharmaceutical Sciences, 66, 1, 63-66.

Meunier A. (2005). *Clays.* Springer, Berlin.

Meunier A. (2013). *Clay Mineralogy Course Materials – International Master in Advanced Clay Science*. University of Poitiers, France.

Mitchel J. K. & Soga K. (2005). *Fundamentals of Soil Behavior*, 3rd Edition, Wiley.

Moore D.M. (1996). *Comment on: definition of clay and clay mineral: joint report of the AIPEA nomenclature and CMS nomenclature committees*. Clays and Clay Minerals 44, 710–712.

Moore D.M., Reynolds Jr. R.C (1997). *Structure, Nomenclature, and occurrences of individual clay minerals, in X-ray Diffraction and the Identification and Analysis of Clay Minerals, 2nd edition.* Oxford University Press, Oxford.

More J., Benazet F., Fioramonti J., Droy-Lefaix M.T. (1987). *Effects of treatment with smectite on gastric and interstinal glycoproteins in the rat: a histochemical study*. Histochemical Journal, 19, 665-670.

Namazi H. & Belali S. (2015). *Starch-g-lactic acid/montmorillonite nanocomposite: Synthesis, characterization and controlled drug release study*. Starch/Stärke 67, 1–11.

Nikolić M.A.L., Dean K., Halley P.J. (2012). Biodegradation *and Applications of Nanobiocomposites, in Environmental Silicate Nano-Biocomposites* (Eds. L. Averous & E. Pollet). Green Energy and Technology, pp. 409 – 441. Springer-Verlag.

Norrish, K., Quirk J.P. (1954). *Crystalline swelling of montmorillonite. Use of electrolytes to control swelling.* Nature, 173, 255.

O'Donnell L. J., Virjee J., & Heaton K. W. (1990). *Detection of pseudodiarrhoea by simple clinical assessment of intestinal transit rate.* BMJ: British Medical Journal 300(6722), 439.

Okada A., Kawasumi M., Usuki A., Kojima Y., Kurauchi T., Kamigaito O. (1989). *Nylon-6 Clay Hybrid*. Materials Research Society Precidings 171, 45-50.

Okada A., Usuki A. (2006). *Twenty Years of Polymer-Clay Nanocomposites*. Macromolecular Materials and Engineering 291, 1449-1476.

Olsson S., Karnland O. (2009). *Characterisation of bentonites from Kutch, India and Milos, Greece– some candidate tunnelback-fill materials.* Swedish Nuclear Fuel and Waste Management Co.

Oze C., Bird D., Fendorf S. (2007). *Genesis of hexavalent chromium from natural sources in soil and groundwater*. Proceedings of the National Academy of Sciences of the United States of America 104, 16, 6544-6549.

Pang J., Luan Y., Li F., Cai X., Du J., Li Z. (2011). *Ibuprofen-loaded poly(lactic-co-glycolic acid) films for controlled drug release.* International Journal of Nanomedicine 6, 659 – 665.

Pansu M. & Gautheyrou J. (2006). *Mineralogical characterization by X-ray Diffractometry, in Handbook of Soil Analysis Mineralogical, Organic and Inorganic Methods*, pp. 83-131. Springer-Verlag Berlin Heidelberg.

Peignot J.F., Giral P., Plique O. (1997). *Etude multicentrique, contrôlée, à double insuface au placebo, de l'efficacité de la diosmectite dans le traitement des gastralgies secondaires à la prise d'anti-inflammatoires non stéroïdiens*. Medicine et chirurgie digestives, 26, 5, 193-202.

Perkins, W.W. (1995). *Ceramic Glossary*. The American Ceramic Society, Westerville, OH.

Perotti G.F., Barud H.S., Messaddeq Y., Ribeiro S.J.L, Constantino V.R.L. (2011). *Bacterial cellulose-laponite clay nanocomposites*. Polymer 52,157-163.

Petrucci R.H., Harwood W.S, Herring F.G. (2002). *General Chemistry, Principles and Modern Applications, 8th edition*, pp. 1122-1148. Prentice Hall.

Pilla S. (2011). *Engineering Applications of Bioplastics and Biocomposites, in* Handbook of Bioplastics and Biocomposites Engineering Applications (Ed. S. Pilla). Wiley.

Plante A., Fernandez J.M., Leifeld J. (2009). *Application of thermal analysis techniques in soil science.* Geoderma 153, 1–10.

Plantefeve J.C., Rene M. (1989). *Modified clays, preparation thereof and therapeutical compositions containing the same*. US Patent, US 4839173 A.

Pongjanyakul T. & Suksri H. (2009). *Alginate-magnesium aluminum silicate films for buccal delivery of nicotine.* Colloids and Surfaces B: Biointerfaces 74,103–113.

Porubcan L.S, Serna C.J., White J.L, Hem S.L. (1978). *Mechanism of Adsorption of Clindamycin and Tetracycline by Montmorillonite*. Journal of Pharmaceutical Sciences, 67, 8, 1081-1087.

Porubcan L.S., Born G.S., White J.L, Hem S.L. (1979). *Interaction of Digoxin and Montmorillonite:Mechanism of Adsorption and Degradation*. Journal of Pharmaceutical Sciences, 68, 3, 358-361.

Prabaharan M. (2011). *Prospective of Guar Gum and Its Derivatives as Controlled Drug Delivery Systems*. International Journal of Biological Macromolecules 49, 2, 117-124.

Prencipe M, Pascale F, Zicovich-Wilson C M, Saunders V R, Orlando R, Dovesi R. (2004). *The vibrational spectrum of calcite ($CaCO_3$): An ab initio quantum-mechanical calculation*. Physics and Chemistry of Minerals 31, 8 559-564.

Quintela A., Terroso D., Ferreira da Silva E., Rocha F. (2012). *Certification and quality criteria of peloids used for therapeutic purposes*. Clay Minerals 47, 441- 451.

Rao K.,M, Nagappan S., Seo D.J., Ha C.-S. (2014). *pH sensitive halloysite-sodium hyaluronate/poly(hydroxyethyl methacrylate) nanocomposites for colon cancer drug delivery.* Applied Clay Science 97–98, 33–42.

Raty J., Peiponen K.E., Asakura T. (2004). *UV-Vis Reflection Spectroscopy od Liquids*. Springer. Verlag, Berlin, Heidelberg, Germany.

Rebelo M., Rocha F., Ferreira da Silva E. (2010). *Mineralogical and physicochemical characterization of selected Portuguese Mesozoic-Cenozoic muddy/clayey raw materials to be potentially used as healing clays*. Clay Minerals, (2010) 229-240.

Reed S.B.J. (2005). *Electron Microprobe Analysis and Scanning Electron Microscopy in Geology*. Cambridge University Press.

Reimer L. (1998). *Intoduction*. *Scanning Electron Microscopy: Physics of Image Formation and Microanalysis, 2nd Edition, in Springer Series in Optical Sciences* (Ed. P.W. Hawkes). Springer-Verlag Berlin Heidelberg.

Ribeiro L.N.M., Alcantara A.C.S., Darder M., Aranda P., Araujo-Moreira F.M., Ruiz-Hitzky F. (2013). Pectin-coated chitosan–LDH bionanocomposite beads as potentialsystems for colon-targeted drug delivery. International Journal of Pharmaceutics 463, 1– 9.

Rojas R., Palena M. C., Jimenez-Kairuz A. F., Manzo R. H., Giacomelli C. E. (2012). *Modeling drug release from a layered double hydroxide–ibuprofen complex*. Applied Clay Science 62, 15-20.

Rouquerol F., Rouquerol J., Llewellyn P. (2013). *Thermal Analysis*, *in Handbook of Clay Science, 2nd edition (*Eds.F. Bergaya & G. Lagaly). Elsevier B.V.

Roussel H., Waterlot C., Pelfrene A., Pruvot C., Mazzuca M., Douay F. (2010). Cd, Pb and Zn Oral Bioaccessibility of Urban Soils Contaminated in the Past by Atmospheric Emissions from Two Lead and Zinc Smelters. Archives of Environmental Contamination and Toxicology 58, 945–954.

Ruiz-Hitzky E., Darder M., Aranda P. (2005). *Functional biopolymer nanocomposites based on layered solids*. Journal of Materials Chemistry 15, 3650–3662.

Ruiz-Hitzky E., Aranda P., Darder M., Fernandes F.M. (2013). *Fibrous Clay Mineral-Polymer Nancomposites , in Handbook of Clay Science, 2nd edition* (Eds. F. Bergaya & G. Lagaly). Elsevier B.V.

Sablinskas V., Steiner G., Hof M., Machan R. (2014). *Applications, in Handbook of Spectroscopy*. (Eds. G. Gauglitz & D.S. Moore). Wiley-VCH Verlag & Co., Germany.

Santos S.C.R, Boaventura R.A.R., Oliveira A.F.M. (2006). *Preliminary Study on the Adsorption of the Cationic Dye Astrazon Red by a Portuguese Bentonite*, *in Combined and Hybrid Adsorbents* (Eds. J.M. Loureiro & M.T. Kartel). Springer, pages 111-116.

Sanz, J., Serratosa, J.M. (1984). *^{29}Si and ^{27}Al high resolution MAS-NMR spectra of phyllosilicates*. Journal of the American Chemical Society 106, 4790– 4793.

Sanz J. & Massiot D. (2013). *Nuclear Magnetic Resonance Spectroscopy, in Handbook of Clay Science, 2nd edition* (Eds. F. Bergaya & G. Lagaly). Elsevier B.V.

Saravanan M., Bhaskar K., Rao G. S., Dhanaraju M.D. (2003). *Ibuprofen-loaded ethylcellulose/polystyrene microspheres: an approach to get prolonged drug release with reduced burst effect and low ethylcellulose content*. Journal of Microencapsulation 20(3), 289-302.

Schoen R.T. & Vender R.J. (1989). *Mechanisms of nonsteroidal anti-inflammatory drug-induced gastric damage*. The American Journal of Medicine 86, 449-58.

Sen G., Mishra S., Jha U., Pal S. (2010). *Microwave initiated synthesis of polyacrylamide grafted guar gum (GG-g-PAM)—Characterizations and application as matrix for controlled release of 5-amino salicylic acid.* International Journal of Biological Macromolecules 47, 164–170.

Shen J. & Burgess D. J. (2013). *In vitro dissolution testing strategies for nanoparticulate drug delivery systems: recent developments and challenges*. Drug delivery and translational research 3(5), 409-415.

Singh V.K., Banerjee I., Agarwala T., Pramanika K. , Bhattacharya M.K., Pala K. (2014). *Guar gum and sesame oil based novel bigels for controlled drug delivery*. Colloids and Surfaces B: Biointerfaces 123, 582–592.

Si-Shen F., Lin M., Panneerselvan A., Gan C.W., Zhou W. (2009). *Poly(lactide)–vitamin E derivative/montmorillonite nanoparticle formulations for the oral delivery of Docetaxel.* Biomaterials 30, 3297–3306.

Soppimath K.S., Kulkarni A.R., Aminabhavi T.M. (2000). *Controlled release of antihypertensive drug from the interpenetrating network poly(vinyl alcohol)–guar gum hydrogel microspheres*. Journal of Biomaterials Science, Polymer Edition, 11:1, 27-43.

Środoń J. (2013). *Identification and Quantitative Analysis of Clay Minerals, in Handbook of Clay Science, 2nd edition* (Eds. F. Bergaya & G. Lagaly). Elsevier B.V.

Steiner G. (2014). Measurement Techniques, in *Handbook of Spectroscopy* (Eds. G. Gauglitz & D.S. Moore). Wiley-VCH Verlag & Co., Germany.

Takahashi T., Yokawa T., Ishihara N., Okubo T., Chu D.-C., Nishigaski E., Kawada Y., Kato M. Juneja L.R.. (2009). *Hydrolyzed guar gum decreases postprandial blood glucose and glucose absorption in the rat small intestine.* Nutrition Research 29, 419–425.

Talibudeen O. (1955). *Complex formation between montmorillonoid clays and amino-acids and proteins*. Transactions of the Faraday Society 51, 582-590.

Thakur S., Chauhan G.,S., Ahn J.-H. (2009). *Synthesis of acryloyl guar gum and its hydrogel materials for use in the slow release of L-DOPA and L-tyrosine.* Carbohydrate Polymers 76, 513–520.

The DrugBank Database, Ibuprofen data; http://www.drugbank.ca/drugs/DB01050#, retrieved in 07.2015.

Theng B.G.K. (2012). *Formation and Properties of Polymer-Clay Nanocomposites, 2nd Edition*. Developments in Clay Science 4. Elsevier B.V.

Tiwari A. & Prabaharan M. (2010) *An Amphiphilic Nanocarrier Based on Guar Gum-graft-Poly(ε- caprolactone) for Potential Drug-Delivery Application*. Journal of Biomaterials Science, Polymer Edition, 21:6-7, 937-949.

Toti U.S. & Aminabhavi T.M. (2003). *Modified guar gum matrix tablet for controlled release of diltiazem hydrochloride*. Journal of Controlled Release 95, 567–577.

Tripathy S.., Das M.K. (2013). *Guar Gum: Present Status and Applications*. Journal of Pharmaceutical and Scientific Innovation 2(4), 24-28.

Turekian, K.K. and Wedepohl, K.H. (1961). *Distribution of the Elements in some major units of the Earth's crust.* Geological Society of America, Bulletin 72: 175-192.

U.S. Pharmacopeia, Buffer Solutions, (www.pharmacopeia.cn/v29240/usp29nf24s0_ris1s119.html)

U.S Pharmacopeial Convention data (2012) referenced in https://www.agilent.com/cs/library/primers/Public/5991-0436EN_Primer_Pharmaceuticals.pdf, pages 29 -30; retrieved 11.2015.

Ueshima M., Tazaki K. (2001). *Possible role of microbial polysaccharides in nontronite formation*. Clays and Clay Minerals, Vol. 49, No. 4, 292-299.

Vaia R.A., Giannelis E.P. (1997). *Polymer melt intercalation in organically modified layered silicates: model predictions and experiment*. Macromolecules 30, 8000–8009.

Van de Wiele TR., Oomen AG., Wragg J., Cave M., Minekus M., Hack A., Cornelis C., Rompelberg CJ., De Zwart LL., Klinck B., Van Wijnen J., Verstraete W., Sips AJ. 2007. *Comparison of five in vitro digestion models to in vivo experimental results: lead bioaccessibility in the human gastrointestinal tract*. Journal of environmental science and health. Part A, Toxic/hazardous substances & environmental engineering, 42(9), 1203-11.

Velde B., Meunier A. (2008). *The Origin of Clay Minerals in Soils and Weathered Rocks*. Springer-Verlag, Berlin Heidelberg.

Velde, B., Barre, P. (2010). *The Alteration – Soil Profile: Transformation of Rocks into Clay, Sand and Organic Matter Complexes, in Soils, Plants and Clay Minerals: Mineral and Biologic Interactions,* pp. 62-75. Springer, Berlin.

Viseras C., Aguzzi C., Cerezo P., Bedmar M.C. (2008). *Biopolymer–clay nanocomposites for controlled drug delivery*. Materials Science and Technology 24(9), 1020-1026.

Viseras C., Cerezo P., Sanchez R., Salcedo I., Aguzzi C. (2010). *Current challenges in clay minerals for drug delivery*. Applied Clay Science 48, 291–295.

Wang Q., Zhang J., Wang A. (2009). *Preparation and characterization of a novel pH-sensitive chitosan-g-poly (acrylic acid)/attapulgite/sodium alginate composite hydrogel bead for controlled release of diclofenac sodium*. Carbohydrate Polymers 78 , 731–737.

Wang Q., Zhang J., Mu B., Fan L., Wang A. (2014). *Facile preparation of magnetic 2-hydroxypropyltrimethyl ammonium chloride chitosan/Fe_3O_4/halloysite nanotubes microspheres for the controlled release of ofloxacin.* Carbohydrate Polymers 102, 877–883.

Waseda Y., Matsubara E., Shinoda K. (2011). *X-Ray diffraction crystallography: introduction, examples and solved problems*. Springer Berlin, Heidelberg New York.

Whistler R.L. (1993). *Introduction to Industrial Gums, in Industrial Gums. Polysaccharides and Their Derivatives, 3rd edition* (Eds. J.N. BeMiller & R.L. Whistler). Academic Press.

Wieczorek M., Krzysztafkiewicz A. (2001). Characteristics of domestic bentonites and possibilities of their application. Prace Naukowe Instytutu Górnictwa, Politechnika Wrocławska nr 31.

Wolfe M.M., Lichtenstein D.R., Singh G. (1999). *Gastrointestinal toxicity of nonsteroidal antiinflammatory drugs.* The New England Journal of Medicine 340 (24), 1888 – 1899.

Wunderlich B. (2005). *Basics of Thermal Analysis, in Thermal Analysis of Polimeric Materials*. Springer Berlin, Heidelberg, New York.

www.webmineral.com.

Xu S. W., Zheng J. P., Tong L.,Yao K. D. (2006). *Interaction of functional groups of gelatin and montmorillonite in nanocomposite*. Journal of applied polymer science,101(3), 1556-1561.

Yang H., Wang W., Zhang J., Wang A. (2013). *Preparation, Characterization, and Drug-Release Behaviors of a pH-Sensitive Composite Hydrogel Bead Based on Guar Gum, Attapulgite, and Sodium Alginate*. International Journal of Polymeric Materials and Polymeric Biomaterials, 62:7, 369-376.

Young S. L., Sherman P. W., Lucks J.B., Pelto G.H. (2011). *Why on Earth?: Evaluating Hypotheses about the Physiological Functions of Human Geophagy*. The Quarterly Review of Biology, Vol. 86, No. 2, 97-120.

Zeng, Q.H., Yu, A.B., Lu, G.Q., Paul, D.R. (2005). *Clay-based polymer nanocomposites: research and commercial development*. Journal of Nanoscience and Nanotechnology 5, 1574–1592.

Zhang Y., Chen J., Zhang G., Lu J., Yan H., Liu K. (2012). *Sustained release of ibuprofen from polymeric micelles with a high loading capacity of ibuprofen in media simulating gastrointestinal tract fluids*. Reactive and Functional Polymers 72(6), 359-364.

Zheng J.P., Li P., Ma Y.L., Tao K.D. (2002). *Gelatin/Montmorillonite Hybrid Nanocomposite. I. Preparation and Properties*. Journal of Applied Polymer Science 86, 1189–1194.

Zheng J.P, Luan L., Wang H.Y., Xi L.F., Yao K.D. (2007). *Study on ibuprofen/montmorillonite intercalation composites as drug release systems*. Applied Clay Science 36, 297 – 301.

Zia K.Z., Zuber M., Barikani M., Hussain R., Jamil T., Anjuma S. (2011). *Cytotoxicity and mechanical behavior of chitin–bentonite clay based polyurethane bio-nanocomposites.* International Journal of Biological Macromolecules 49,1131– 1136.